INÊS FILIPA ACÁCIO GRENHO

GENERATION OF DRUG-RESISTANT CELL LINES AS A MODEL TO STUDY PANCREATIC CANCER

Faculdade de Medicina e Ciências Biomédicas

2021

INÊS FILIPA ACÁCIO GRENHO

GENERATION OF DRUG-RESISTANT CELL LINES AS A MODEL TO STUDY PANCREATIC CANCER

Master in Oncobiology: Molecular Mechanisms of Cancer

Work developed under the supervision of:

Bibiana I. Ferreira, PhD

Wolfgang Link, PhD

UAlg
UNIVERSIDADE DO ALGARVE

Faculdade de Medicina e Ciências Biomédicas

2021

GENERATION OF DRUG-RESISTANT CELL LINES AS A MODEL TO STUDY PANCREATIC CANCER

Authorship Statement

I declare to be the author of this work, which is original and unpublished. Authors and papers consulted are properly cited in the text and are listed in the included references.

_____

(Signature)

To you.

Abstract

Pancreatic cancer (PC) is among the most aggressive cancers in the world, characterized by an extremely high mortality/incidence ratio. Besides its aggressiveness, PC is usually diagnosed in an advanced and metastatic stage, which limits the treatment options available. Most of these tumors are unresectable by surgery, thus chemotherapy remains the only option available for treatment. However, a majority of these patients relapse within months and have a recurrence of the disease, usually more aggressive and no longer sensitive to the initial treatment. The major responsible for this relapse is the development of acquired therapy resistance.

Our work focused on generating cell lines resistant to the current first line chemotherapy drug, Gemcitabine, and on their characterization. This allowed us to generate tools that will be crucial to unveil the mechanism driving acquired resistance in PC. Previous studies from our group and others demonstrated an association between the expression profiles of TRIBBLES pseudokinases and drug resistant phenotypes in other cancers. We evaluated the sensitivity of the generated cell lines to Gemcitabine and characterized them in terms of migration ability, cell death rate under stress and the expression of TRIBBLES proteins and EMT markers.

Our results show that we successfully generated Gemcitabine-resistant cell lines, and that these cell lines are phenotypically different from the sensitive ones, showing fibroblastic-like features. Furthermore, we observed a reversible phenotypic switch when these cells undergo Gemcitabine treatment. They show different migration ability and increased mRNA expression of EMT markers, a hallmark of the epithelial-to-mesenchymal transition process. Moreover, in the resistant cells we observed higher TRIB2 protein expression levels and a decrease in the TRIB3 protein expression, compared with the sensitive cell lines. Overall, the phenotype associated with the resistant cells is concordant with drug resistance development by chronic Gemcitabine exposure.

Keywords: pancreatic cancer; gemcitabine; drug-resistance; resistance mechanisms; TRIB2; TRIB3

Resumo

Cancro, ou neoplasias malignas, é um conjunto de doenças que afetam a população mundial veemente de uma forma recorrente. Atualmente, estas doenças contam com uma crescente incidência e representam a causa de grande percentagem da mortalidade a nível mundial.

O cancro pancreático encontra-se em 14º lugar como o tipo de cancro mais diagnosticado nos últimos tempos, e representa o 7º cancro mais mortífero. De acordo com os dados mais recentes, possui um rácio de mortalidade/incidência de 94%. Para além da sua agressividade, o cancro pancreático é usualmente diagnosticado em fases tardias do seu desenvolvimento. Cerca de 52% destes tumores são detetados em estado avançado ou com presença de metástases, o que contribui para um desvantajoso prognóstico destes pacientes. Em causa estão a falta de sintomas em fases precoces do desenvolvimento deste tumor e a escassez de novos e específicos biomarcadores.

As opções de tratamento disponíveis para o cancro pancreático estão correlacionadas com o estádio do tumor na altura do diagnóstico. Relativamente aos tumores metastáticos, a primeira linha de tratamento baseia-se em protocolos de quimioterapia. No geral, seja em terapias adjuvantes ou neoadjuvantes ou em tratamentos de primeira linha com quimioterapia, o fármaco Gemcitabina está recorrentemente presente no tratamento de pacientes com cancro do pâncreas.

A Gemcitabina (2',2'-difluoro-2'-deoxycytidin; dFdC) é um análogo de nucleósidos, frequentemente utilizado no tratamento do cancro do pâncreas, mas também no tratamento de cancro da mama, ovário, bexiga, e pulmão de células não pequenas. O mecanismo de ação principal da Gemcitabina baseia-se na inibição da síntese de DNA, atuando na fase S do ciclo celular. A sua forma ativa e trifosfatada, dFdCTP, compete com os nucleótidos e é incorporada na cadeia, impedindo a elongação da cadeia de DNA e mimetizando a sua terminação. Para além disso, a Gemcitabina é também reconhecida por conseguir auto potenciar a sua ação e por induzir o processo de apoptose, por ativação da enzima quinase p38-MAPK, em células tumorais e pela via de sinalização AMPK/mTOR.

Contudo, apesar do desenvolvimento das terapias, a percentagem de sobrevivência destes pacientes ao fim de 5 anos continua diminuta. A taxa de sobrevivência varia de 39% para pacientes com tumores ressecáveis ou locais (11%),

para 3% em tumores avançados ou metastáticos (52%). Para além disso, a taxa de progressão livre de desenvolvimento da doença apenas se mantém na ordem dos meses. Ensaios clínicos em pacientes com doença avançada demonstram que a maioria apresenta uma recaída da doença em apenas 2 a 6 meses após tratamento.

O desenvolvimento de resistência à terapia é um dos principais fatores associados ao mau prognóstico do cancro pancreático. Apesar de detetado tardiamente, a maioria dos pacientes submetidos a tratamento acabam por sofrer uma recaída, com evolução de um tumor mais agressivo e não sensível às terapias previamente administradas. Contudo, os mecanismos desta resistência adquirida são ainda pouco conhecidos, sendo a maioria dos já descritos considerados intrínsecos.

O presente projeto baseia-se na criação de um modelo celular pancreático resistente à Gemcitabina. O principal objetivo foca-se no desenvolvimento de ferramentas essenciais para a investigação de mecanismos de resistência adquirida. De forma a gerar o modelo resistente, selecionámos duas linhas celulares descritas como sensíveis à Gemcitabina, MIA PaCa-2 e PANC-1. Através de exposição crónica ao fármaco, por administração de ciclos consecutivos de tratamento gerámos três linhas celulares, MUTIR28, MUTIR01 e PUTIR23.

A caracterização das linhas celulares resistentes é crucial para futuramente compreender os mecanismos que conduzem a esta resistência. Desta forma, avaliámos os níveis de resistência das linhas celulares geradas, pela avaliação dos valores de *IC50* (metade da concentração inibitória máxima) correspondentes. De acordo com a definição de resistência, este valor deve ser duas vezes superior ao da linha celular sensível correspondente. Considerando este princípio, apesar de todas as linhas celulares mostraram aumento dos seus valores de IC50, apenas as linhas MUTIR28 e PUTIR23 são resistentes. Ao longo deste trabalho referimo-nos às três linhas como resistentes, de forma a melhor serem identificadas em comparação com as parentais.

Durante o protocolo de tratamentos com a Gemcitabina para gerar as novas linhas, observámos uma mudança de fenótipo por parte das células expostas ao fármaco. A linha celular parental apresenta uma morfologia epitelial, com adesões entre as células, que apresentam conformação quadrangular. Contudo, as células resistentes, quando submetidas a um novo ciclo de tratamento, perdem aderência, encontrando-se em suspensão e aderindo tardiamente à superfície de cultura (com características fusiformes). Desta forma, avaliámos os níveis de marcadores de EMT nas células que sofreram esta alteração fenotípica e observámos um padrão de aumento dos níveis dos marcadores mesenquimais, relativamente às linhas celulares parentais.

As células foram também caracterizadas relativamente à sua capacidade de migração. Surpreendentemente, as linhas derivadas de MIA PaCa-2 apresentam níveis inferiores de migração quando comparado com a linha sensível. Relativamente à linha derivada de PANC-1, esta apresenta níveis superiores quando comparados com a linha parental.

Após a criação das linhas, caracterizámos a sua viabilidade e níveis de morte celular quando expostas a uma concentração específica do fármaco. Para tal, as células foram tratadas com a concentração de Gemcitabina correspondente ao IC50 das células parentais e executámos ensaios de viabilidade (ensaio de viabilidade *MTT*) e morte celular (ensaio de exclusão de *Trypan Blue*). Como observado, as linhas derivadas de MIA PaCa-2 demonstram alterações nos níveis de morte (induzida por Gemcitabina) e viabilidade comparadas com a linha parental. Contudo, o mesmo não acontece para PUTIR23 comparando com a linha sensível PANC-1, quando tratadas com baixas concentrações de Gemcitabina.

Por fim, caracterizámos as linhas resistentes relativamente à expressão de proteínas TRIBBLES. Alguns trabalhos anteriores demonstraram uma associação entre os níveis de TRIB2 e de TRIB3 e os fenótipos resistentes em outros tipos de cancro. Desta forma, considerámos importante avaliar se estas proteínas são possíveis alvos na resistência desenvolvida no cancro pancreático. Através de uma avaliação aos níveis transcricionais e proteicos, observámos um aumento de TRIB2 nas linhas resistentes e um decréscimo na expressão de TRIB3.

De uma forma geral, o fenótipo associado às linhas resistentes é concordante com o desenvolvimento de resistência por exposição crónica à Gemcitabina, tal como sucede na clínica.

Palavras-chave: cancro pancreático, gemcitabina, resistência a fármacos; mecanismos de resistência; TRIB2; TRIB3

General Index

Abstract xi
Resumo xiii
General Index xvii
List of Figures xxi
List of Tables xxv
List of Equations xxvi
List of abbreviations, acronyms, and symbols xxvii
1 Introduction 3
1.1 Cancer 3
1.2 Pancreatic cancer 5
1.2.1 Epidemiology 5
1.2.2 Carcinogenesis 6
1.2.3 Pancreatic cancer classification and subtypes 10
1.3 Pancreatic cancer treatment 15
1.3.1 Diagnosis 15
1.3.2 Surgery 17
1.3.3 Adjuvant therapy 17
1.3.4 Neo-adjuvant therapy 18
1.3.5 Palliative treatment 19
1.4 Gemcitabine 20
1.4.1 Gemcitabine metabolism 20
1.4.2 Mechanism of action 21
1.5 Therapy resistance 22
1.5.1 Gemcitabine resistance in PC 23
1.5.2 Tribbles in cancer and therapy resistance 27
2 Methodology 31
2.1 Cell culture and maintenance 31

2.1.1 Cell counting 31
2.1.2 Cell freezing and thawing 33
2.2 Drug-resistant cell lines generation 33
2.3 Thiazolyl Blue Tetrazolium Bromide (MTT) assay 35
2.3.1 Gemcitabine dose-response curves for pancreatic cancer cell lines 36
2.3.2 Cell viability upon Gemcitabine treatment 37
2.4 Trypan Blue Exclusion assay 38
2.4.1 Gemcitabine-induced cell death 38
2.5 Migration ability assay 39
2.5.1 Wound-healing migration assay 40
2.6 Western Blot 41
2.6.1 Biological sample collection 41
2.6.2 Protein extraction 41
2.6.3 Total protein quantification 42
2.6.4 Sample calibration and preparation 43
2.6.5 SDS - Polyacrylamide gel electrophoresis 43
2.6.6 Protein transfer to a PVDF membrane 44
2.6.7 Membrane blocking 44
2.6.8 Antibody incubation 45
2.6.9 Chemiluminescent protein detection 46
2.7 Real-time quantitative polymerase chain reaction 46
2.7.1 Sample collection 47
2.7.2 RNA extraction and purification 47
2.7.3 cDNA synthesis 48
2.7.4 Quantitative Real-Time Polymerase Chain Reaction (qPCR) 49
3 Results 55
3.1 Pancreatic cell lines sensitivity to Gemcitabine 56
3.2 Generation of Gemcitabine-resistant cell lines 58

3.2.1 New emerging phenotypes of MUTIR28 and MUTIR01 cell lines .. 58
3.2.2 Different morphology of the PUTIR23 cell line 62
3.2.3 IC50 determination of the Gemcitabine-resistant cell lines at T5 ... 64
3.2.4 IC50 determination of the Gemcitabine-resistant cell lines at T9 ... 66
3.3 Viability of Gemcitabine resistant cell lines 69
3.3.1 Characterization of MUTIR28, MUTIR01 and PUTIR23 cell lines after treatment with the Gemcitabine IC50 concentration for the parental cell lines at T5 69
3.3.2 Characterization of MUTIR28, MUTIR01 and PUTIR23 cell lines after treatment with the Gemcitabine IC50 concentration for the parental cell lines at T9 72
3.4 Resistant versus Parental cell lines motility capacity 79
3.4.1 Optimization of the starvation protocol 79
3.4.1 Wound healing of MIA Paca-2 and PANC-1 and the derived resistant cell lines 83
3.5 TRIBBLES expression in the generated cell lines..... 89
3.5.1 TRIB1, TRIB2 and TRIB3 mRNA levels 89
3.5.2 TRIB2 and TRIB3 protein levels 94
3.6 Epithelial to mesenchymal transition markers evaluation..... 99
3.6.1 EMT mRNA levels..... 100
4 Discussion..... 105
5 Conclusion 117
6 Future Perspectives 123
7 Bibliography 127

List of Figures

Figure I.1. Progression model for pancreatic cancer carcinogenesis and histological representation of the different PanIN lesions grades 9

Figure I..2. Molecular features that contribute to the different PC molecular subtypes 12

Figure I.3. Different stages and clinical classification of pancreatic cancer.. 16

Figure I.4. Review of the drug resistance mechanisms in cancer cell lines.. 23

Figure II.2. Representation of the Neubauer Chambers with its four quadrants A, B, C and D.…..... 32

Figure II.3. Schematic representation of the Gemcitabine treatment protocol cycles.. 34

Figure II.4. Calibration curve for protein quantification using the Bradford assay.. 42

Figure III.1. Diagram representation of our project timeline. 55

Figure III.2. Drug-response curves for MIA PaCa-2 and PANC-1 cell lines, after 72 hours Gemcitabine treatments. 57

Figure III.3. Representation of the project timeline, emphasizing the moment when the new phenotypes emerge.. 59

Figure III.4. Representation of the phenotypic switch observed in the MIA PaCa-2 derived cell lines.. 61

Figure III.5. Representation of the morphologic changes in the PUTIR23 cell line after Gemcitabine administration.. 63

Figure III.6. MIA PaCa-2 and the derived cell lines, MUTIR28 and MUTIR01, drug-responses to Gemcitabine exposure at T5..... 65

Figure III.7. MIA PaCa-2, MUTIR28 and MUTIR01 drug-responses after Gemcitabine treatment at T9..... 67

Figure III.8. PANC-1 and PUTIR23 drug-responses after Gemcitabine treatment at T9.. 68

Figure III.9. MIA PaCa-2 and its derived resistant cell lines under high dose of Gemcitabine treatment at T5. 71

Figure III.10. Evaluation of the cell viability levels for the Parental versus Resistant cell lines when exposed to low levels of Gemcitabine for 48 hours..... 74

Figure III.11. Evaluation of the cell viability levels for the Parental versus Resistant cell lines when exposed to low levels of Gemcitabine for 72 hours..... 75

Figure III.12. Evaluation of the parental versus resistant cell lines cell death after Gemcitabine treatment..... 78

Figure III.13. Wound healing assay performed for 15 hours to evaluate starvation conditions.. 81

Figure III.14. Optimization of starvation conditions for the wound healing migration assay..... 82

Figure III.15. Wound healing assay to analyze the migration ability of MIA PaCa-2 and the derived cell lines..... 84

Figure III.16. Wound healing assay to analyze the migration ability of PANC-1 and derived cell line. 86

Figure III.17. MIA PaCa-2 and derived cell lines present different levels of wound closure ability..... 87

Figure III.18. PANC-1 and PUTIR23 cell lines wound closure ability.. 88

Figure III.19. Characterization of MIA PaCa-2 and PANC-1 cell lines regarding TRIBBLES mRNA levels. 90

Figure III.20. TRIBBLES mRNA levels in the newly generated Gemcitabine-resistant cell lines. 93

Figure III.21. Levels of TRIB2 and TRIB3 proteins in MIA PaCa-2, PANC-1, and UACC-62. 94

Figure III.22. TRIB2 and TRIB3 proteins expression levels in the emerging MIA PaCa-2 resistant phenotypes. 96

Figure III.23. TRIB2 and TRIB3 proteins expression levels in PANC-1 and PUTIR23 cell lines.. 97

Figure III.24. TRIB2 and TRIB3 levels in MIA PaCa-2, MUTIR28 and MUTIR01 cell lines under Gemcitabine treatment. 98

Figure III.25. TRIB2 and TRIB3 levels in PANC-1 and PUTIR23 cell lines under Gemcitabine treatment. 99

*Figure III.26. Epithelial to mesenchymal markers mRNA expression levels in the Parental versus Resistant cell lines and in the emerging MIA PaCa-2 phenotypes and in PANC-1 derived resistant cell line. **101***

List of Tables

Table II.1. The antibodies used for Western Blot in the present study. 45

Table II.2. The primers used for RT-qPCR analysis. 50

Table III.1. Calculation of the percentage of viable and non-viable cells upon Gemcitabine treatment for 48 and 72 hours. 76

Table III.2. Wound size measurements for optimization of the starvation conditions 80

Table III.3. Wound size measurements in the 15 hours Migration Assay. 83

List of Equations

Equation II.1. Equation used to calculate the number of viable cells..... 32

Equation II.2. Equation correspondent to the log (inhibitor) vs response non-linear regression used to calculate the IC50 values of the cell lines. 37

Equation II.3. Percentage of cell death calculation considering the number of non-viable cells using Trypan Blue Exclusion Assay.. 39

Equation II.4. Fold change of gene expression calculation. 51

List of abbreviations, acronyms, and symbols

A

ACC: acinar cell carcinoma

ADEX: aberrantly differentiated endocrine exocrine subtype

AMPK: AMP-activated protein kinase

B

BRAF: proto-oncogene B-Raf

C

CA: carbohydrate antigens

CDKN2: cyclin-dependent kinase inhibitor 2

CEA: carcinoembryonic antigen

CSC: cancer stem cells

D

dCK: deoxycytidine kinase

dFdC: 2',2'-difluoro-2'-deoxycytidine

dFdCDP: 2',2'-difluoro-2'-deoxycytidine diphosphate

dFdCMP: 2',2'-difluoro-2'-deoxycytidine monophosphate

dFdCTP: 2',2'-difluoro-2'-deoxycytidine triphosphate

DNA: deoxyribonucleic acid

DPC4: Deleted in Pancreatic Cancer-4 gene

E

EUS: endoscopic ultrasound

F

FOXO: class O of forkhead box transcription factors

G

Gem: Gemcitabine

GLOBOCAN: global cancer observatory toll

H

hCNTs: concentrative nucleoside transporters

hENTs: equilibrative nucleoside transporters

HER-2/neu: Receptor tyrosine-protein kinase erbB-2

hNTs: human nucleoside transporters

I

IC50: half maximal inhibitory concentration

IPMN: intraductal papillary mucinous neoplasms

K

KRAS: kirsten rat sarcoma vírus gene

M

MCN: invasive mucinous cystic neoplasm

MRCP: the magnetic resonance cholangiopancreatography

MRI: magnetic resonance imaging

mTOR: mammalian target of Rapamycin

MTT: 3-(4,5-Dimethylthiazol-2-yl)-2,5-Diphenyltetrazolium Bromide

N

NF-kβ: nuclear factor kappa-light-chain-enhancer of activated B cells

nM: nanomolar

NTPs: nucleoside triphosphate

O

OS: overall survival

P

p38-MAPK: p38 mitogen-activated protein kinase

PanIN: pancreatic intraepithelial neoplasia

PC: pancreatic cancer

PDX1: pancreatic and duodenal homeobox 1

PFS: progression-free survival

pNET: pancreatic neuroendocrine tumor

PX: pixels

Q

qPCR: quantitative Real-time polymerase chain reaction

R

RNA: Ribonucleic acid

RR: Ribonucleotide reductase

RT: real time

S

SCC: squamous cell carcinoma

SPT: invasive solid pseudopapillary tumor

T

TB: Trypan Blue

TNM: tumor staging system

TRIB: Tribbles pseudokinase homolog

U

UMP-CMP: pyrimidine nucleoside monophosphate kinase

W

WB: western blot

WHO: World Health Organization

OTHERS

µg: micrograms

µL: microliters

5-FU: 5-Fluorouracil

CHAPTER I

INTRODUCTION

1 Introduction

1.1 Cancer

Cancer is one of the major leading causes of death worldwide and became a public health problem in the past decades. According to the World Health Organization, in 2020, cancer is a leading cause of death worldwide. The International Agency for Research on Cancer estimated, through GLOBOCAN 2020 database, 19,3 million new cases of cancer and ≈ 10 million deaths by this cause globally in 2020 [1]. The Eastern Europe holds the highest mortality/incidence ratio calculated in 2020, with around 165 deaths per 100 000 cases [1].

Irrefutably, neoplastic diseases and, ultimately, cancer is devastating for our society, and there is a constant need to expand the prognosis and survival of cancer patients. Indeed, emerging diagnostic tools, biomarkers, and improved treatment approaches, associated with adequate disease monitoring, are crucial factors that could help overcome these complex diseases.

Neoplastic diseases result from a multistep and progressive process, where normal cells acquire specific and distinct characteristics and advantages, now known as "*The Hallmarks of Cancer*" [2]. After recognizing these aspects, some crucial knowledge regarding the molecular and cellular mechanisms, and the surrounding interactive microenvironment, uncovered the principles for interpreting tumor development and progression, which is called carcinogenesis.

All the cells that compose an organism have a specific predisposition or susceptibility to become tumorigenic, and throughout this process, genetic and epigenetic alterations are being accumulated, favoring the transformation and posterior proliferation of abnormal cells [3,4]. With an increasing level of changes and abnormality, tissues start to show no orderly architecture and possibly evolve and acquire a malignant arrangement, along with an uncontrolled proliferation status [5]. Indeed, it takes many years to achieve a metastatic stage, the most clinically advanced status of abnormality [6]. The malignant tumors, also known as cancer, exhibit the most aggressive phenotype by invading the surrounding areas and spreading throughout the body, metastasizing in secondary locations. These are certainly the most concerning and lethal tumors, conversely to the benign ones, that are confined, and most are harmless to the patients [5].

Mutations are well-defined significant alterations in this multistage process of carcinogenesis and are also related to disease progression. However, the mutational signature underlying the carcinogenesis of each cancer type is specific and written in each tumor genome [7]. Several different causes can induce these mutations, some of them unknown yet, but they can be categorized into environmental, hereditary, or age-related causes [8].

Three different gene classes, the gatekeepers (oncogenes and tumor suppressor genes), the caretakers (DNA repair genes), and the landscapers (microenvironment associated), are cancer-susceptibility genes and the main targets of these mutations. The regulation of survival signaling, cell proliferation, cell cycle progression and differentiation, and the genomic integrity and stability are then compromised and controlled by these altered genes, contributing to the tumorigenic process and distorted cell microenvironment [9].

Despite that, not all mutations that can occur in a normal cell have the same contribution to its phenotype. These mutations can be classified into three categories: gatekeepers, drivers, or passengers, according to their cellular impact and if they confer (driver) or not (passenger) a growth advantage to the cells. Gatekeeper refers to the first mutation that provides a tumorigenic advantage and is usually followed by driver or passenger ones. On average, a solid tumor comprises between 33 and 66 somatic mutations, being only 2 to 8 of them driver mutations [6]. Moreover, we should also consider the age factor has a contributor for the mutational status of the cells. The increased replication number of the cells is associated with a higher mutational level, contributing to the accumulation of tumor-triggering alterations [10].

Moreover, in the past 15-20 years, the importance of epigenetic alterations has emerged as a significant determinant in cancer. According to the *Holliday* definition, and posterior *Wu and Morris* contribution, epigenetic corresponds to “the study of changes in gene function that are mitotically and/or meiotically heritable and that do not entail change in DNA sequence” [11–13]. Alterations at an epigenetic level lead to gene expression changes, but the opposite may also occur with mutations in the epigenome contributing to cancer development [3,14]. The continuous crosstalk between genetic and epigenetic helped to understand and explain tumor heterogeneity underlying the selective stress of tumor microenvironment [14,15].

In conclusion, normal cells overcome specific determinants through all this complex process and gain the capacity to sustain their own survival signaling and evade growth suppressors, enabling their replicative immortality and resisting cell death.

Inducing the angiogenesis process and activating invasion and metastasis for their purpose, through avoiding immune destruction and deregulating cellular energetics, these cells can promote genome instability and a mutation status with the maintenance of a tumor-promoting inflammation, essential features of a tumorigenic cell. – "*The Hallmarks of Cancer*" [2].

1.2 Pancreatic cancer

1.2.1 Epidemiology

Pancreatic cancer (PC) is among the most aggressive and lethal cancers throughout the world. In 2020, 495 9773 new cases and 466 003 deaths caused by this tumor were estimated on GLOBOCAN, with an expected mortality/incidence ratio of ≈ 94% (94 deaths per 100 cases) [1]. This data ranked PC as the 14th most common type of cancer and the 7th leading cause of cancer death worldwide. This tumor has a higher incidence and mortality rate in countries with high or very high human development index. Both incidence and mortality rates increase with age, being 90% of the deaths verified in patients with more than 55 years [16]. In fact, is expected that PC become the third leading cause of cancer death in 2025 in the European Union countries [17].

Despite all the advances in pancreatic cancer research, disease diagnosis, and therapy development, only ≈ 9% of the patients with pancreatic cancer survive for five years after being diagnosed [18]. The clinical stage of the tumor at the time of diagnosis is a critical determinant of the 5-year overall survival for these patients, which effortlessly varies from ≈ 37% to 3% [19]. However, many other factors could influence, such as the age and sex of the patient, and the treatment options and healthcare systems available [16]. A lack of biomarkers, screening tests, and symptoms in the early stages of PC development, lead to a late diagnosis, being the tumors detected in an advanced and unresectable status. These factors influence the treatment options available for those patients, contributing to the poor prognosis of this disease [16,20,21].

The number of PC new cases is still increasing worldwide, and more people will suffer from this complex disease over the years. Until 2040 it is expected an incidence increase of 77,7%, with more 79,9% of deaths [16,18,22].

1.2.2 Carcinogenesis

In 2000, Hruban and his team, inspired by the progression model for colorectal cancer proposed by Vogelstein [23], developed a similar prototype for pancreatic cancer carcinogenesis [24], as represented in Figure I.1. They found a correlation between primary pancreatic lesions (PanINs - Pancreatic intraepithelial neoplasia) and PC development, basing their model on some representative evidence and clinical studies that suggest them precursors of PC [24]. Previous findings from Cubilla and Fitzgerald, through pancreatic tissue evaluation, demonstrated histologically distinct lesions in the pancreas, adjacent to carcinomas. They also demonstrated their higher prevalence in tissues with PC and suggested them as significant primary *in situ* alterations [25]. However, it was essential to define a temporal association between these lesions and the invasive carcinoma, which was performed by Hruban and its team [24].

These microscopic lesions can be categorized into different classes: PanIN-1A (flat), PanIN-1B (papillary), PanIN-2, and PanIN-3, depending on its histological grade and nuclear atypia and polarity [26]. PanIN1 are the lowest graded lesions and progressively evolve into PanIN-3, already considered as a carcinoma in situ, as represented in Figure I.1.

Additionally, some macroscopic alterations have also been detected as precursors of pancreatic. The IPMNs (intraductal papillary mucinous neoplasms) and mucinous cystic neoplasms can also represent the carcinoma evolution and reflect a preinvasive condition [26].

In fact, most of the well-characterized mutations discovered in pancreatic carcinomas are also present in PanINs and IPMNs, indicating a stepwise progression from these lesions to the invasive status. PC, such as other cancers, is a genetic disease caused by possible inherited mutations and some acquired somatic alterations, possibly associated with these lesions evolution [27]. Normal epithelia acquire specific genetic alterations during the tumorigenesis process, contributing to precursor lesions development (neoplasia – abnormal and tissue growth) and further evolution to carcinoma [24,26].

KRAS activation by point mutations is one of the primary alterations in the pancreatic cells, being this gene activated in more than 90% of pancreatic cancers [28,29]. Specifically codon 12 and, more rarely, codon 13 and 61 are the main targets of these mutations [26,30]. Among these, $KRAS^{G12D}$ is the most frequent mutation, representing the shift from glycine to aspartic acid [31,32]. Due to its oncogenic role, KRAS abnormal

activation drives an uncontrolled and exacerbated stimulus that promotes proliferation and cell survival. Occurring prematurely in this neoplasia development (PanIN1-A), these are significant alterations at a clinical level, possibly allowing earlier detection of these neoplasms and monitoring the disease [27,33]. Nonetheless, KRAS mutations are not PC exclusive and can occur in other pathologic situations, even in infectious cases, where a neoplasm is not developed [26].

Another significant event in PC carcinogens affects the BRAF gene, which is usually altered in approximately 3% of pancreatic carcinomas and 30% of KRAS wildtype pancreatic carcinomas, being mutations in the KRAS and BRAF genes mutually exclusive [34,35]. Indeed, $BRAF^{V600E}$ mutation was associated with the development of PanIN lesions, precursors of an invasive pancreatic neoplasia [36]. Mutations in the BRAF gene are usually associated with higher kinase activity and promotion of a proliferative status [37].

The overexpression of HER-2/neu protein also seems to provide an advantage to pancreatic cells. This protein overexpression detected in most of pancreatic neoplasia and carcinomas is rare in normal pancreatic ducts [38–40]. Due to its oncogenic role, its activation increases proliferative and survival signaling, being associated with a poor prognosis of PC patients [41–43].

Later in the evolution of pancreatic lesions, the loss of CDKN2 gene, that encodes for the p16 tumor suppressor gene, located at chromosome 9p, seems to contribute to PC evolution [44]. The p16 inactivation is mainly detected in more advanced lesions, with higher atypia, but not yet invasive [45]. Loss of p16 function, a cyclin-dependent kinase inhibitor (CDIs), is associated with cell cycle progression, proliferation and tumorigenesis in PC [46]. Moreover, p16 mutations are detected in already KRAS mutated lesions, indicated that KRAS activation is a primary event [47].

Moreover, the loss of p53, DPC4 and BRCA2 have also been detected in pancreatic cancer ductal lesions [24]. The TP53 tumor suppressor gene encodes for the p53 protein that, in normal conditions, is associated with cell cycle arrest and activation of apoptotic signaling, in response to DNA damage [48,49]. Moreover, the DPC4 or SMAD4 protein is also associated with tumor suppressive functions. This protein is a mediator of the TGF-β signaling pathway, that induces cell cycle arrest and promotes angiogenesis [50,51]. Furthermore, the BRCA2 gene is associated with DNA repair, cell cycle arrest and apoptosis, being required for chromosomal stability[52]. Overall, the loss of p53, DPC4 and BRCA2 contributes to PC carcinogenesis and tumor progression.

However, the loss of these tumor suppressor genes occurs biologically late in the development of pancreatic cancer [53–55]. While KRAS mutations are very frequent in low grade PanIN lesions, p53, DPC4 and BRCA2 loss is associated with more advanced lesions, being even more frequent in invasive pancreatic carcinoma [56].

Also, the PI3K/AKT signaling pathway, one of the most mutated pathways in cancer, is overactivated in pancreatic cancer, controlling proliferation and cell cycle progression [57]. Mutations in the PIK3CA gene, that encodes for the p110α catalytic subunit of PI3K protein, have been identified in IPMN and carcinomas, suggesting its contribution to this tumorigenesis [58]. Besides that, downregulation of PTEN, a PI3K/AKT inhibitor, seems to have an aberrant expression in pancreatic cancer, deregulating this survival signaling pathway and its main targets expression [59].

Hedgehog pathway has also been identified as intervenient in pancreatic cancer initiation, progression, and maintenance [60–62]. On the contrary, in normal pancreatic ducts, expression of proteins associated with this signaling pathway is rarely detectable. Moreover, enhanced Hedgehog signaling is associated with KRAS overexpression [63], a frequent phenomenon in pancreatic cancer.

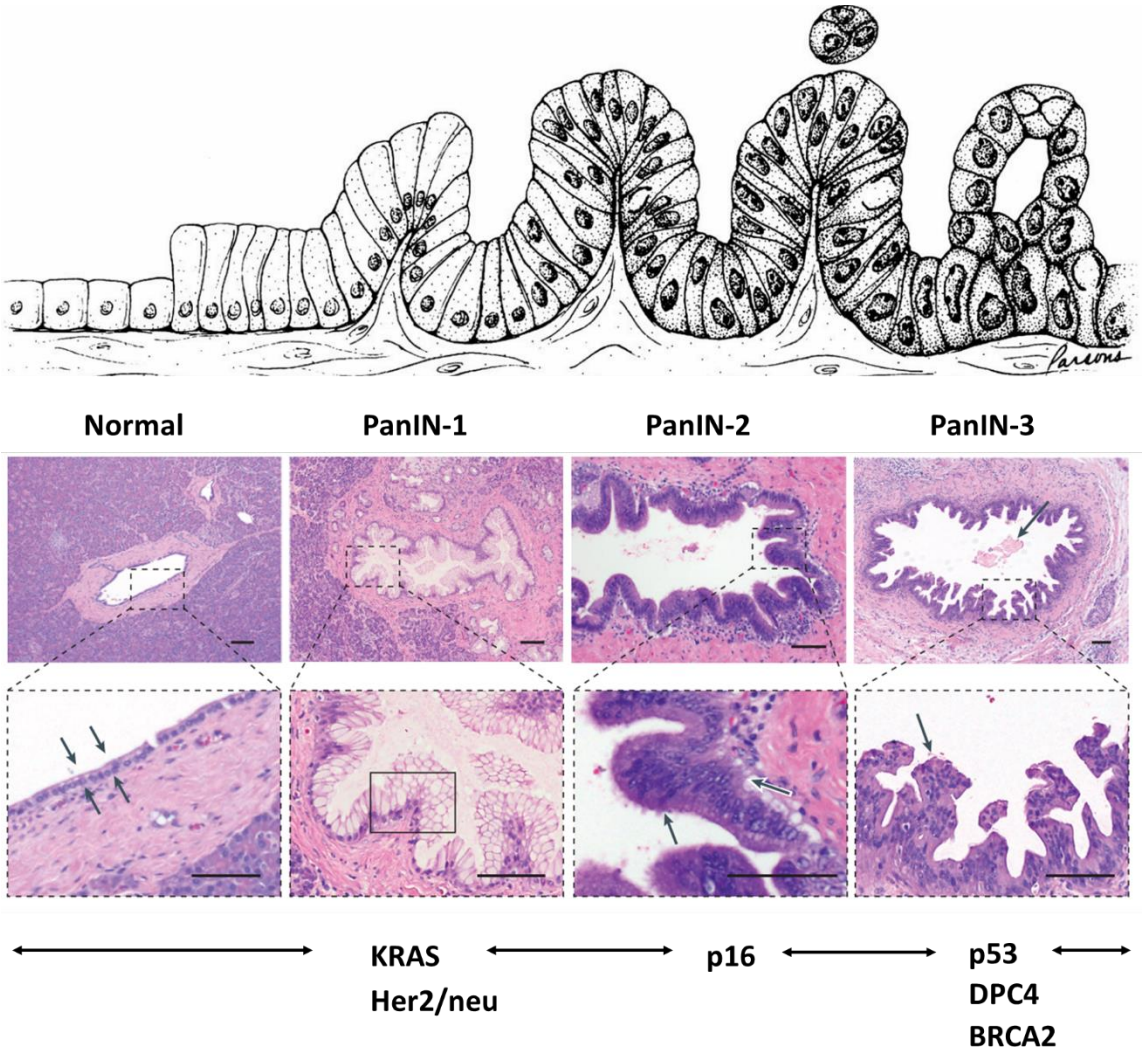

Figure I.5. Progression model for pancreatic cancer carcinogenesis and histological representation of the different PanIN lesions grades. The pre-invasive neoplasms (PanIN) are precursor lesions of PC present in pancreas tissue, that can be classified into different categories according to its histological grade. PanIN-1 lesions show low-grade dysplasia, PanIN-2 moderate dysplasia and PanIN-3 high-grade dysplasia. Activation of KRAS oncogene and overexpression of HER2/neu product are primary alterations in pancreatic cancer carcinogenesis, frequently found in PanIN-1 lesions. Following inactivation of tumor suppressor p16, and posterior loss of p53, DPC4 and BRCA4 functions, are associated with higher grade lesions, but still associated with pre-invasive neoplasms. Figure adapted from *Hruban et al., 2000* and *A & CA, 2016.*

1.2.3 Pancreatic cancer classification and subtypes

Pancreatic tumors can be divided according to different classifications, regarding their initial cell type and its molecular and cellular proprieties. With the increased knowledge about pancreatic cancer, it became important to discriminate its different types. We can no longer classify it as one unique disease. Different pathologic proprieties can benefit from different treatments, and this information is useful to improve treatment protocols and hopefully arrive to a personalized treatment [64].

1.2.3.1 Histological subtypes

The majority of PCs, around 86%, are adenocarcinomas, originated from the exocrine portion of the pancreas, more specifically from the ductal cells (ductal adenocarcinoma) [65]. Adenocarcinomas are tumors derived from specialized epithelial cells, with secretory ability, just like the exocrine pancreas epithelia [5]. This is the most studied subtype of pancreatic cancer, since it is the most frequent and aggressive one, with the highest impact on patient's survival.

This type of PC is usually more frequent in older patients, being the majority developed in the pancreas head. It is often characterized by a solid mass however it can manifest through an emerging fluid cyst and designated as a cystic tumor. Associated with the lack of symptoms in the early stages of development, when a pancreatic adenocarcinoma reaches a significant and inconvenient size, possible to detect, is already spreading out [20,66]. Indeed, it became widely accepted that after tumor initiation, the pancreatic ductal adenocarcinoma spreads quickly, which contributes to the late diagnosis of this tumor, at an advanced or metastatic stage [67].

Moreover, a smaller portion of these tumors, around 14%, display uncommon histological subtypes, such as: invasive intraductal papillary mucinous neoplasm (IPMN) and invasive mucinous cystic neoplasm (MCN), that correspond to cystic precursor lesions, pancreatic neuroendocrine tumor (pNET), adenosquamous carcinoma (with glandular and squamous differentiation), acinar cell carcinoma (ACC), squamous cell carcinoma (SCC), and invasive solid pseudopapillary tumor (SPT) [65,68].

According to a recent study, the uncommon subtypes of pancreatic cancer were less aggressive when compared with the adenocarcinoma type. The authors also observed that pNET, IPMN, MCN, SPT, and ACC can be classified as less violent,

whereas the adenocarcinoma, adenosquamous, and SCC are highly aggressive [65]. They also referred the importance of the early detection of the less aggressive subtypes since it seems to highly improve the patient's prognosis and survival [65].

However, more detailed information is required for clinical improved decisions on the treatment regimens, that could be provided by the classification of molecular subtypes.

1.2.3.2 Molecular subtypes

The molecular subtypes of PC account more than genetic information about the different pancreatic tumors [27]. As represented in Figure I.2, a variety of molecular changes, such as chromosomal instability and changes in the transcriptome, metabolome and epigenome could determine different pancreatic cancer subtypes [69]. The molecular taxonomy provides novel information that will contribute to distinguish between biological features that interfere in the therapeutic outcome [64,68–70].

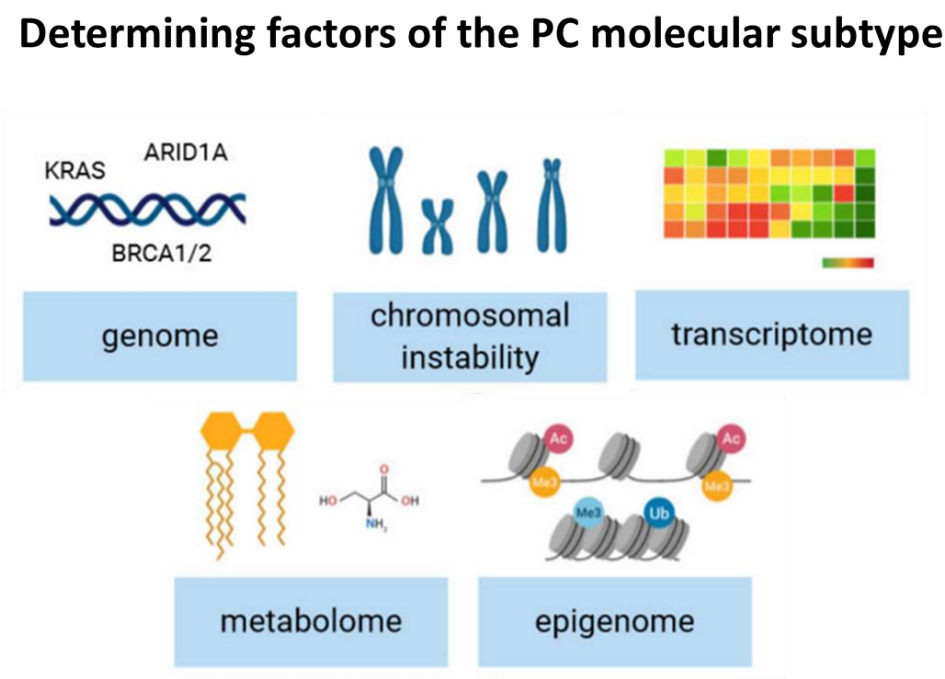

Figure I.2. Molecular features that contribute to the different PC molecular subtypes. The molecular classification of pancreatic cancer can be divided according with different tumor characteristics. Particular mutations in the genome seem to cluster in specific pathways associated with cancer development. However, the analysis of chromosomal instability, transcriptome, metabolome, and epigenome revealed their contribution to the identification of emerging PC subtypes. Figure adapted from *Regel, Mayerle, & Mahajan, 2020.*

As previously mentioned, there are four genes constantly associated with PC tumorigenesis: KRAS, p16, p53 and DPC4 [24]. Mutations associated with these genes are constantly detected in most of PCs. However, mutations in around 32 other genes appear to be common in PC, however with a lower frequency. These mutations are aggregated and associated with the same tumor processes and signaling pathways, such as KRAS, TGF-β, WNT, NOTCH and ROBO/SLIT signaling, G1/S transition, SWItch/Sucrose Non-Fermentable complex, chromatin modification, DNA repair and RNA processing [64,68–70]. Overall, the genomic analysis of PC tissues shows different subtypes around the mutational signature of different pancreatic tumors. In terms of cancer therapy, targeting these pathways could be a good therapeutic approach, since some of these mutated genes cannot be targeted, which has been the case of mutated KRAS in the past decades. Due to its particular structure, the design of targeted inhibitors has not been a success [71].

The pancreatic tumors can also be classified according to their chromosomal stability. This feature characterizes four new molecular subtypes of PC: stable, locally rearranged, scattered, and unstable and relies on chromosomal rearrangement phenomenon and genomic aberrations [68,69,72]. The frequency and distribution of chromosomal rearrangements determines this classification. The stable subtype comprises ≤50 structural changes in the genome and is commonly associated with cell cycle and mitosis defects. The locally rearranged subtype is characterized by focal events on 1 or 2 chromosomes, such as focal amplifications or rearrangements. The scattered subtype is the most frequent (36%) and is characterized by the presence of less 200 alterations, while the unstable subtype contemplates between 200 and 558 structural variations [72].

Moreover, the analysis of RNA sequencing data from PC tumor tissue revealed that different genetic expression profiles could be associated with different PC subtypes. Over the years, different authors have contributed with several classifications based on the transcriptomic data from PC tissue. In 2011, *Collisson et al.*, defined three new molecular subtypes: exocrine, classical and quasi-mesenchymal subtypes. This classification revealed three subtypes that have different impacts in the overall survival of PC patients and are characterized by distinct progression rates and therapy responses. The quasi-mesenchymal subtype was associated with the worst prognosis, but it seems to be the most sensitive to the treatment with Gemcitabine, a chemotherapeutic drug frequently used in PC therapy. They also demonstrated different KRAS dependence between the three subtypes, indicating the classical subtype as the most dependent on KRAS function for its maintenance [69,73].

A different classification suggested by *Bailey et al., 2016* revealed four other subtypes of PC named squamous, pancreatic progenitor, immunogenic and aberrantly differentiated endocrine exocrine (ADEX). These are associated with differences in the expression of transcription factors and the correspondent target genes involved in lineage specification and differentiation in PC [70]. The authors indicated that part of their classification overlaps with the subtypes determined by *Collisson et al.* and for that reason they renamed the previous subtypes to better represent the molecular mechanisms according to their analysis. The quasi-mesenchymal corresponds to the squamous subtype, characterized by the expression of genes associated with inflammation, metabolic reprogramming, hypoxia response and TGF-β signaling, which are also involved in other squamous-like cancers. The classical one was called pancreatic progenitor because it is associated with the expression of transcription factors, such as the pancreatic and duodenal homeobox 1 (PDX1), that are crucial for

cell fate determination into the pancreatic lineage. The exocrine subtype was renamed ADEX, which is characterized by an expression profile associated with the pancreatic late development and because it also includes overexpression of genes associated with the differentiation of both exocrine and endocrine cells. However, a novel immunogenic subtype was proposed by *Bailey et al.* This subtype is associated with the expression of a transcriptional network characteristic of several immune cell types, such as B and T immune cells.

Based on the investigation of the RNA sequence data, *Moffitt et al., 2015* also contributed with a new classification for PC. They were able to identify two subtypes of PC based on the stroma gene expression, which they named normal and activated subtypes, being the activated subtype associated with a worst prognosis. This classification raises the important question of stroma contribution in cancer development. They identified expression patterns associated with the stroma, that were not found in tumors cells, and categorized them into two subclasses.

Another approach to PC classification is based on the different metabolic profiles found in PC cells. The metabolome of these tumor cells, that corresponds to the entire group of metabolic products, seem to distinguish different subtypes of P*C. Daemen et al., 2015* suggested a different classification based on these features and suggested the following subtypes: slow proliferating, glycolytic and lipogenic subtypes [75]. The slow proliferating subtype was characterized by low concentration of amino acids and carbohydrates, and increased doubling time. The glycolytic subtype was enriched in components of the glycolytic and serine pathways, whereas the lipogenic subtype seem to be associated with higher levels of lipid metabolites. The different metabolic subtypes are consequently associated with different responses to metabolic inhibitors, which influences the tumor treatment [75].

Some other classifications of PC are being evaluated, such as the subtypes based on different epigenome modifications profiles [76]. The increasing knowledge of PC cancer at the molecular level will improve its classification over the years and contribute to the discovery of novel and specific biomarkers. Ultimately, this information can be used for the design of new therapies and to decomplicate this complex disease.

1.3 Pancreatic cancer treatment

1.3.1 Diagnosis

Patients with PC are commonly asymptomatic in the early stages of cancer development. The location of the pancreas in the organism directly influences the lack of symptoms, and their appearance is usually associated with an already advanced disease [77–79]. The pancreas is located in the retroperitoneum and its close proximity to blood vessels facilitates the cancer propagation through the organism, contributing to the rapid disease dissemination [77,78].

Moreover, also the location of the tumor in the pancreas can influence its late detection. Tumors that develop in the head of the pancreas are commonly associated with more aggressive symptoms, whereas the tumors that develop in the body and tail of the pancreas are frequently diagnosed in late and advanced stages [80]. Around 65% of PC tumors arise in the head of the pancreas [78].

The diagnosis of PC can be made by different methods. The carcinoembryonic antigen (CEA) and the carbohydrate antigens CA 19-9, CA 72-4, CA 50 and CA 242, are biomarkers of pancreatic cancer [81]. Increased CEA levels are associated with a diversity of cancer types (colorectal, lung, breast, and thyroid cancer), but also with pancreatic cancer. They are overexpressed in around 30-60% of pancreatic tumors and seem to be associated with poor prognosis [82]. Currently, only CA 19-9 is recommended for PC diagnosis in the clinic [82], however it holds a low predictive value, with a sensitivity of 70% to 90% and a specificity of 68% to 91% [77]. Overall, finding novel and specific biomarkers for PC remains a challenge in today's research.

Furthermore, other medical techniques are used to PC diagnosis. The endoscopic ultrasound (EUS), the magnetic resonance imaging (MRI), and the magnetic resonance cholangiopancreatography (MRCP) are the most frequent imaging systems utilized [78,83]. These non-invasive techniques allow the detection of pancreatic disease, and posterior classification according to the stage of the tumor.

The options for PC treatment are directly associated with the status of the disease at the time of diagnosis and consequently to the tumor clinical stage. According to *Varadhachary et al., 2006,* four different stages are proposed: Local or resectable, borderline resectable, locally advanced or unresectable and metastatic [84]. This classification is based on the TNM staging system [85], which considers the tumor size (T)

and expansion to nearby tissues, its occurrence in lymph nodes (N) and the presence of metastasis (M) as represented in Figure I.3 [77,84].

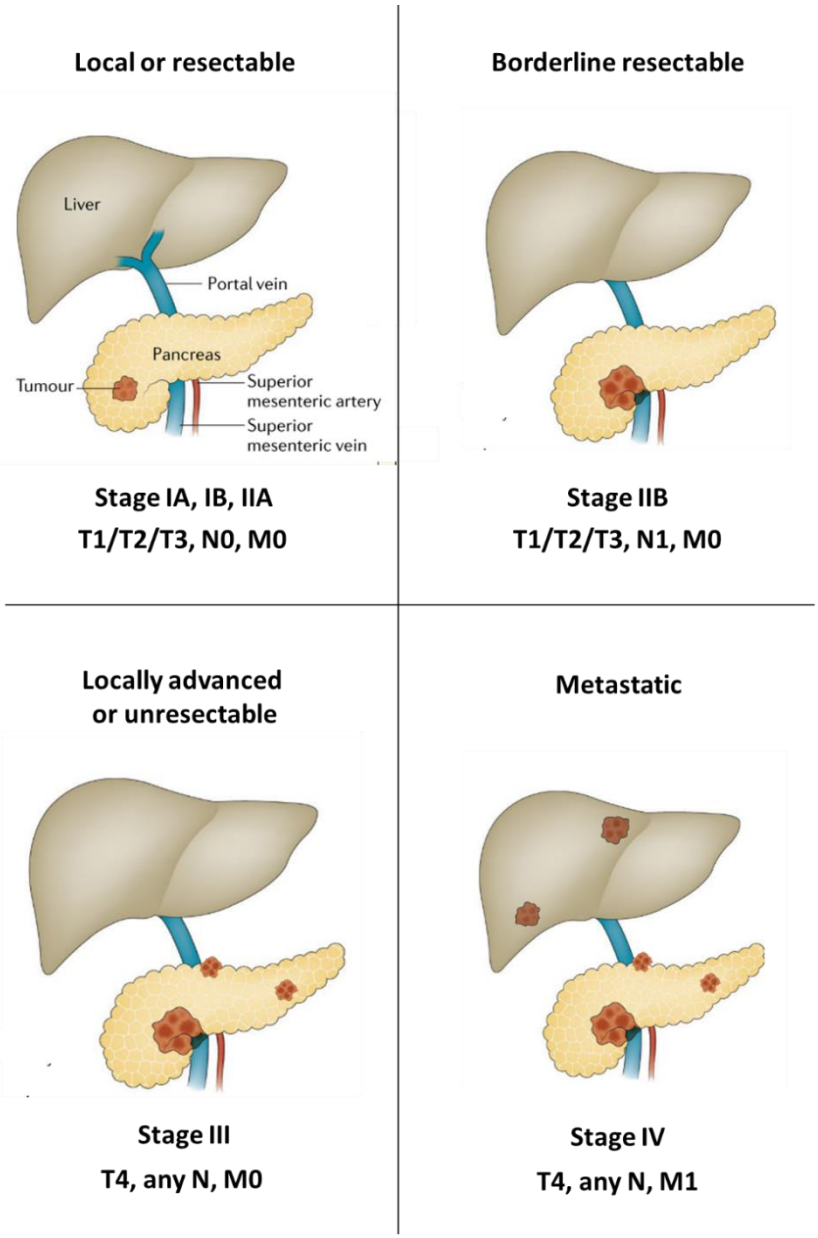

Figure I.3. Different stages and clinical classification of pancreatic cancer. The PC is classified according to the clinical stage at the time of diagnosis into local or resectable, borderline resectable, locally advanced or unresectable, and metastatic. These stages are distinguished according to the TNM staging system, which considers the size and expansion of the tumor at the time of diagnosis (T), the number affected lymph nodes (N) and the presence of metastasis (M). Figure adapted from *Neoptolemos et al., 2018.*

1.3.2 Surgery

The only curative treatment for PC is the tumor resection by surgery [86]. However, the late detection of these type of tumors implies that only around 15% of these patients are suitable for surgery [78].

Over the years, it has been a significant improvement of the surgical techniques used for PC resection, that reflects in the outcome of the patients [87,88]. The most common type of surgeries is the Whipple's procedure or pancreaticoduodenectomy (pancreas head removal), the distal pancreatectomy (pancreas body and tail removal) and the total pancreatectomy (total pancreas removal) [78]. The best surgical option is selected for each case and considering the location of the tumor.

The main goal of the surgery is to achieve a R0 resection, which represents the total resection of the tumor mass, without residual tumor [89]. The R0 classification is associated with a better prognosis and higher survival levels in PC patients [78]. However, this condition is very difficult to achieve, due to the location of the pancreas and the PC severity [80]. Moreover, around 90% of the PC patients that undergo surgery ends up relapsing if no additional therapy was administered [83,88]. For this reason, other therapy approaches are now recommended to improve the outcome of patients with possibly resectable tumors, such as the adjuvant and neo-adjuvant treatment. These treatments are based on chemotherapy, radiotherapy, or chemo-radiotherapy protocols, and seem to improve the patients 5-year overall survival, when comparing with the surgical treatment only [80].

1.3.3 Adjuvant therapy

Due to the bad prognosis still associated with surgical removal of PC, the adjuvant treatment is recommended to improve the survival of these patients, being administered after the surgical procedure. This helps to impair tumor recurrence and improves the patient's prognosis.

The ESPAC-1 clinical trial, in 2001, demonstrated a beneficial role of chemotherapy administration after tumor resection, when compared with the administration of chemoradiotherapy or no further therapy [90]. This study revealed the role

of 5-Fluorouracil (5-FU) in adjuvant therapy and in the improvement of the 5-year overall survival of PC patients, that doubled (10% versus 21%).

However, further studies were performed, such as the CONKO-001 trial, that introduced the role of 2',2'-difluoro-2'-deoxycytidine (Gemcitabine) in the adjuvant treatment. This study demonstrated an improved overall (21% vs 10%) and progression-free survival (13 months vs 7 months) (time without disease evolution) in the patients treated with Gemcitabine when compared with the observation group [91].

From this study on, multiple clinical trials were performed in order to analyze the best adjuvant treatment options for PC [88]. According to the results of these studies, especially the ESPAC-3 trial, Gemcitabine became the preferential adjuvant chemotherapy drug for PC. No differences in the overall survival and progression-free survival were observed comparing Gemcitabine treatment with 5-FU treatment, however Gemcitabine showed lower cytotoxicity when compared with 5-FU treatment [92]. The combination of Gemcitabine and Capecitabine was posteriorly evaluated and compared with Gemcitabine monotherapy. This study showed a beneficial role of the combined therapy, with an improved overall survival (28 months vs 25.5 months) [92].

Two recent clinical trials, NCT0196443 and NCT01526135, aim to evaluate the role of nab-paclitaxel and the role of the 5-fluorouracil, Leucovorin, Irinotecan and Oxaliplatin protocol (modified FOLFIRINOX), respectively. The available results for the study comparing Gemcitabine with Nab-paclitaxel plus Gemcitabine, showed an improved overall survival for the patients treated with the combined therapy [93]. However, there are still no results available for the study with modified FOLFIRINOX therapy and Gemcitabine [94].

1.3.4 Neo-adjuvant therapy

As mentioned in previous sections, most of the PC patients are not suitable for tumor resection at the time of diagnosis. The neo-adjuvant therapy seems to play an advantage role in these patients, allowing the reduction of the primary tumor size and the elimination of micro-metastasis [78,95].

The neo-adjuvant therapy in the treatment of PC patients, especially to the ones presenting borderline or locally advanced tumors, has been studied in the past years [95].

The downstaging of these tumors to resectable improve the prognosis and overall survival of these patients and increase the possibility to achieve a R0 surgical resection [96].

The most effective treatment regimens for neo-adjuvant treatment in PC are Gemcitabine plus Nab-paclitaxel, the FOLFIRINOX protocol and chemo-radiotherapy, mostly combined with Gemcitabine [97]. The ESPAC-5F clinical trial compared the treatment of PC patients with surgery and with different protocols of neo-adjuvant therapy, Gemcitabine plus Capecitabine, FOLFIRINOX and Capecitabine-based chemoradiation. Their results did not show significant differences between the neo-adjuvant protocols in the resection rates but demonstrated improved survival rates in neo-adjuvant therapy compared with surgery alone [98].

Several ongoing clinical trials are being performed to evaluate the best neo-adjuvant treatment protocols for PC patients. A clinical study comparing Gemcitabine plus Nab-paclitaxel and the FOLFIRINOX protocol is being performed in locally advanced PC to evaluate the best suitable chemotherapy protocol for advanced tumor reduction and survival [99].

1.3.5 Palliative treatment

PC patients with advanced or metastatic tumors are frequently qualified for palliative treatment, mostly to reduce disease symptoms and improve their quality of life [100].

The majority of PC patients (around 52%) are diagnosed in an advanced or metastatic stage, due to the late diagnosis of this type of tumors [101]. The first treatment option suggested for metastatic patients was the 5-FU monotherapy. However, the low response rates and the high cytotoxicity of this drug raised the need for improved treatment protocols [96]. In 1997, a clinical trial comparing 5-FU and Gemcitabine monotherapy in advanced PC showed better clinical response to Gemcitabine (24% vs 5%) and improved overall survival (6 months vs 4 months) [102]. Different combination chemotherapy protocols have been evaluated in these patients, however, until 2011, Gemcitabine monotherapy was the gold standard for advanced and metastatic PC [88].

In the same year, a study comparing FOLFIRINOX and Gemcitabine monotherapy in PC metastatic patients revealed better results on the overall survival for the FOLFIRINOX protocol (11 months versus 7 months) [103]. Later, a study comparing

Nab-paclitaxel plus Gemcitabine with Gemcitabine alone revealed a benefit role for the combined therapy in patients overall survival (8.7 months vs 6.6 months) [104]. In line with these results, the current first line treatment protocols for metastatic PC patients are FOLFIRINOX and Nab-paclitaxel plus Gemcitabine [88]. As mentioned before, an ongoing study is being performed to compare both of these regimens [99].

1.4 Gemcitabine

Gemcitabine (2',2'-difluoro-2'-deoxycytidin*;* dFdC) is a chemotherapeutic drug, more specifically a nucleoside analogue, commonly used in the treatment of breast, ovarian, bladder and non-small cell lung cancers [105]. However, it is also very frequent in the therapy regimens for PC treatment. As showed in the previous sections, the administration of Gemcitabine seems to be beneficial in adjuvant, neo-adjuvant, and palliative treatment protocols for PC, improving the overall survival and prognosis of the patients.

1.4.1 Gemcitabine metabolism

As a prodrug, the 2',2'-difluoro-2'-deoxycytidine (dFdC) needs to be metabolized, through different phosphorylation steps, into its triphosphate and active form (dFdCTP). The uptake of dFdC into the cells is mediated by the human nucleoside transporters (hNTs), displayed in the cytoplasmatic membrane. Moreover, the equilibrative and concentrative nucleoside transporters (hENTs and hCNTs) type of hNTs were found to be important in the Gemcitabine uptake, in particular the hENT1, hENT2, hCNT1 and hCNT3 transporters [106]. Therefore, the expression of the nucleoside transporters is critical for Gemcitabine uptake and necessary for its pharmacology activity [107].

After entering the cell, dFdC undergoes post-translational modifications. The deoxycytidine kinase (dCK) is responsible for the first phosphorylation of dFdC into its monophosphate form, dFdCMP. Posteriorly phosphorylation by the pyrimidine nucleoside monophosphate kinase (UMP-CMP kinase) transforms it into the Gemcitabine diphosphate, dFdCDP [105]. However, it has been demonstrated that other enzymes could be also contributing to the second phosphorylation [108]. Furthermore, a third phosphorylation occurs, and Gemcitabine presents its most active form, dFdCTP [107].

1.4.2 Mechanism of action

The principal Gemcitabine mechanism of action is associated with its ability to inhibit the DNA synthesis, acting in the S phase of the cell cycle. Being a nucleoside analogue, the triphosphate and active form, dFdCTP, is able to compete with nucleotides for incorporation into the DNA chain. After its incorporation, a single deoxynucleotide is able to join the chain [109]. This phenomenon prevents DNA polymerases activity, that can no longer proceed with DNA synthesis. Gemcitabine incorporation mimics the chain termination that is masked by the posterior nucleotide addition, which inhibits its exclusion by DNA repair enzymes [109]. By inhibiting DNA synthesis and cell proliferation, Gemcitabine induces cell damage and contributes to the activation of cell death [105].

Moreover, Gemcitabine is recognized by its self-potentiation ability. The deoxycytidylate deaminase (dCTD) is an enzyme directly associated with the inactivation of Gemcitabine. However, it seems that both dFdCDP and dFdCTP metabolites are associated with dCTD inhibition [110]. In fact, dFdCDP seems to bind to the ribonucleotide reductase (RR), which is a crucial enzyme for nucleotides formation [111,112]. This phenomenon interferes with the pool of available nucleotides (dNTPs) for DNA synthesis [110]. Furthermore, the decreased pool of dNTPs also contributes to an increased probability of dFdCTP incorporation and increased cell death [105].

Gemcitabine is also able to directly induce apoptotic signaling, through the activation of the p38 mitogen-activated protein kinase (MAPK). The map kinase kinase isoforms 3 and 6 MKK3/6, an upstream activator of p38-MAPK, seems to be phosphorylated by Gemcitabine, activating an apoptotic signaling pathway [113]. Furthermore, Gemcitabine activates apoptotic and autophagy signaling via the activation of the AMP-activated protein kinase (AMPK)/mammalian target of Rapamycin (mTOR) pathway, which increases the levels of AMPK and decreases mTOR, resulting in cell autophagy [114].

1.5 Therapy resistance

The most frequently methods used for tumors treatment are based on chemotherapy or targeted therapies. However, the success of the chosen therapeutic regimens can be impaired by the tumor resistance to the given drugs. The prevalence of drug resistance limits the effectiveness of these treatments and remains one of the biggest barriers, affecting the patients outcome [115,116].

The resistance to chemotherapeutic drugs can be divided in two different categories: intrinsic and acquired. The intrinsic type of resistance exists before treatment and is caused by pre-existing resistant factors, present in the tumor cells or microenvironment. Conversely, the acquired resistance is developed while the patients are being exposed to the chemotherapeutic drugs, to which the tumor was initially sensitive [112,115]. The acquired therapy resistance is the most concerning because it can silently develop months after the first treatment and reduces further treatment possibilities for these patients.

Thus, there is a constant need to understand how the tumors develop drug resistance and the mechanisms behind the resistant phenotype. This will contribute to the development of new therapies and to improve the treatment regimens, in order to achieve the personalized medicine goal: the best treatment options according to the features of each tumor.

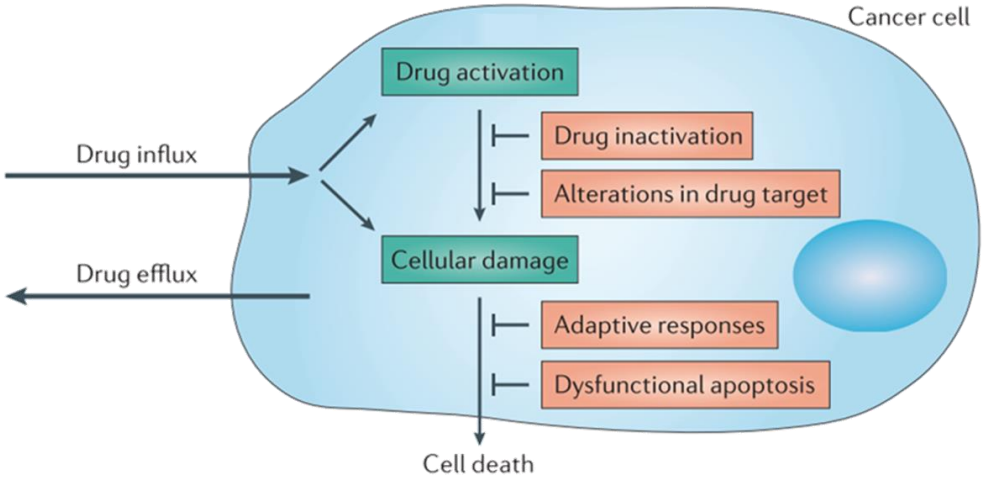

PHARMACOLOGIC CHANGES	CELLULAR DAMAGE	MICROENVIRONMENT
Drug influx and efflux	Aberrant signaling	Tumor heterogeneity
Deregulation of drug metabolism	Secondary mutations	Tumor microenvironment
Release of extracellular vesicles	Amplification of drug target	
	Drug target modification	
	Epigenetic alterations	

Figure I.4. Review of the drug resistance mechanisms in cancer cell lines. The commonly described resistance mechanisms are associated with three different processes: changes in drug metabolism and delivery, cellular and molecular changes, and the microenvironment contribution. Figure adapted from *Holohan et al., 2013*.

1.5.1 Gemcitabine resistance in PC

The mechanisms underlying drug resistance are not yet fully understood. However, that are many reports of a diversity of mechanisms suggested by different authors. Mainly, the described mechanisms are based on genetic, epigenetic or microenvironmental factors [116].

The majority of the patients with PC are probably treated with the chemotherapeutic drug Gemcitabine, in combined or monotherapy. However, even in the clinical trials with the best responses and overall survival results, these patients are characterized by low progression-free survival (PFS) rates. The PFS corresponds to the

period of time after the treatment that a patient lives with the disease, but the disease does not evolve. In the oncology field, PFS is usually measured in months [117].

As previously mentioned in the early sections, around 52% of the PC patients are diagnosed in advanced or metastatic stages [101]. According to the current treatment approaches for PC, the patients in these stages of the disease are frequently indicated for palliate treatment with the FOLFIRINOX protocol or the combined therapy of Nab-paclitaxel plus Gemcitabine. However, if we take a look into the PFS rates of these regimens, we observe a very low life expectancy for the patients.

In the clinical trial NCT00112658, the FOLFIRINOX treatment improves the PFS of PC patients to 6,4 months when compared with the 3,3 months in the Gemcitabine group [103]. Moreover, in the clinical trial NCT00844649, Nab-paclitaxel plus Gemcitabine treatment seem to be associated with 5,5 months of PFS when compared with the 3,3 months for Gemcitabine [104]. Overall, the treatment with Gemcitabine is associated with poor PFS rates and the remaining options for advanced PC treatment are only able to improve it in 2 or 3 months.

The current problematic in PC treatment with Gemcitabine is the development of acquired drug resistance. The patients that initially respond to therapy end up relapsing within months and have a recurrence of the disease, that is usually more aggressive and no longer sensitive to the initial therapy [118,119].

1.5.1.1 Alterations in the Gemcitabine metabolism

Gemcitabine resistance in PC has been associated with the majority of the described mechanisms for other cancer types [115,120]. Alterations in the factors associated with Gemcitabine metabolism and mechanism of action, is one of the mechanisms associated with drug resistance in PC [121]. The downregulation of nucleoside transporters, such as hENT1, hCNT1, hCNT3, crucial for Gemcitabine efflux into the cells, is correlated with the resistant phenotype. In fact, the higher expression of nucleoside transporters is associated with improved overall survival and PFS in PC patients treated with Gemcitabine [122–126]. Moreover, downregulation of the dCK, a rate limiting enzyme in the Gemcitabine metabolism, seems to be a mechanism associated with PC resistance to this drug [127,128]. Increased expression of dCK in Gemcitabine resistant models restores the initial sensitivity to this drug [129–131]

On the contrary, overexpression of the cytidine deaminase (CDA) and the RR enzymes, are associated with higher levels of Gemcitabine inactivation. CDA is responsible for Gemcitabine deamination into the dFdU form, which causes its degradation and inactivation, associated with lower drug effectiveness [132]. The overexpression of the RR enzyme, which is associated with the nucleoside formation, increases the pool of available NTPs, which are direct competitors of Gemcitabine incorporation into the DNA chain. The increased competitions leads to lower Gemcitabine incorporation and consequently drug resistance [133].

1.5.1.2 Drug delivery, and efflux

One of the characteristic features of PC is its complex stroma composition [134]. Around the PC cancer cells is commonly a desmoplastic stroma, composed by fibrous and connective tissue. The PC stroma is very heterogenous and comprises fibroblasts, myofibroblasts, pancreatic stellate cells, immune cells, blood vessels, extracellular matrix (ECM), and soluble proteins [134,135]. Over the years, the microenvironment of PC got the attention of the researchers. The features of the PC tumor stroma, and especially the increased concentration of ECM components, seem to be correlated with a physical barrier to drug delivery [135]. In fact, previous studies have demonstrated that tumors with a rich stroma are associated with low concentrations of Gemcitabine in the tumor cells, when compared with tumors that are poor in stroma [136,137]. Moreover, the high density associated with this microenvironment increases the pressure in the blood vessels, which also difficult blood perfusion and drug delivery [135].

Besides that, changes in the drug influx and efflux in the cells also contributes to different tumor responses to the chemotherapy. The family of ABC transporters, involved in metabolites transport through the membrane, seem to be associated with drug resistance [138,139]. The ABC transporters ABCB4, ABCB11, ABCC1, ABCC3, ABCC5, ABCC10, and ABCG2, are overexpressed in PC and seem to contribute to the poor response to treatment [140]. Furthermore, the overexpression of the breast cancer resistant protein (BCRP), the P- glycoprotein (P-gp) and the multidrug resistance protein (MRP) transporters also play an important role in the PC drug efflux, contributing to low intracellular drug concentrations [120].

1.5.1.3 Epithelial-to-mesenchymal transition (EMT)

The EMT activation have been associated with a diversity of process in oncobiology, such as tumor progression, metastasis, and drug resistance [145,146]. In fact, this process seems to be frequently active in PC and correlated with the Gemcitabine chemoresistance [147–150]. PC cell lines that are resistant to Gemcitabine present higher migration ability and expression profiles associated with the acquired EMT phenotype, such as higher expression of the mesenchymal biomarkers [151–153].

The epithelial-to-mesenchymal transition is a phenotypic change, that can occur in normal physiological processes or in cancer cells. This process is characterized by a switch to a mesenchymal phenotype, associated with morphological, genomic and proteomic changes from the cells [141].

The epithelial cells are characterized by their high adherence to one another and to the culture surface, as well as by presenting cell polarity. The mesenchymal cells differ in the epithelial cells in these two aspects, losing their adhesion and consequently their polarity, which is associated with higher migration ability [142]. The epithelial cells present a square morphology, whereas the mesenchymal cells have an elongated and fibroblastic appearance. Moreover, the expression profiles are specific for each cell type. The epithelial cells are characterized be higher expression of β-catenin and E-cadherin, that forms an important complex in the cell membrane, crucial for cell adhesion [143]. On the other hand, the mesenchymal cells seem to express higher levels of the markers Vimentin, N-cadherin and TGF-β, and the transcription factors Snail, Slug and Twist. These are proteins with important functions in the activation of the mesenchymal features and biomarkers of the EMT activation [142,144].

Furthermore, a recent study demonstrated that the maintenance of this phenotype by drug exposure has been associated the expression of ZEB-1, that when abolished reverts drug resistance [154]. Similar results were verified for the expression of the microRNA (miR)-223. Downregulation of miR-223 restores the sensitivity of Gemcitabine resistant cell lines, by reverting the EMT phenotype [155]. The downregulation of the forkhead box O3 (FOXO3) transcription factor in PC seems also to regulate the EMT activation, which contributes to PC metastasis [156]. Additionally, the expression of the AMPK-related kinase 5 (ARK5) is associated with the activation of EMT and regulates the PC sensitivity to Gemcitabine [157].

1.5.1.4 Cancer Stem Cells (CSCs)

Cancer stem cells (CSCs) are cells that are present in the tumors and show similar features to the normal stem cells. Their self-renewal ability and poor differentiation allow their differentiation into different cell types, according to different stimuli, which contributes to the tumor heterogeneity [158].

The role of CSCs in tumor progression and metastasis has been studied in the past years, however they seem also to be associated with drug resistance mechanisms [158–160]. In fact, populations of CSCs have been found in PC. These cells show expression of stem markers such as CD133, CD184, CD24 and CD44 [161–163]. Moreover, Gemcitabine induced resistant in PC cell lines increases the cancer stem cell markers [152].

The presence of CSCs in PC and the contribution of Gemcitabine treatment to increase their population seem to play an important role for Gemcitabine resistance in this cancer type [164]. Moreover, CSCs are important for tumor recurrence, which associated with an acquired therapy resistance can contribute to the development of a more aggressive tumor [160].

1.5.2 Tribbles in cancer and therapy resistance

The Tribbles family of pseudokinases (TRIB1, TRIB2 and TRIB3) is a family of proteins that regulates mitosis, cell cycle, proliferation, metabolism and differentiation processes [165,166].

The function of these proteins in cancer development and progression has been evaluated in the past years [167]. Their oncogenic role has been shown in different cancer types, such as leukemia, melanoma, pancreatic, ovarian, liver, lung and colorectal cancer [167–173]. However, there is an increasing evidence that these proteins are drivers of drug resistance and can contribute to the poor outcome of the current chemotherapeutic drugs [174].

The Tribbles pseudokinase homolog 2 (TRIB2) is the most relevant protein of the family in the drug resistance field. TRIB2 seems to interact with different signaling pathways, associated with cell survival, proliferation and immune response, such as MAPKK, AKT and NF-kβ signaling [175].

In fact, higher expression of TRIB2 seem to regulate the sensitive to chemotherapy drugs by promoting AKT activation and impairing drug response [176]. Deregulated AKT activation is associated with increased survival signaling, proliferation, migration, and angiogenesis, which contributes to an aggressive tumor behavior [177]. Moreover, TRIB2 contribution in tumor growth is associated with the repression and abrogation of the class O of forkhead box transcription factors (FOXO) [168], downstream effectors of the AKT signaling [178].

A recent study from our group on the characterization of the TRIB2 mediated expression profile showed that TRIB2 is associated with a specific transcriptome. Its overexpression induces the expression of several genes and its pharmacological abrogation reverts sensitivity to anti-cancer treatments [179].

Conversely, another member of the family, TRIB3, seems to play a dubious role in carcinogenesis. Its downregulation has been associated with different cancer types, such as melanoma and endometrial cancer [180–184]. However, some other studies demonstrate an oncogenic role for TRIB3 and associate it with a poor prognosis [185–187].

TRIB3 was found to deregulate the mTORC2/AKT/FOXO signaling pathway [180]. In this case, TRIB3 acts as a tumor suppressor and its genetic inhibition helps tumor progression and proliferation [180]. Moreover, the treatment of lung cancer cells with an anti-cancer compound induces apoptosis through TRIB3/ NF-kβ signaling activation [181]. A similar phenomenon was previously identified in pancreatic cells [188].

However, TRIB3 seem to be highly expressed in endometrial cancer, with an important role in proliferation and apoptosis. The authors present an inconsistent role of TRIB3 in these cells, since its overexpression seem to impair proliferation and migration and induce apoptosis in these cells and suggest further investigation [182]. Furthermore, a study on breast cancer associated the expression of TRIB3 with the poor prognosis in these patients, in response to the hypoxic conditions of this tumor [187].

CHAPTER II

METHODOLOGY

2 Methodology

2.1 Cell culture and maintenance

MIA PaCa-2 and PANC-1 cell lines were a kind gift from Dr. Bruno Sainz (IIBM, CSIC-UAM, Madrid, Spain).

All the cell lines utilized in this study were cultured in Dulbecco's Modified Eagle's Medium with High Glucose, 4 mM L-glutamine and sodium pyruvate (HyClone, GE Healthcare, USA), supplemented with 10% Fetal Bovine Serum (Corning, USA) and 1% of 100X Penicillin Streptomycin (Corning, USA). The medium was changed every 2-3 days and when cells reached ≈ 80% confluence, we reseeded cells, using a 1:5 to 1:8 dilution. The medium was removed, cells were washed 1-2 times with 1X Phosphate Buffered Saline (VWR, USA) and covered with 1X Trypsin solution (Sigma Aldrich, USA) diluted in 1X PBS for 3-5 minutes at 37ºC or room temperature. Trypsin is a protease that allows cells separation, and, for its inactivation, we added supplemented medium when the cells were no longer attached. We collected the cells in suspension into a 15 mL conical tube. In order to remove trypsin from the media we centrifuged the cell suspension at 175,2 g for 4 minutes and removed the medium. We resuspended the cell pellet in fresh supplemented medium and reseeded the cells. Cell lines were cultured in 6 or 10 cm culture dishes (SPL Life Sciences, Korea) and maintained in an incubator at 37ºC and 5% carbon dioxide (CO_2). DMEM, Trypsin Solution and PBS were previously warmed in a 37ºC water bath (Clifton, UK) before used in cell culture.

All the procedures that require a sterilized environment, as cell lines maintenance and solutions preparation for culture use, were performed inside a Class II Laminar Flow Hood (Telstar, UK). We used Ethanol at 70% as a disinfectant solution for all the surfaces and materials and we autoclaved the cell culture materials for sterilization before use.

2.1.1 Cell counting

Whenever a specific number of cells was necessary for plating, we counted cells in a Neubauer Chamber after being dyed with Trypan Blue (Sigma Aldrich, USA), a dye that specifically labels dead cells. A mix of 10 µL of cell suspension and 10 µL of Trypan Blue was prepared and loaded into the Neubauer chamber, covered with a coverslip

(VWR, USA). Cells from the four quadrants (A, B, C, and D) were counted on a Microscope as represented in Figure II.1 and calculated using the Equation II.1.

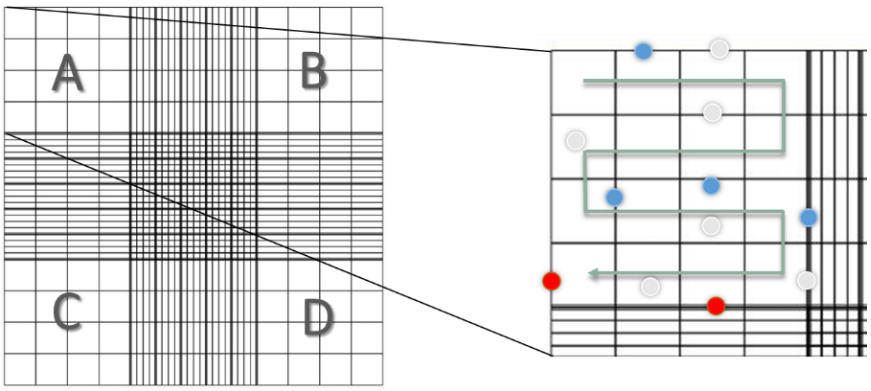

Figure II.6. Representation of the Neubauer Chambers with its four quadrants A, B, C and D. The Neubauer chamber was used to calculate the number of cells in a cell suspension. We counted the cells in four of the nine chambers quadrants. Each quadrant presents 1 mm long and 1 mm wide (1 mm^2 area) and 0,1 mm of depth, which corresponds to 0,1 mm^3 or 10^{-4} mL of quadrant volume. Blue cells represent the non-viablecells, and clear or unstained cells represent the viable cells. We performed the counting from left to right, bottom from top. We did not include the cells in the left and bottom line of the grid, as represented with the red colored cells.

$$Number\ of\ viable\ cells/mL\ = \frac{A + B + C + D}{4} \times 2\ \times 10^4$$

´

Equation II.5. Equation used to calculate the number of viable cells. Cells were resuspended in DMEM after centrifugation and posteriorly diluted 1:2 in Trypan Blue. We used a Neubauer Chamber's covered with a coverslip to calculate the cells in the suspension using a microscope. A, B, C, and D represent the number of cells counted in each of the Neubauer Chamber's four quadrants. The average of these values was calculated. We considered the dilution factor in Trypan Blue (1:2) and the Chamber's total volume, 10^{-4} mL, to the final calculation. The value calculated indicates the number of viable cells per mL of cell suspension.

2.1.2 Cell freezing and thawing

To store and freeze cells when not being used in an experiment, a mix of 90% cell suspension and 10% of Dimethyl sulfoxide (DMSO) (VWR, USA) was prepared and stored in Low Temperature Freezer Vials cryotubes (VWR, USA). For a slow freezing process, we reserved the cryotubes in a Mr. Frosty ® freezing container (Thermo Fisher Scientific, USA) and exposed them to an initial temperature of -80ºC and posterior -150ºC. DMSO acts as a cryoprotectant agent, preventing ice crystals formation and cellular lysis through membrane rupture under low temperatures.

Frozen vials were thawed in a water bath at 37ºC for 30 seconds to 1 minute, and the cells were resuspended and collected to a 15 mL conical tube. We centrifuged the cell suspension at 175,2 g for 4 minutes to pellet cells and removed DMSO residues. Fresh medium was posteriorly added, and the cells resuspended for seeding in a culture dish, already prepared with fresh warm medium.

2.2 Drug-resistant cell lines generation

We generated drug-resistant pancreatic cancer cell lines from the parental pancreatic cell lines MIA Paca-2 and PANC-1. The corresponding derived resistant cell lines, which we named MUTIR28, MUTIR01, and PUTIR23, were generated through cyclic exposure to 2',2'-difluorodeoxycytidine (Gemcitabine) treatments. We let the cells grow in the absence of Gemcitabine for at least 14 days before the experiments. The final cells were maintained without drug exposure and stored at -80ºC. [189–191].

Gemcitabine (LC Laboratories, G-4177) powder was reconstituted at a stock concentration of 10 and 50 mM, using sterile DMSO, and stored in 50 µL aliquots at -80ºC. We kept working dilutions at lower concentrations in DMSO at -20ºC. For direct use in cell culture, we freshly diluted the compound in DMEM at the desired concentration.

Drug treatments were administered to cells in culture at ≈ 50% of confluence for 2-3 days. We used 6 cm culture dishes (SPL, Korea) to maintain cells in culture during the treatment protocol. After treatment, medium was replaced for drug-free fresh medium, allowing cells to grow in normal conditions, recovering their proliferative status. The next Gemcitabine cycle was only administered after a few passages, necessary for cells to overcome drug-induced stress (Figure II.2). We calculated Gemcitabine

concentration for the initial treatment administration upon drug-response assays conducted in MIA PaCa-2 and PANC-1 cell lines (described in the section 2.3.1). We choose a higher concentration than the half maximum inhibitory concentration (IC50) calculated in these assays to select only a few initial cells. In line with this, we started the Gemcitabine treatments at 40nM and sequentially increased the dose at each drug cycle (increasing in 20nM until the 100nM level and in 100nM from then on). Maximum concentration administrated was 1µM for MUTIR28 (MIA PaCa-2 derived cell line), 600nM for MUTIR01 (MIA PaCa-2 derived cell line), and 500nM for PUTIR23 (PANC-1 derived cell line).

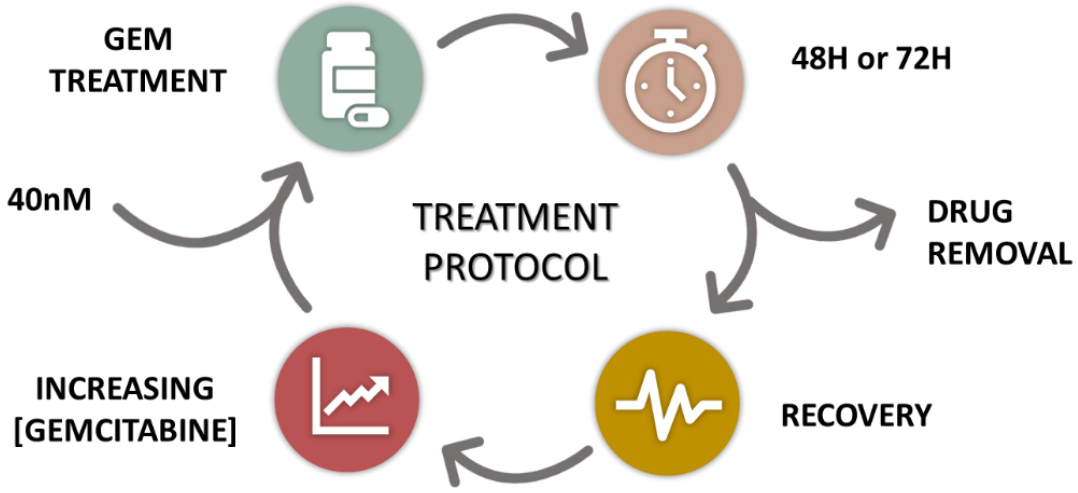

Figure II.7. Schematic representation of the Gemcitabine treatment protocol cycles. We generated the resistant cell lines by exposing the sensitive cell lines to consecutive cycles of Gemcitabine exposure, as represented in the figure. The Gemcitabine concentration to initiate the treatments was chosen regarding the IC50 values previously calculated for both of the parental cell lines, as mentioned above. Aft each Gemcitabine administration, we let the cells incubate for 48 or 72 hours with the drug. Posteriorly, the drug was removed, and we let the remaining cells recover and repopulate the cells. When the cells reach around 50% of confluence, we administered another Gemcitabine cycle, with increasing dosage.

2.3 Thiazolyl Blue Tetrazolium Bromide (MTT) assay

Thiazolyl Blue Tetrazolium Bromide (MTT) assay was used to calculate cell viability and proliferation rate. It consists of a colorimetric assay used to measure cellular metabolic activity. Using MTT assay, we can infer cell viability since only viable cells have the metabolic capacity that is essential for MTT compound conversion into formazan [192,193]. 3-(4,5-dimethylthiazol-2-yl)-2,5-diphenyltetrazolium bromide (MTT) is a yellow-green water-soluble compound that is metabolized by cycling cells into purple formazan, which is insoluble in water, forming purple crystals. The reduction of MTT into formazan is possible due to mitochondrial activity and some cytoplasmatic vesicle's interference, such as endosomes or lysosomes cytosolic enzymes [193–195]. MTT assay is an endpoint assay due to its capacity to quantify a product, in this case, formazan, which is derived from an irreversible reaction.

A 5 mg/mL stock solution of MTT (Alfa Aesar, USA) was prepared in 1X PBS, filtered and aliquoted in 1,5 mL microcentrifuge tubes. Before each experiment, we prepared a working solution of 0,5 mg/mL in fresh DMEM and plated cells on a flat bottom 96-well cell culture microplate (SPL, Korea) for posterior use. Columns 1 and 12 and Line A and H were filled with 100 µL of 1X PBS, avoiding the "edge-effect" of these wells. "Edge-effect" refers to discrepancies in the absorbance reads caused by the well's position in the microplate and not by the biological process in study[196]. During an incubation period of more than 72 hours, DMEM starts to evaporate on the plate edges. Evaporation was also avoided, by following these precautions, since PBS helped to maintain a humid environment.

We maintained cells in culture for at least 48 hours before MTT addition, according to each experimental design's timepoints (see sections X). After this period, we removed the culture media covering the cells and added 100 µL of MTT solution at 0,5 mg/mL. Cells were incubated for 3 hours for MTT metabolization into formazan. After the incubation period, MTT was removed, and formazan crystals were solubilized with 100 µL DMSO. We measured each well's absorbance using the Promega GloMax Plate Reader Luminometer (Promega, USA), at two different wavelengths, 560 and 750 nanometers, since the maximum absorbance by formazan occurs at 550-600 nanometers. The 750 nm wavelength was used as a reference wavelength (> 630 nm) to correct and normalize small differences that can be caused by well variations independent of the reaction[197,198].

The number of cells per well depends on the experimental design and its duration. Accordingly to the literature, the optical density read should be between 0,75 and 1,25,

which represents the linearity window in the absorbance versus the number of cells correlation[197,199]. Accordingly, we optimized all the conditions of our experiments to have these aspects into consideration.

We used cells treated with 0,1% DMSO in DMEM as a positive control for cell viability calculations (100% of cell viability). This control will exclude any cytotoxic or cytostatic effects caused by the solvent and cancel any artifacts that it could generate in the absorbance reads. Additionally, we also included wells with no cells as negative controls (blank wells). Each experimental condition was tested in triplicate.

2.3.1 Gemcitabine dose-response curves for pancreatic cancer cell lines

We assessed Gemcitabine sensitivity/resistance in the parental cell lines (MIA PaCa-2 and PANC-1) and in the generated resistant cell lines (MUTIR28, MUTIR01, and PUTIR23), by exposing them to serial dilutions of this drug and assessing the IC50 values. The IC50 value corresponds to the half of the maximum inhibitory concentration of a drug to a specific cell line, indicating the amount of drug needed to produce half of its maximum effect. In line with this, we used MTT assay to assess the IC50 values of the cell lines in our study.

To evaluate cells' sensibility to Gemcitabine, we plated 2 000 cells per well in a 96-well flat-bottom microplate (SPL, Korea), in a total of 100 µL of DMEM, at day 0 of the experiment. We previously determined the ideal number of cells to a 96-hour duration assay for Mia PaCa-2 and PANC-1 cell lines, considering cell confluence at the end of the experimental time course. Twenty-four hours after cell seeding, we aspirated the medium covering the cells and exposed them to Gemcitabine treatments.

To test a wide range of concentrations, we screened 20 different Gemcitabine concentrations ranging between 0,1nM and 50 µM, with an approximately 2-fold increment (0,1nM; 0,2nM; 0,4nM; 0,8nM; 1,5nM; 3nM; 6nM; 12nM; 25nM; 50nM; 0,1µM; 0,2µM; 0,4µM; 0,8µM; 1,5µM, 3µM; 6µM; 12µM; 25µM and 50µM). Being DMSO a solvent with toxic features to the cells, these must be only exposed to a maximum of 0,1% DMSO concentration to minimize the cytotoxic effects of this compound. Consequently, the maximum concentration possible in our study and, consequently, the maximum dose administrated to the cells, was 50 µM.

After treatments, we performed MTT assays to assess the correspondent cell viability at 48 and 72 hours after drug exposure. The cell's sensitivity to Gemcitabine was posteriorly determined using this data. We calculated the percentage of cell viability for

each condition and represented it as a function of the Gemcitabine concentration administrated. Using the GraphPad Prism7 we further applied a non-linear regression (log(inhibitor) vs. response -- Variable slope) to these results and extrapolated the IC50 values correspondent to each cell line (Equation II.2) [200].

$$\mathrm{Y} = \mathrm{Bottom} + (\mathrm{Top} - \mathrm{Bottom})/(1 + 10\hat{}((\mathrm{LogIC50} - \mathrm{X}) * \mathrm{HillSlope}))$$

Equation II.6. Equation correspondent to the log (inhibitor) vs response non-linear regression used to calculate the IC50 values of the cell lines. The results of the cell viability assays were represented in dose response plots to assess the IC50 values for each cell line. We applied an automatic non-linear regression to the calculated cell viability points and extrapolated the IC50 values (Y). Bottom and Top refers to the plateaus of the maximum and minimal response values and LogIC50 to the Log of the Gemcitabine concentration that causes a response halfway between the two plateaus. Considering that each cell line could behave differently to the Gemcitabine treatments, we chose a model that did not assume a standard slope (1) and considers each plot's hill slope.

2.3.2 Cell viability upon Gemcitabine treatment

To evaluate cell viability upon specific Gemcitabine treatments, we tested the generated cell lines, MUTIR28, MUTIR01 and PUTIR23, and the correspondent parental ones, Mia PaCa-2, and PANC-1, against Gemcitabine.

We plated 2 000 cells at day 0, per well, in a 96-well flat-bottom microplate (SPL, Korea). After 24 hours, Gemcitabine was administrated. For this experiment, we choose the Gemcitabine concentration correspondent to the previously calculated IC50 values for the parental cell lines. For Mia PaCa-2, MUTIR28 and MUTIR01 we used 22nM, and for PANC-1 and PUTIR23 we administered 26nM. We prepared Gemcitabine stock solutions 1000x higher concentrated than the value of interest in DMSO. At the time of drug administration, a working dilution (1:1000) in DMEM was prepared and used in cell culture, guaranteeing the 0,1% as the DMSO maximum concentration. We measured cell viability by adding MTT at 48 and 72 hours after treatment.

2.4 Trypan Blue Exclusion assay

Trypan Blue is a blue dye commonly used in cell culture maintenance and cell viability assays. Its specific proprieties allow it to penetrate through the cytoplasmatic membranes of non-viable cells, labelling their cytoplasm blue. According to this assay principle, viable cells would present intact membranes, that are able to exclude the dye, maintaining their cytoplasm clear [201,202]. Using Trypan Blue Exclusion assay, it is possible to distinguish viable cells from dead cells in a cell suspension, which allows us to quantify cellular dead and infer cell viability [203].

2.4.1 Gemcitabine-induced cell death

Cell lines were plated in a 6-well microplate (SPL, Korea), at a seeding confluence of 80 x 10^3 cells, in supplemented DMEM. Twenty-four hours later, the medium was removed and replaced with DMEM containing 22nM (for Mia PaCa-2 and derived cells) and 26nM (for PANC-1 and derived cells) of Gemcitabine. We previously calculated Gemcitabine IC50 concentrations in section 2.3.1. To evaluate the Gemcitabine-induced cell death levels, we evaluated cell death at 48 and 72 hours of treatment.

After treatment, we collected cells into a 15 mL conical tube. The medium covering the cells was also collected due to the presence of dead cells in suspension. We carefully washed the wells with DMEM and collected most of the cells. Cells were centrifuged at 175,2 g for 4 minutes and resuspended into 100-500 µL of DMEM. We diluted 10 µL of cell suspension (1:2) in 10 µL of Trypan Blue and loaded the mix into a Neubauer Chamber, covered with a coverslip. The number of both death (blue) and viable (unstained, clear) cells were posteriorly counted in a microscope, as represented in section 2.1.1. We calculated the total number of cells by the sum of both dead and alive cells, considering each suspension's final volume, as represented in Equation II.3. The results were analyzed using GraphPad Prism 7.

$$C_{V\ or\ U} = \frac{(N\ \times 2 \times 10^4) \times V}{1000}$$

$$\%\ C_U = \frac{C_U}{C_U + C_V}$$

Equation II.7. Percentage of cell death calculation considering the number of non-viable cells using Trypan Blue Exclusion Assay. We calculated the number of viable (C_V) and non-viable cells (C_U) using the Trypan Blue Exclusion assay and by counting the cells in a microscope. According to this assay principle, blue cells are considered non-viable whereas clear/unstained cells are considered viable. We counted the number of cells in each of the Neubauer chamber four quadrants and calculate the average value (N). We posteriorly multiplied it by the Trypan Blue dilution factor (2) and the total volume of the chamber, 10^{-4} mL, to obtain the number of cells per mL of suspension. Gemcitabine treatments induced cell death and a reduction in the total number of cells. For that reason, we needed to resuspend the cells in different volumes (µL), which we accounted in these calculations (V). We calculated the percentage of cell death ($\%\ C_U$) at each condition, by dividing the number of non-viable cells (C_U) by the total number of cells, which corresponds to the sum of the viable (C_V) and the non-viable cells (C_U).

2.5 Migration ability assay

Migration capacity is a well-recognized cellular ability that occurs in a diversity of basal processes. It is essential for healing and repairing processes, for structure development and organism's evolution [204]. In the Oncobiology field, migration is associated with multiple cancer hallmarks, such as metastasis development and tumor's aggressiveness [205,206].

2.5.1 Wound-healing migration assay

To quantify the cellular migration of the cell lines in our study, we performed wound-healing migration assays. This technique relies on the evaluation of a wound closure over time, after we performed a scratch [207–209].

In a 6-well microplate (SPL, Korea), a specific number of cells was plated per well in order to achieve a 100% confluence 24 hours later. We plated 880 000 cells for MIA PaCa-2 cell line, 2 200 000 cells for MUTIR28, 2 200 000 cells for MUTIR01, 1 100 000 cells for PANC-1 and 1 650 000 cells for PUTIR23. In the present study, we conducted preliminary assays to optimize this condition for all cell lines. We seeded the cells in normal conditions, with DMEM complemented with 10% FBS.

At the 24-hour timepoint, the covering DMEM was removed with a vacuum system's help. Recurring to a 200 µL pipette tip, we made a precisely wound in the cell's monolayer. It is essential to generate a straight vertical wound without scratching the well's surface. The remaining DMEM was then aspirated and replaced by DMEM with only 2% FBS. It is crucial to inhibit cell proliferation after scratch to guarantee that wound closure is only due to cell migration. For migration registration, we took microscopic photographs every 3 hours starting at T = 0 hours (immediately after scratching) and ending at T= 15 hours, using the VisiCam® 5 Plus (VWR, USA) microscopic camera and the Wave Image software, coupled to a microscope. Wound size was posteriorly measured using Wave Image software for each timepoint, and we analyzed data with GraphPad Prism7. We represented the data by the fold change of the wound size at each timepoint regarding the values calculated for T=0. We performed this experiment twice, using all the cell lines simultaneously.

2.6 Western Blot

Western Blot is a protein-based technique that allows the separation of different proteins by their size and molecular weight. From a biological sample, a complex mixture of proteins can be isolated. These are posteriorly separated via electrophoresis and then transferred to a membrane. After this, it is possible to label the proteins of interest with different approaches, using antibodies [210,211]. Using this method, we can evaluate a protein's relative quantity, changes in post-translational modifications and protein-protein interactions.

2.6.1 Biological sample collection

Cells at ≈ 80-90% confluency were collected and centrifuged in a 15 mL canonical tube. Following, we performed two washing steps, by adding 1 mL of cold 1X PBS, we resuspended the pellet resuspension and posterior centrifuged it at 175,2 g for 4 minutes, discarding the supernatant. On the last washing step, after resuspension, we transferred all the volume to a 1,5 mL centrifuge tube, centrifuged again for 30 seconds, and carefully discarded the supernatant. Finally, we stored the cell pellets at -20ºC for posterior use.

2.6.2 Protein extraction

For total protein extraction, we used a Lysis Buffer (Cell Signalling Technology, USA) (1M Tris pH 7.5 (Fisher Scientific, USA), 5M sodium chloride (NaCl) (Merck, Germany), 5% Triton X-100 (Amresco, USA), 1M NaF (VWR, USA), 0.5M ethylenediaminetetraacetic acid (EDTA) (Sigma Aldrich, USA), 0.5M aminopolycarboxylic acid (EGTA) (AppliChem, Germany), 200mM pyrophosphate (Santa Cruz, USA), 1M β-glycerophosphate (b-g-p) (Santa Cruz, USA), 100M OVO4 (Sigma Aldrich, USA), calyculin A (Santa Cruz, USA) and protease inhibitors cocktail (Sigma Aldrich, USA)). This buffer cause membrane disruption and cellular lysis, without protein degradation, allowing to obtain protein extracts. Cell pellets (from 1 or 2 -10 cm plates) were resuspended in 100µL of CST buffer, incubated for 20 minutes at 4ºC, and vortexed every 5 minutes. Next, we centrifuged protein extracts at the maximum speed in a bench centrifuge for 20-minute at 4ºC (VWR, USA), and collected the supernatant into a 1,5 mL centrifuge tube.

2.6.3 Total protein quantification

The amount of protein in each biological sample was normalized for the same final concentration (3µg/µL), so we can compare the results. We used the Bradford assay for protein quantification, a colorimetric assay based on Coomassie Brilliant Blue G-250 dye color change from brown to blue in the presence of protein.

To determine the protein amount in each sample, we prepared a calibration curve recurring to bovine serum albumin (BSA) protein (Thermo Fisher Scientific, USA) at 2mg/mL (stock solution), as represented in Figure II.3. The calibration curve and the samples were tested simultaneously at a 96-well microplate (SPL, Korea), by adding 250 µL of Bradford solution (Alfa Aesar, USA) to each well, followed by a 10-minute incubation at room temperature. We diluted each sample 1:15 and Bradford solution 1:2 in dH_2O before use. Finally, we measured absorbance at 595/600 nm at the GloMax Luminometer (Promega, USA) and calculated each sample's protein concentration using the values from the calibration curve.

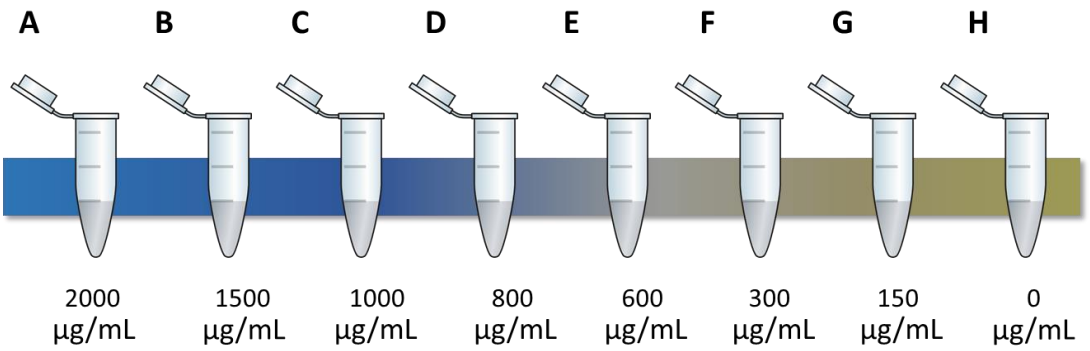

Figure II.8. Calibration curve for protein quantification using the Bradford assay. To quantify the amount of protein in our samples, we performed a calibration curve using BSA at the initial concentration of 2000 µg/mL. We performed serial dilutions of BSA in *dH_2O* to obtain seven different concentrations, as represented in the figure. After the incubation with Bradford reagent, the color range is related to the amount of protein in each sample, as represented in the diagram.

2.6.4 Sample calibration and preparation

We calibrated all samples to the same final concentration with Laemmli Buffer (6x) and CST Lysis Buffer. Laemmli Buffer is constituted by 0.2M Tris HCl pH 6.8 (Sigma Aldrich, USA), 40% glycerol (Sigma Aldrich, USA), 0,4% bromophenol blue (Santa Cruz, USA), 0.3M sodium dodecyl sulfate (SDS) (AppliChem, Germany) and 20% β-mercaptoethanol (Sigma Aldrich, USA). Both SDS and β-mercaptoethanol induce changes in protein conformation. SDS detergent coats the proteins with negative charges, while β-mercaptoethanol disrupts disulfide bonds, denaturing proteins and conferring them a linear conformation. Glycerol confers density to the samples, helping on loading them to the gel, and bromophenol blue is a dye that allows following the run status. After sample's calibration, we denatured proteins through heat exposure at 100ºC for 5 minutes, using a Thermo Shaker (BioSan, Latvia).

Sample calibration and protein denaturation will confer the needed proprieties for the proteins to migrate through the gel when an electric current is applied, from the negative to the positive pole.

2.6.5 SDS - Polyacrylamide gel electrophoresis

SDS-PAGE, or SDS - Polyacrylamide gel electrophoresis, is a technique that allows protein separation through their molecular weight, based on their length, when an electric current is applied. We loaded samples into a polyacrylamide gel, formed by two different elements, a stacking gel, and a running gel. We prepared the stacking gel with 312.5 µL of 1M Tris pH 6.8 (Sigma Aldrich, USA), 312.5 µL of 40% bis-acrylamide (Thermo Fischer Scientific, USA), 2.6 mL of H_2O, 25 µL of 10% sodium dodecyl sulfate (SDS) (AppliChem, Germany), 12.5 µL of 25% ammonium persulfate (APS) (Sigma Aldrich, USA) and 7.5 µL of tetramethylethylenediamine (TEMED) (Santa Cruz, USA). This a low-density gel with large pores for rapid protein migration and is needed to condense samples in a band, to allow all the proteins to start to migrate at the same time. We prepared the running gel at 10%, using 3 mL of 1M Tris pH 6.8 (Sigma Aldrich, USA), 2 mL of 40% bis-acrylamide (Thermo Fischer Scientific, USA), 2.9 mL of H_2O, 80 µL of 10% sodium dodecyl sulfate (SDS) (AppliChem, Germany), 32 µL of 25% ammonium persulfate (APS) (Sigma Aldrich, USA) and 12 µL of tetramethylethylenediamine (TEMED) (Santa Cruz, USA). We choose a 10% gel, according to the proteins we were

studying. APS and TEMED are the reagents in charge of acrylamide polymerization, being TEMED the catalytic component. We used 10-well combs for this experiment.

When the gel polymerized, we loaded 20 µL of each sample on the wells, which corresponded to 60 µg of total protein. We also used3 µL of NZY Blue Protein Marker (NZYTech, Portugal) in every run. The protein marker will serve as a reference for protein weight. The running was performed in an electrophoresis chamber filled with Running Buffer, composed of 1X Tris (Sigma Aldrich, USA), Glycine (Sigma Aldrich, USA), SDS (AppliChem, Germany), and distilled H_2O. Finally, we applied an electric current (initially 75V, and after proteins crossed to the running gel, 150V), during 1h30m, recurring to a power supply (BioRad, USA).

2.6.6 Protein transfer to a PVDF membrane

After SDS-PAGE, we transferred proteins to an Amersham® Hybond 0.2 µm polyvinylidene (PVDF) membrane (GE Healthcare, Germany). These are sensible membranes with a high capacity for protein binding that we activated before use with a methanol bath (VWR, USA). We performed the transference through the Sandwich Method, consisting of assembling two sponges, filter paper, a membrane, and the gel in the correct order to make the proteins transfer. The sandwich was then incorporated into a chamber, filled with Transfer Buffer, constituted by 1X Tris (Sigma Aldrich, USA), Glycine (Sigma Aldrich, USA), 20% Methanol (VWR, USA), and ddH_2O, and covered with ice. An electric charge of 75V was then applied, for 1h30min, recurring to a power supply (BioRad, USA).

2.6.7 Membrane blocking

We sequentially blocked the PVDF membrane with 5% non-fat milk in 1X Tris-Buffer Saline with 0.1% Tween (TBS-T), composed by Tris (Sigma Aldrich, USA), sodium chloride (NaCl) (Merck, Germany), Tween (Merck, Germany) and H_2O. The membrane was incubated in the blocking solution for 1 hour, with agitation, at room temperature. Blocking the membrane will cancel the nonspecific binding of antibodies to proteins in the membrane, guaranteeing that we will only label proteins of interest.

2.6.8 Antibody incubation

To label the proteins of interest, we used specific antibodies against them, as detailed below in Table II.1. Following the blocking step, we washed the membranes three times with 1X TBS-T, for 5 minutes, with agitation at room temperature. Incubation with primary antibodies was performed at 4ºC with agitation for 24h to 48h. After incubation, membranes were washed three times, for 5 minutes, with 1X TBS-T, at room temperature, with agitation. The secondary antibody was freshly prepared in 5% non-fat milk in 1X TBS-T at the recommended concentration. Finally, we incubated the membranes with the secondary antibody for 1 hour, at room temperature, with agitation. While primary antibodies are specifically against the proteins of interest, secondary antibodies will recognize the primary ones while conjugated to horseradish peroxidase enzyme (HRP), necessary for posterior protein revealing and detection.

Table II.3. The antibodies used for Western Blot in the present study. The type (primary or secondary), catalog number, dilution, type of solvent, specie and supplier information are described for each one of the antibodies that we used in the present study.

PROTEIN	ANTIBODY	CATALOG NUMBER	DILUTION	SOLVENT	SPECIE	SUPPLIER
TRIB2	Primary	#13533	1:1000	MILK	Rabbit	Cell Signaling Technology
TRIB3	Primary	ab75846	1:1000	BSA	Rabbit	Abcam
GAPDH	Primary	SC-25778	1:5000	BSA	Rabbit	Santa Cruz Biotechnology
α-Rb (rabbit)	Secondary	NA934V	1:10000	MILK	Donkey	GE Healthcare

2.6.9 Chemiluminescent protein detection

Before protein detection, we rewashed the membranes three times for 5 minutes, with 1X TBS-T. A revealing solution (ECL) containing luminol, the chemiluminescent substrate for the HRP enzyme, was prepared. HRP enzyme will catalyze the oxidation of luminol in the presence of hydrogen peroxide (H_2O_2), which excites the substrate, ending up emitting light.

We prepared ECL in two separated solutions: ECL1, which consists of 250 mM luminol (in DMSO) (Sigma Aldrich, USA), 90 mM p-coumaric acid (in DMSO) (Sigma Aldrich, USA), 1M Tris pH 8.5 (Sigma Aldrich, USA) and H_2O, carefully protected from light, and ECL2, that consists of 30% H_2O_2 (VWR, USA), 1M Tris pH 8.5 (Sigma Aldrich, USA) and H_2O. Both ECL solutions were freshly prepared and mixed by the exact time of use. We incubate membranes in the revealing solution for 5 minutes, with agitation, and the light signaling was detected and analyzed by ChemiDoc XRS+ System (BioRad, USA) and the ImageLab software.

2.7 Real-time quantitative polymerase chain reaction

Real-time quantitative polymerase chain reaction (RT-qPCR) is a molecular biology technique used to detect specific mRNA molecules, allowing gene expression evaluation. From RNA molecules, cDNA is synthesized and posteriorly amplified, which makes this a very sensitive technique. It makes possible to detect a specific mRNA, even if only a few molecules are present in the study sample. The addition of a fluorescent dye to the cDNA molecules during the reaction allows monitoring PCR product accumulation. Over time, the emitted fluorescent is measured, making this technique a quantitative method. Thereby, using RT-qPCR, we can identify different gene expression profiles in biological samples and monitor variations in a specific target's expression.

2.7.1 Sample collection

Pancreatic cell lines MIA Paca-2, PANC-1, and the correspondent generated cells were submitted to RNA extraction and posterior RT-qPCR analysis. We collected cells from 10 cm plates at ≈80-90% confluence. After collection, we performed two washing steps with 1X PBS, separated by one centrifugation at 175,2 g for 4 minutes. Pellets were stored in 1,5 mL centrifuge tubes at -20ºC for posterior use.

2.7.2 RNA extraction and purification

RNA is a very sensitive and highly degradable molecule. Because of its instability, all the following procedures were carefully executed, always attending to the necessary cleaning needs. We used 70% ethanol and RNAse cleaner (NZYTech, USA) for surfaces and material frequent cleaning.

We performed the RNA extraction from all samples using the E.Z.N.A. TOTAL RNA KIT I (OMEGA Bio-Tek, USA), following the manufacturer's protocol and instructions. Cell pellets that we previously stored at -20ºC were utilized. We also performed an additional on-membrane DNase treatment following the On-Column PureLink® DNase Treatment Protocol (Invitrogen, USA) to guarantee higher quality and pure RNA extraction.

Total RNA concentration (in µg/ µL) and quality were analyzed using the NanoDrop™ 2000/c Spectrophotometer (ThermoScientific, USA). The ratio between absorbances measured at 260 and 280 nm (A260/A280) is frequently used to determine protein contamination in RNA samples since it absorbs at 280 nm. To a considerable pure RNA, this ratio should be approximately 2. Moreover, to access other types of contamination with organic compounds or extraction residues, the ratio A260/A230 is analyzed. Values between 2 and 2,2 are representative of RNA purity. We stored RNA samples at -80ºC for posterior use.

2.7.3 cDNA synthesis

Complementary DNA (cDNA) was synthesized from previously stored RNA samples using the NZY First-Strand cDNA Synthesis Kit (NZYTech, Portugal), and following manufacturer protocol and instructions were followed. For cDNA synthesis, we transformed 2 µg of RNA into approximately 2 µg of cDNA. Finally, we stored the PCR product at -20ºC.

We prepared a mix containing 10 µL of NZYRT 2X Master Mix, 2 µL of NZYRT Enzyme Mix, and the RNA template for each sample. We used diethylpyrocarbonate (DEPC)-treated H_2O to perform a final reaction volume of 20 µL, at 0.2 mL PCR tubes. According to the manufacturer's instructions, NZYRT 2X Master Mix already contains the primers, deoxyribose nucleoside triphosphate molecules (dNTPs), magnesium chloride ($MgCl_2$), and an already optimized buffer. Similarly, the NZYRT Enzyme Mix contains all the enzymes needed for the following reactions, such as the reverse transcriptase (RNAse H minus) and the NZY Ribonuclease Inhibitor, which cancels any RNA degradation from ribonucleases action.

Samples were posteriorly subjected to thermal incubation periods using the C1000 Touch Thermal Cycler (BioRad, USA). cDNA synthesis is characterized by three different phases, delimited in the PCR by temperature variations. The first phase consists of primer annealing to the single-stranded RNA template. For this annealing, we performed an initial 10-minute incubation at 25ºC. The second phase is characterized by chain extension, from the previous annealed primers, with a reverse transcriptase (RT) enzyme. We applied a temperature increase to achieve an optimal reaction temperature for the RT enzyme, in this case, 50ºC, during 30 minutes of incubation. Finally, after cDNA elongation, RT reaction needed to be stopped by A 5-minute incubation at 85ºC. Moreover, 1 µL of NZY RNase H was added in the final step of PCR, followed by incubation at 37ºC for 20 minutes. RNase H will remove any remaining RNA fragments and their bond to DNA, allowing an increase in qPCR sensitivity.

2.7.4 Quantitative Real-Time Polymerase Chain Reaction (qPCR)

qPCR is a technique that allows product reaction quantification. Through a PCR reaction, cDNA molecules previously generated were used as a template, while a fluorescent dye is incorporated into the newly synthesized DNA molecules. Using specific primers for the genes of interest, these sequences' presence or absence can be detected and quantified.

Besides the genes of interest, described in Table II.2, we also evaluated a housekeeping gene expression. Housekeeping genes are conserved regions of the genome, with constant expression at all cells. They are frequently used as reference genes to normalize other's expression, canceling any variations that are not driven from the biological process in study. In the present study, we used glyceraldehyde 3-phosphate dehydrogenase (GAPDH) as the reference gene.

Experimental design for each qPCR was previously prepared, always attending to the number of samples and genes we analyzed. We prepared a Mix containing both primers, forward and reverse, Power Up SYBR® Green Master Mix (Applied Biosystems, USA), and DEPC-treated H2O for each gene. Forward and Reverse primers were previously designed for each target, recurring to the Primer3 Input (v.0.4.0) software. Power Up SYBR® Green Master Mix already contains all the necessary reagents for the PCR reaction, as well as the fluorescent dye SYBR® Green. While reaction occurs, SYBR® Green is incorporated into the newly synthesized double-stranded DNA, emitting fluorescence when excited by a light beam. During qPCR protocol, this fluorescence is accumulated and measured at the end of each cycle. As a result, the amount of fluorescence quantified at each PCR cycle is proportional to the amount of the target molecules produced. We performed a 1:10 dilution of the template cDNA before use. The total reaction volume was 10 µL, and we performed it at a 384-well PCR plate. We also included no-template controls as negative controls of the reaction.

Table II.4. The primers used for RT-qPCR analysis. The primers sequence (from 5' to 3'), direction (Forward or Reverse), size (as base pairs) and supplier, are described for each one of the genes analyzed in the present study.

GENE	FW/RV	SEQUENCE 5' → 3'	SIZE (BP)	SUPPLIER
B-catenin	FW	GACCACAAGCAGAGTGCTGA	20	Eurofins
	RV	TGCAGCATCTGAAAGATTCCT	21	Eurofins
Slug	FW	CCTTCCTGGTCAAGAAGCAT	20	Eurofins
	RV	CACAGTGATGGGGCTGTATG	20	Eurofins
Snail	FW	GAAAGGCCTTCAACTGCAAA	20	Eurofins
	RV	CAGTGGGGACAGGAGAAGG	19	Eurofins
Vimentin	FW	CCTTGAACGCAAAGTGGAAT	20	Eurofins
	RV	TTGGCAGCCACACTTTCATA	20	Eurofins
ZEB-1	FW	GCACCTGAAGAGGACCAGAG	20	Eurofins
	RV	GTGTAACTGCACAGGGAGCA	20	Eurofins
TRIB1	FW	ATCGCCGACTACCTGCTG	18	Eurofins
	RV	GTAATGTTGCTGTGCGATGG	20	Eurofins
TRIB2	FW	GACTCCGAACTTGTCGCATT	20	Eurofins
	RV	ATGAGCAGACAGGCAAAAGC	20	Eurofins
TRIB3	FW	TGCCCTACAGGCACTGAGTA	20	Eurofins
	RV	GTCCGAGTGAAAAAGGCGTA	20	Eurofins
GAPDH	FW	CAATGACCCCTTCATTGACC	20	Eurofins
	RV	TTGATTTTGGAGGGATCTCG	20	Eurofins

The qPCR reaction protocol consisted of an initial enzyme activation phase, constituted by a 50ºC incubation for 2 minutes, to uracil-DNA glycosylase (UDG) activation, which prevents DNA mutagenesis through uracil removal, and a 95ºC 2-minute period for Dual-Lock DNA polymerase initiation. Next, DNA was denatured for 15 seconds at 95ºC, followed by 40 cycles of primer annealing at 58ºC for 15 seconds and chain extension at 72ºC for 1 minute. The annealing temperature should consider the melting point of primers in use. We also performed dissociation curves for melting temperature calculation during each qPCR to analyze primer specificity and primer dimer formation. As the temperature rises, double-stranded DNA starts to dissociate, releasing

fluorescent dye, representing a decrease in the emitted fluorescence. When half of the DNA dissociates, we achieved the melting temperature.

During qPCR reaction and cycle progression, variations in fluorescence are reported, through a sigmoidal amplification curve, composed of 3 phases, an initial linear phase, a log phase, and a plateau phase. The threshold is then automatically calculated by the software in use and represents a baseline for background fluorescence. The Ct (cycle threshold) value for each amplification curve is also calculated and represents the number of cycles necessary for the fluorescence to cross the threshold.

The instrument used for this technique was the CFX384 Touch Real-Time PCR Detection System (BioRad, USA), being the results analyzed with the CFX Maestro Software (BioRad, USA). We tested all samples in triplicate and used the relative gene expression quantification to compare various genes' expression levels between different samples. GAPDH was used as a reference gene to normalize gene expression. Besides that, we also chose a control sample, depending on the experimental design. The ratio between Ct_{TARGET} and Ct_{GAPDH} was calculated for both control and test samples, as represented in Equation II.4, allowing fold change calculation between both of them. These results were analyzed using GraphPad Prism7 and represented as a fold change of the mRNA levels comparing with the control cell line.

$$\Delta Ct\ (control) = Ct\ (target) - Ct\ (GAPDH)$$

$$\Delta Ct\ (test\ sample) = Ct\ (target) - Ct\ (GAPDH)$$

$$\Delta\Delta Ct = \Delta Ct\ (control) - \Delta Ct\ (test\ sample)$$

$$Fold\ Change = 2^{-\Delta\Delta Ct}$$

Equation II.8. Fold change of gene expression calculation. RT-qPCR results for gene expression evaluation were analyzed considering the gene expression of a control cell line. For both the control and the test samples, we normalized the Ct values correspondent to a specific gene amplification (ΔCt) against the Ct values obtained for a reference gene (GAPDH). To accomplish that, we performed the ratio between the Ct value for our target gene and the Ct value for the reference gene, for both our control and test samples. Moreover, we normalized the ΔCt of our test sample to the ΔCt of our control and calculate the ΔΔCt. ΔΔCt value represents the change in the expression of our target gene between our test sample and our control cell line. To represent the results in fold change, we calculated the $2^{-\Delta\Delta Ct}$, which represents the normalized expression ratio.

CHAPTER III

RESULTS

3 Results

The aim of our study was to generate and characterize Gemcitabine-resistant pancreatic cell lines to study resistance mechanisms in pancreatic cancer. A resistant cell line is characterized by a fold change of at least 2 times in its IC50 value, when comparing to the parental cell line. According to *McDermott et al., 2014*, a clinically relevant resistance model should present an IC50 fold change of 2 to 5, based on their evaluation of patients samples before and after chemotherapy. However, the establishment and characterization of drug-resistant cell lines is a long term and time-consuming process. For this reason, we divided our work in different phases, as represented in Figure III.1.

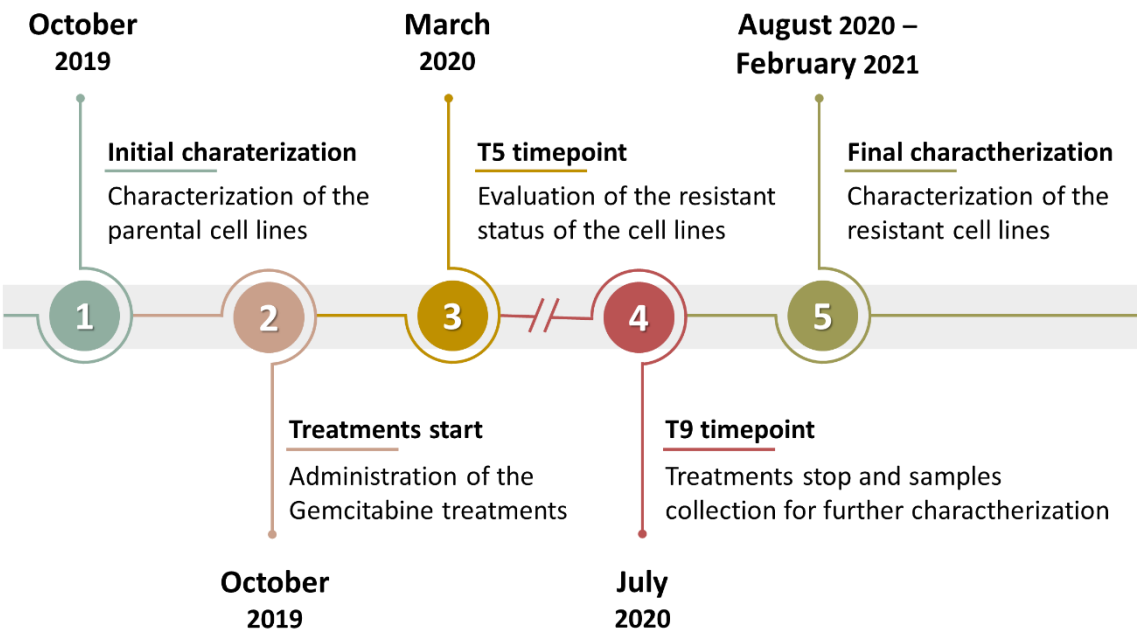

Figure III.1. Diagram representation of our project timeline. In the beginning of our project started by the characterization of the parental cell lines, MIA PaCa-2 and PANC-1 (1). After we analyze their IC50 values for Gemcitabine, we started the treatment protocols (2). Five months after the first treatment (T5), we analyzed the resistance levels of the newly generated cell lines, to evaluate the success of the chosen resistance protocol (3). Due to adverse reasons we needed to stop the treatments for around 2 and a half months, however we restarted them in June and stopped the protocol in July of 2020 (represented by the two parallel red lines). At this moment, T9, we collected the final cells for further experiments (4). We performed the characterization of the newly generated cell lines in the following months (5).

We started by analyzing the sensitivity of the established PC cell lines (MIA PaCa-2 and PANC-1) to Gemcitabine. This data allowed us to determine the ideal concentration to initiate the treatment protocol. To evaluate the success of the protocol, we characterized the generated cell lines in two different moments, T5 and T9, which corresponds to 5 and 9 months after treatment initiation, respectively.

We generated two different cell lines for MIA PaCa-2 and two other cell lines for PANC-1. MUTIR28 and MUTIR01 cell lines are MIA PaCa-2 derived cell lines. PUTIR23 is the only cell line successfully generated from PANC-1, since PUTIR27 did not tolerate drug treatments and died in the process.

3.1 Pancreatic cell lines sensitivity to Gemcitabine

To evaluate the sensitivity of the pancreatic cell lines (MIA PaCa-2 and PANC-1), Gemcitabine, a chemotherapeutic drug used in first-line treatment of PC, we performed MTT assays. The data obtained from these assays allowed us to perform a dose-response curve for each cell line. We represented the decrease in the percentage of cell viability as an effect of the drug concentration (dose-response), represented as logarithm (log_2 drug concentration). This allowed us to calculate the half maximum inhibitory concentration (IC50) of Gemcitabine.

Comparing the dose-response curves, the IC50 was 22nM and 26nM of Gemcitabine for MIA PaCa-2 and PANC-1 cell lines, respectively, at 72 hours of treatments (Figure III.2. A and B). This indicates that the PANC-1 cell line is less sensitive to drug treatment than MIA PaCa-2 cell line. Moreover, we saw differences in the maximum Gemcitabine effect for both cell lines. At the highest concentration, 50 µM of Gemcitabine, 21% of the MIA PaCa-2 cells were viable (Figure III.2 A), compared to approximately 37% of the PANC-1 cells (Figure III.2 B).

To conclude, the parental cell lines, MIA PaCa-2 and PANC-1 showed similar IC50 values for Gemcitabine, in the nanomolar range. However, at the highest Gemcitabine concentration, MIA PaCa-2 presented lower cell viability levels when compared to PANC-1 cell line.

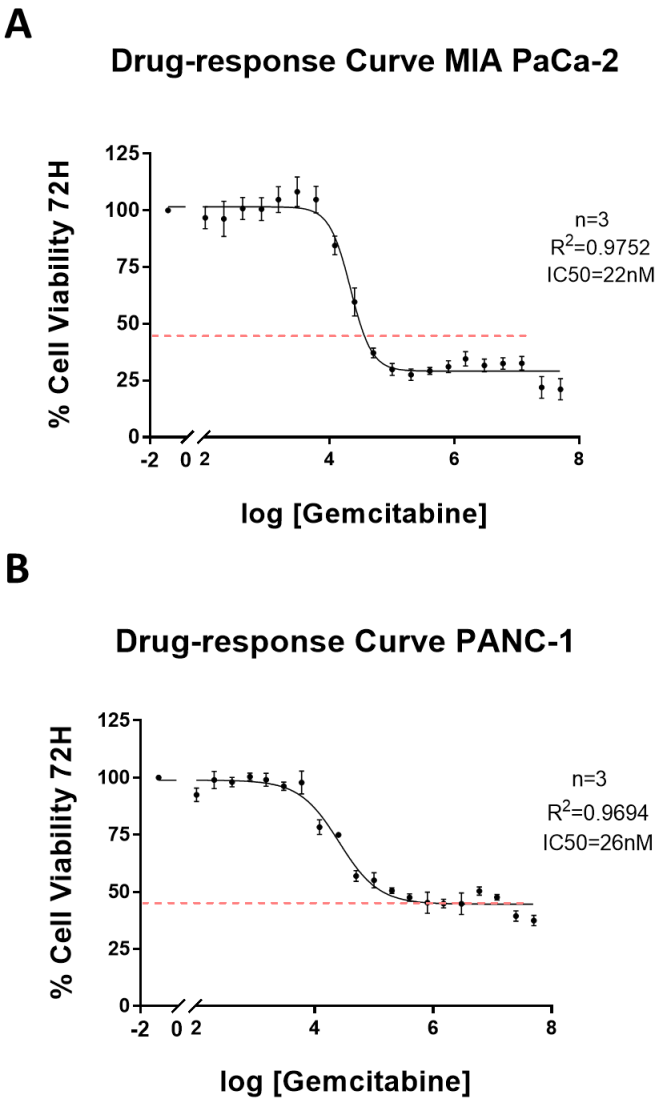

Figure III.2. Drug-response curves for MIA PaCa-2 and PANC-1 cell lines, after 72 hours Gemcitabine treatments. MIA PaCa-2 and PANC-1 were exposed to 0,0001 – 50 µM Gemcitabine for 72 hours. Drug-response curves for MIA PaCa-2 (**A**) and PANC-1 (**B**) cell lines were generated using viability values determined by MTT. The MTT assay display the cell viability of each cell line when the cells are treated with different Gemcitabine concentrations, when compared with de DMSO-treated controls (100% of cell viability). Experiments were performed in triplicate and the represented data is the mean ± SEM, with n=3. Non-linear fitting curves were achieved using the log(inhibitor) vs. response -- variable slope (four parameters) function. Dashed red line indicates the threshold of 50% of cell viability.

3.2 Generation of Gemcitabine-resistant cell lines

In order to further understand the mechanisms underlying Gemcitabine resistance in pancreatic cancer, we generated drug-resistant cell lines. This enabled us to characterize the resistant cell lines and uncover molecular signatures, responsible for this resistance.

To generate drug-resistant cell lines, we chronically exposed MIA PaCa-2 and PANC-1 cell lines to Gemcitabine, in consecutive cycles of drug exposure and recovery (Figure II.2). The cell lines generated were named MUTIR28 (MIA PaCa-2 derived cell line), MUTIR01 (MIA PaCa-2 derived cell line), and PUTIR23 (PANC-1 derived cell line). In order to minimize effect of passage number, we subjected the parental cell lines (MIA PaCa-2 and PANC-1) to the same passages as the drug treated cell lines.

Resistant cells can be achieved using different protocols. To assess if the protocol we used, generated resistant paired isogenic cell lines according to the definition provided above, we re-analyzed sensitivity to Gemcitabine at two different moments, T5 and T9 (5 and 9 months after first Gemcitabine exposure).

3.2.1 New emerging phenotypes of MUTIR28 and MUTIR01 cell lines

During the generation of the resistant cell lines, we were confronted with a phenotypic switch from the MIA PaCa-2 derived cell lines, that were being exposed to the chemotherapy drug. We only observed this phenomenon for MUTIR28 and MUTIR01 cell lines while PANC-1 and PUTIR23 failed to significantly change phenotype during the process. As represented in Figure III.3, we noticed the phenotypic changes after 2 months of treatments initiation.

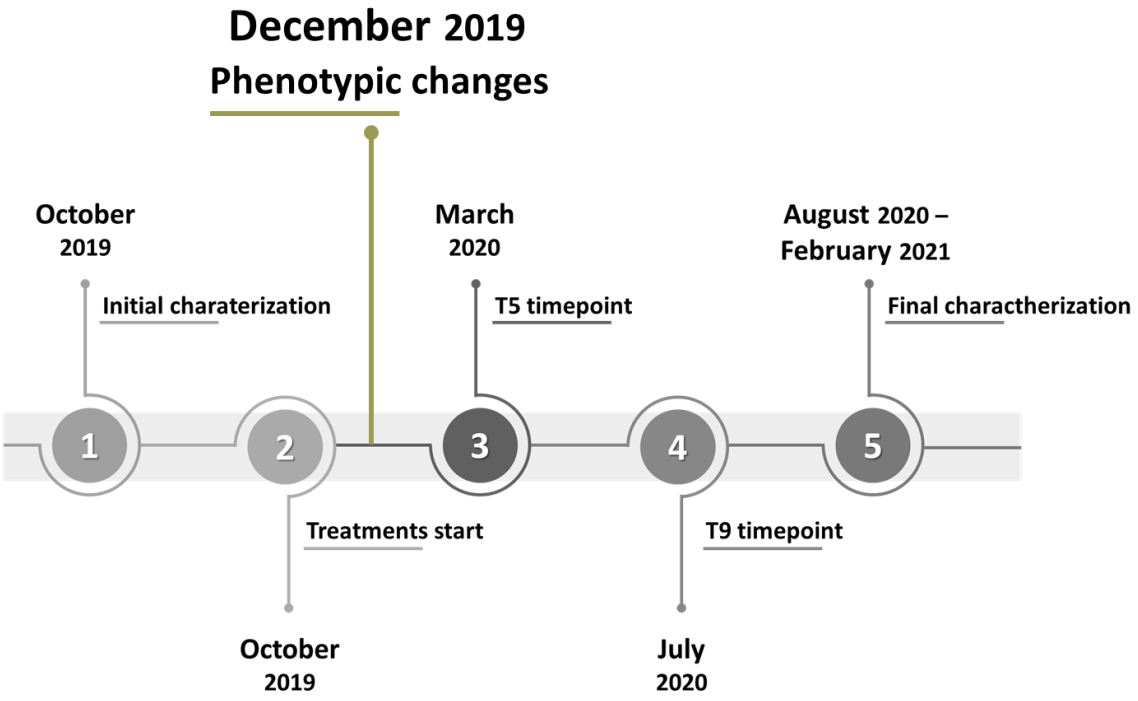

Figure III.3. Representation of the project timeline, emphasizing the moment when the new phenotypes emerge. As represented in the diagram, 2 months after we start the treatment protocol, we observed new emerging phenotypes from the cells that were being exposed to Gemcitabine. Only MIA PaCa-2 derived cell lines showed this phenotypic switch.

As we observed, the parental cell line, MIA PaCa-2, presented an initial epithelial phenotype (Figure III.4A). However, after 2 months of Gemcitabine treatments, MUTIR28 and MUTIR01 changed their phenotype. When the cells were under Gemcitabine treatment, they were under stress and showed an elongated cytoplasm (Figure III.4B). However, after 48 or 72 hours of treatment, we removed the drug and the cells changed to a rounder phenotype keeping in suspension while viable, as represented in Figure III.4C. Interestingly, it took around 5 days for these cells to attach to the plate, instead of a few hours as parental MIA Pa-Ca cells (Figure III.4D). Surprisingly, when the cells attached to the plate, they presented a mesenchymal and fibroblastic-like phenotype in contrast to the original epithelial appearance (Figure III.4D). As represented in Figure III.4, we named each phenotype differently. DR refers to the cells with drug, ROU refers to the cells with the rounder phenotype (observed after drug removal) and FUS refers to the fusiform phenotype when the cells attach to the plate (after being in suspension). MUTIR28 and MUTIR01 represents the phenotype of the resistant cells in basal conditions.

To evaluate if this new phenotype was stable over time, we let some of these cells without drug exposure for six weeks. After this period of time, the cells recover their original phenotype, as represented in Figure III.4E.

In summary, we observed that the Gemcitabine treatments induced phenotypic changes in these cell lines, that switch from an epithelial to a fibroblastic-like phenotype. However, this switch was reversible over time in the absence of the drug suggesting that the changes were not based on stable alterations in the genome of these cells.

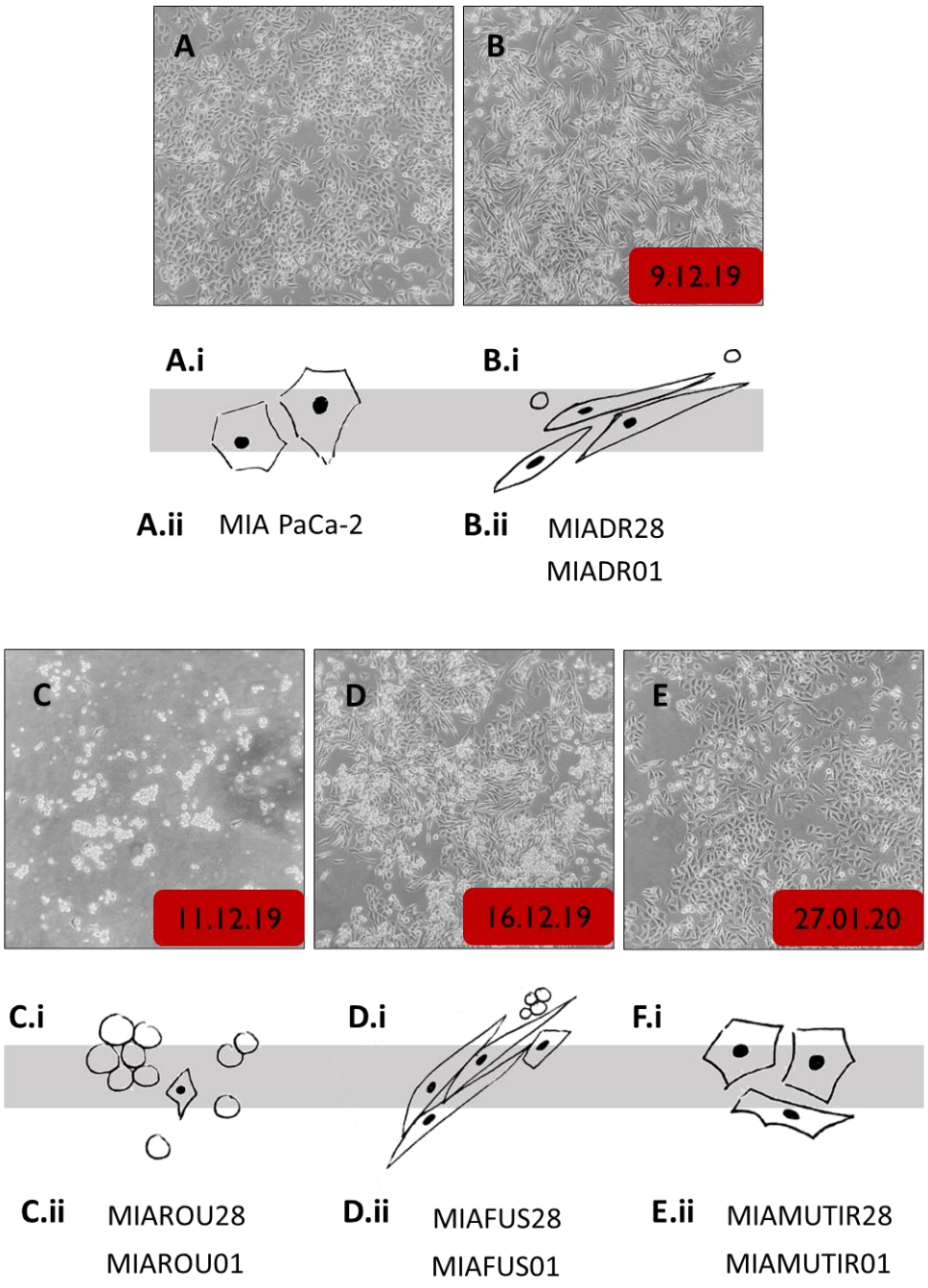

Figure III.4. Representation of the phenotypic switch observed in the MIA PaCa-2 derived cell lines. **A)** Original Mia PaCa-2 cell line epithelial phenotype; **B)** The phenotype that both of the resistant cell lines presented under Gemcitabine treatment (MIADR); **C)** After drug removal, the cells switch to a rounder phenotype and were in suspension (MIAROU); **D)** The cells attach to the culture dish only after 5 days and showing a mesenchymal like phenotype (MIAFUS); **E)** The cells grew in drug absence for 6 weeks and revert their phenotype to the original epithelial appearance. We named each one of the new emerging phenotypes and collected samples for future experiments. In the red boxes, we included the date of the first time that we observed each one of the phenotypes, for a better understanding of the timeline. In the grey bar we represented each phenotype schematically. **A.i, B.i, C.i, D.i, E.i** are schematic representations of the phenotypes. **A.ii, B.ii, C.ii, D.ii, E.ii** correspond to the names of each phenotype.

3.2.2 Different morphology of the PUTIR23 cell line

The PANC-1 derived cell line, PUTIR23 did not showed a phenotypic switch as we observed for the MIA PaCa-2 derived cell lines. However, after two cycles of Gemcitabine treatment, we noticed that these cells took longer to recover from each Gemcitabine administration. Moreover, after drug removal, PUTIR23 cells showed an enlarge size, with cytoplasmatic extensions, features that are not present in the PANC-1 cell line, as represented in Figure III.5. Furthermore, this morphology is reversible with the cells reverting it after recover.

In conclusion, PUTIR23 cells did not undergo a phenotypic switch under Gemcitabine treatment but changed their morphology in response to this stimulus from a quadrangular to a circular shape with cytoplasmatic extensions.

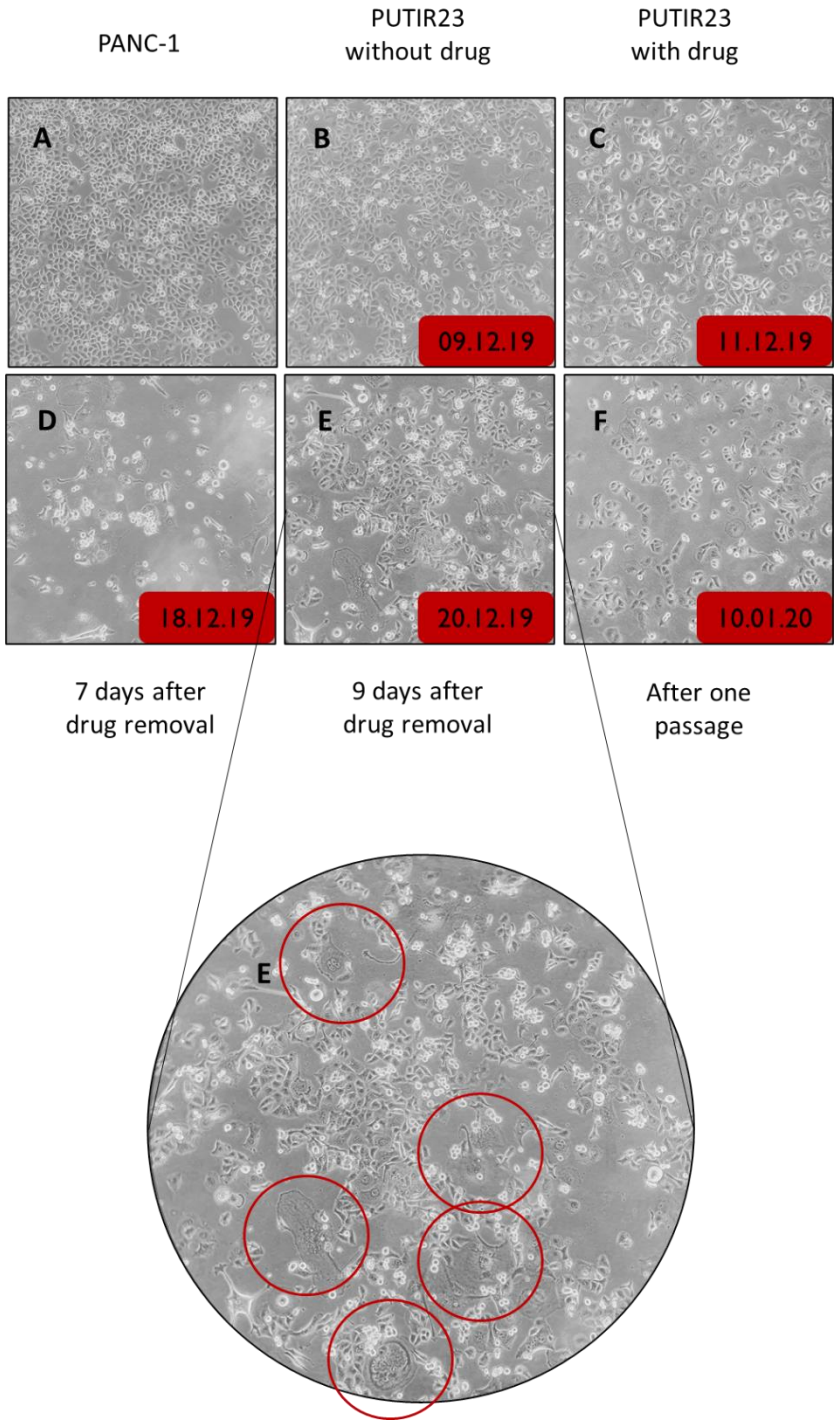

Figure III.5. Representation of the morphologic changes in the PUTIR23 cell line after Gemcitabine administration. A) PANC-1 original phenotype; B) PUTIR23 cell line appearance in normal conditions; C) When we exposed PUTIR23 cell lines to Gemcitabine, the cells show a stressed morphology; D) After 7 days of drug removal, the cells start to show extensions of their cytoplasm; E) After 9 days of drug removal, we observed the frequent appearance of enlarge cells, with large cytoplasm and protuberances; A bigger plan of these cells in culture is showed in the big circle. F) When the cells reach around 80% of confluence, we reseed them and observed a recover of the initial phenotype. Red circles indicate the location of the cells with different morphology. In the red boxes, we included the date of the first time that we observed each one of the phenotypes, for a better understanding of the timeline.

3.2.3 IC50 determination of the Gemcitabine-resistant cell lines at T5

For this experiment, we used MIA PaCa-2 and the derived resistant cell lines, MUTIR28 and MUTIR01. We observed an increase in the IC50 values of MUTIR28 and MUTIR01 upon Gemcitabine treatment when compared to MIA PaCa-2 parental cell line. In this experiment, the IC50 of the MIA PaCa-2 cell line was 18Nm (Figure III.6A). This result corroborates the IC50 value of 22nM previously obtained (Figure III.2A). The IC50 values calculated for MUTIR28 and MUTIR01 cell lines were 54nM and 37nM, respectively (Figure III.6A). This represents a two-fold increase of the IC50 values for MUTIR01 and a three-fold increment for MUTIR28, when compared to MIA PaCa-2 cell line (Figure III.6B). At 50 µM of Gemcitabine, the maximum dose administered, the cell viability was 35% on MUTIR28 and 30% on MUTIR01, which represents a two-fold increment when compared with the 15% for MIA PaCa-2 cell line.

In conclusion, the cell lines that were being exposed to consecutive cycles of Gemcitabine exposure, MUTIR28 and MUTIR01, showed increased IC50 values when compared with the sensitive parental cell line, MIA PaCa-2.

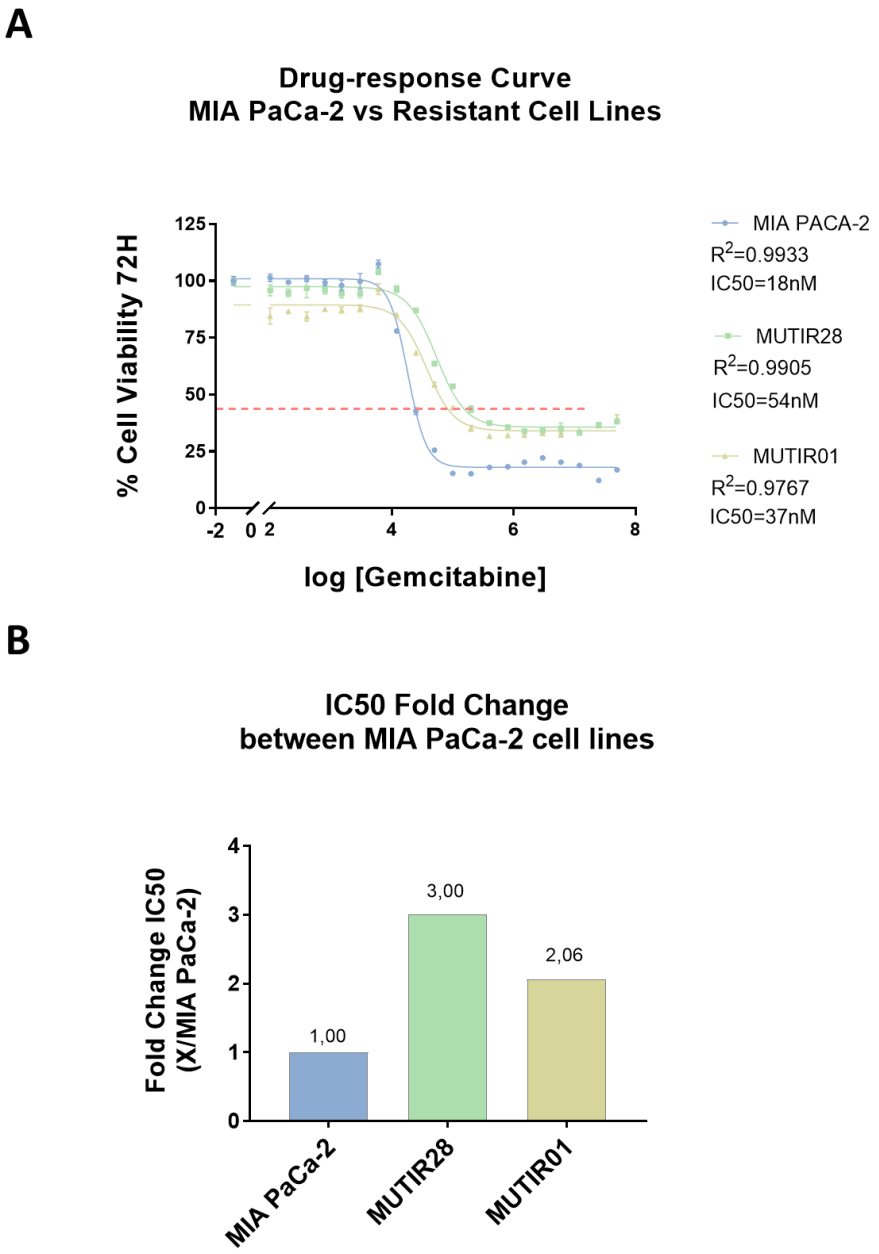

Figure III.6. MIA PaCa-2 and the derived cell lines, MUTIR28 and MUTIR01, drug-responses to Gemcitabine exposure at T5. MIA PaCa-2, MUTIR28 and MUTIR01 were exposed to Gemcitabine treatments for 72 hours to evaluate their resistance level. In this experiment we used Gemcitabine concentrations between 0,0001 – 50 µM, with a two-fold increment in each dose. **A)** Drug-responses to increasing Gemcitabine concentrations are displayed for MIA PaCa-2, MUTIR28 and MUTIR01. Cell viability analysis by MTT assay represent the cell viability of the cell lines under specific Gemcitabine concentrations, when compared with the DMSO-treated control (100% of cell viability). Non-linear fitting curves were performed using the log(inhibitor) vs. response -- variable slope (four parameters) function. Dashed red line indicates the threshold of 50% of cell viability. **B)** IC50 fold change of the generated cell lines is displayed for both of the resistant cell lines, MUTIR28 and MUTIR01, comparing their IC50 values with the MIA PaCa-2. The experiment was only performed once, to analyze resistance status during the Gemcitabine treatments.

3.2.4 IC50 determination of the Gemcitabine-resistant cell lines at T9

After the treatments, we reevaluated the cell lines sensitivity to Gemcitabine. For this experiment we used both MIA PaCa-2 and PANC-1 – derived cell lines, MUTIR28, MUTIR01 and PUTIR23.

The IC50 values calculated were 55nM for MUTIR28 and 32nM for MUTIR01, which indicates an increase in the IC50 values for the generated cell lines when compared with the 17nM value calculated for MIA PaCa-2 (III.7A, B, and C). This data corroborates the results obtained in the previous analysis, at T5. These values represent a fold increase of 2,7 ± 1,2 for MUTIR28 and 1,4 ± 0,19 for MUTIR01 in the IC50 values when compared to MIA PaCa-2 cell line (Figure III.7D). At the highest concentration of Gemcitabine, all the cell lines presented similar values of cell viability. Around 28% of the cells were viable on MIA PaCa-2 cell line, 32% on MUTIR28 cell line and 26% on MUTIR01 cell line (Figure III.7A, B, and C).

For PUTIR23, the IC50 value calculated was 141nm of Gemcitabine (Figure III.8B), which corresponds to a fold increase of 7,0 ± 1,5 of the 16nM value calculated for the PANC-1 cell line (Figure III.8A and C). At the maximum concentration of Gemcitabine (50 µM of Gemcitabine), 63% of the cells were viable on PANC-1 cell line compared with 24% on PUTIR23 cell line (Figure III.8A and B). These results show that at higher Gemcitabine concentrations, PUTIR23 presented three times less viable cells than PANC-1 cell line, despite its lower IC50 value.

Taken together these data indicate, that the MIA PaCa-2 derived cell lines, MUTIR28 and MUTIR01 as well as the PANC-1 derived cell line, PUTIR23, presented higher IC50 values, when compared with the parental cell lines. While MUTIR01 cells increased their IC50 value only 1,4-fold and therefore do not comply with the definition of resistance, MUTIR28 and PUTIR23 cell lines are considered resistant to Gemcitabine.

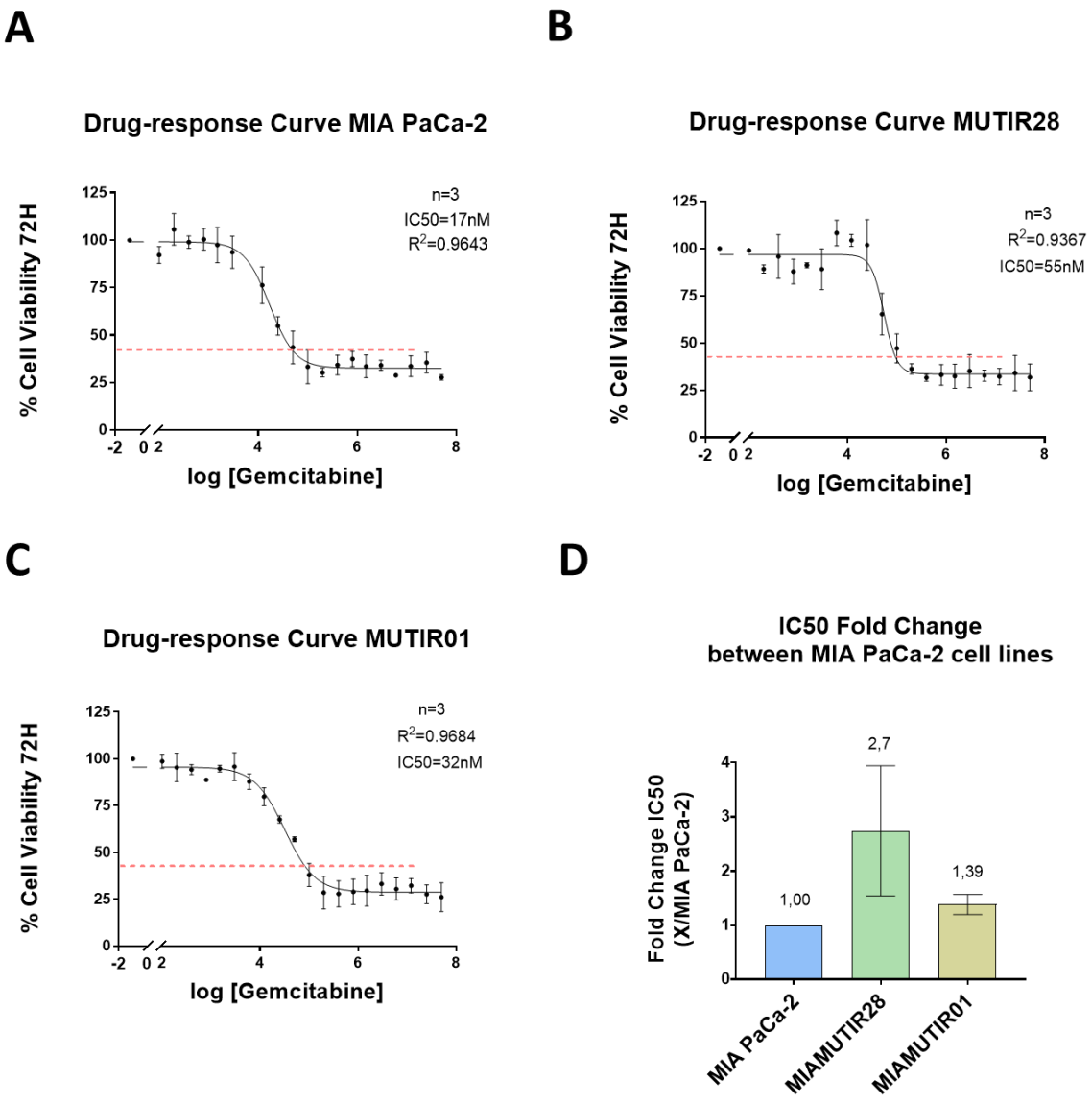

Figure III.7. MIA PaCa-2, MUTIR28 and MUTIR01 drug-responses after Gemcitabine treatment at T9. To evaluate Gemcitabine sensibility in the final stage of the protocol treatment, we exposed these cell lines to 0,0001 – 50 µM of Gemcitabine, for 72 hours treatments. The cell viability was evaluated by MTT assays, comparing the viability in each Gemcitabine concentration with the DMSO-treated control (100% of cell viability). We performed drug-response curves for MIA PaCa-2 (**A**), MUTIR28 (**B**) and MUTIR01 (**C**) cell lines. Non-linear fitting curves were executed using the log(inhibitor) vs. response -- variable slope (four parameters) function. These experiments were performed in triplicate and the represented data is the mean ± SEM, with n=3. Dashed red line indicates the threshold of 50% of cell viability. We calculated the IC50 fold change to evaluate the differences in cells resistance to Gemcitabine, comparing to the sensitive MIA PaCa-2 cell line IC50 value, as displayed in **D**.

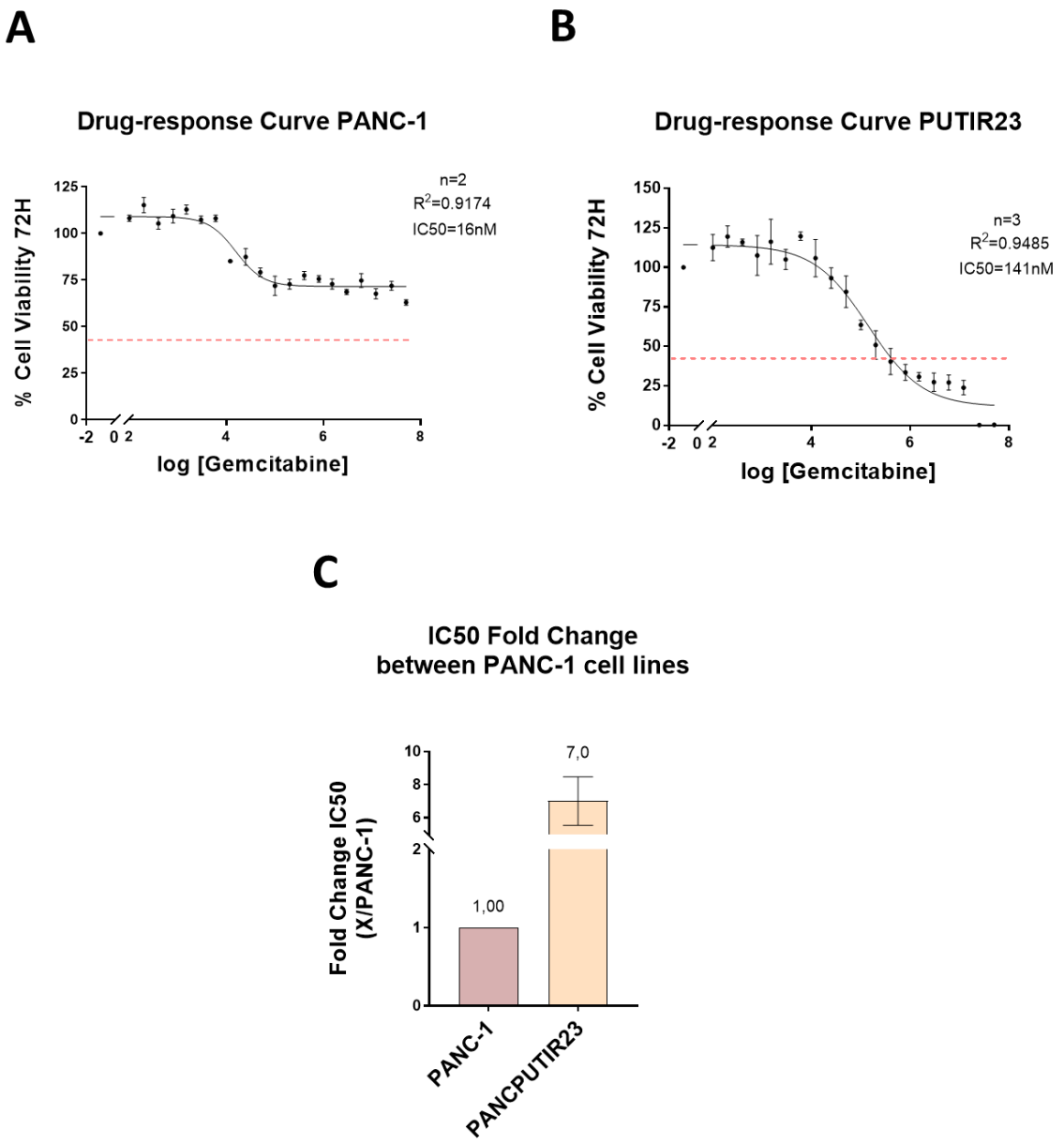

Figure III.8. PANC-1 and PUTIR23 drug-responses after Gemcitabine treatment at T9. To evaluate how the generated cell line PUTIR23 would react under Gemcitabine exposure, we treated both PANC-1 (**A**) and PUTIR23 (**B**) cell lines with Gemcitabine, for 72 hours. We exposed the cell lines to 0,0001 – 50 µM of Gemcitabine and performed drug-response curves for each cell line. The cell viability in each Gemcitabine treatment was evaluated comparing to the DMSO-treated control (100% of cell viability), using the MTT assay. Non-linear fitting curves were performed using the log(inhibitor) vs. response -- variable slope (four parameters) function, and the dashed red line indicates the threshold of 50% of cell viability. This allowed us to calculate the correspondent IC50 values for both cell lines. Moreover, we calculated the IC50 fold change of PUTIR23, comparing with PANC-1 cell line, that allowed us to evaluate the resistance level of the generated cell line (**C**).

3.3 Viability of Gemcitabine resistant cell lines

After the calculation of the IC50 values for the generated cell lines, we exposed them to the corresponding IC50 concentrations of Gemcitabine previously determined for the parental cell lines (MIA Paca-2 and PANC-1). This allowed us to verify the differences in cell viability between the parental and the derived resistant cell lines for a specific, non-extrapolated, drug concentration. For this purpose, we applied Gemcitabine treatments in the cells for 24, 48 or 72 hours.

3.3.1 Characterization of MUTIR28, MUTIR01 and PUTIR23 cell lines after treatment with the Gemcitabine IC50 concentration for the parental cell lines at T5

For this experiment, we used MIA PaCa-2 and the derived resistant cell lines, MUTIR28 and MUTIR01. We did not test PUTIR23 cell line at this moment due to its difficulty recovering from the initial drug treatments. At T5, to verify if the cells were successfully turning resistant, we applied 300nM of Gemcitabine, during 24-, 48- and 72-hours treatments. We choose this value because it corresponded to the concentration of the last drug treatment administrated.

According to our results, 24 hours of drug exposure were not enough to induce changes in the cell viability of the tested cell lines, as represented in Figure III.9. At the 48 hours timepoint, our results showed a decrease in the viability of all the cell lines, after drug administration. The percentage of viable cells in MIA PaCa-2 cell line decreased to 50% when compared to the DMSO-treated control, to 76% in MUTIR28 and 64% in MUTIR01 cell lines (Figure III.9C). When comparing with treated MIA PaCa-2 cell line, these values represent a 1,52-fold increase of the cell viability for MUTIR28 and a 1,29-fold increase of the cell viability for MUTIR01 (Figure III.9D). Our statistical analysis by the Welch's t-test demonstrated a significant decrease in the cell viability of all the tested cell lines after Gemcitabine treatment. Moreover, and according to the same test, our data indicated that the resistant cell lines MUTIR28 and MUTIR01 showed significantly increased cell viability values when compared to MIA PaCa-2 cell line, after Gemcitabine treatment (Figure III.9D).

After 72 hours of drug exposure our results showed a decrease in the cell viability of all the cell lines after Gemcitabine treatment. For MIA PaCa-2 cell line, we observed

a decrease to 13% when compared with the 100% calculated for the DMSO-treated control. For MUTIR28 and MUTIR01, the percentage of cell viability decreased to approximately 36% and 28%, respectively, when compared to the values calculated for the DMSO-treated controls (100%) (Figure III.9E). These values indicated an increase of the cell viability for both MUTIR28 (2,7-fold increase) and MUTIR01 (2,1-fold increase) cell lines, when compared to the treated MIA PaCa-2 cell line (Figure III.9F). According to the Welch's t-test, the cell viability decrease in all the cell lines after drug exposure was statistically significant, such as the differences between MIA PaCa-2 and the resistant cell lines after Gemcitabine treatment.

In conclusion, when we treated the cells with a high dose of Gemcitabine, MUTIR28 and MUTIR01 presented higher cell viability levels when compared with MIA PaCa-2. This corroborated the fact that both MUTIR28 and MUTIR01 presented higher levels of resistance when compared with the parental cell line, tolerating well high Gemcitabine concentrations.

A

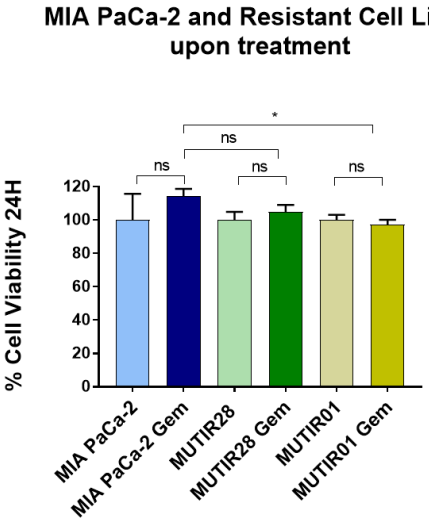
MIA PaCa-2 and Resistant Cell Lines upon treatment
% Cell Viability 24H
ns
ns
ns
*
120
100
80
60
40
20
0
MIA PaCa-2
MIA PaCa-2 Gem
MUTIR28
MUTIR28 Gem
MUTIR01
MUTIR01 Gem

B

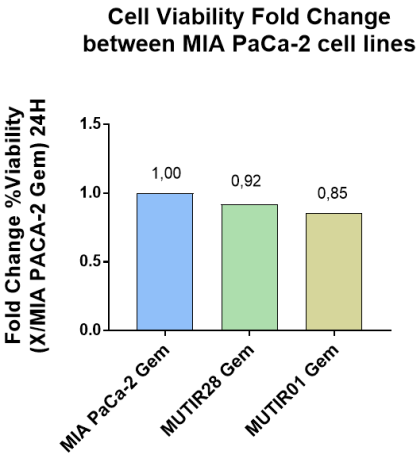
Cell Viability Fold Change between MIA PaCa-2 cell lines
Fold Change %Viability (X/MIA PACA-2 Gem) 24H
1.5
1.0
0.5
0.0
1,00
0,92
0,85
MIA PaCa-2 Gem
MUTIR28 Gem
MUTIR01 Gem

C

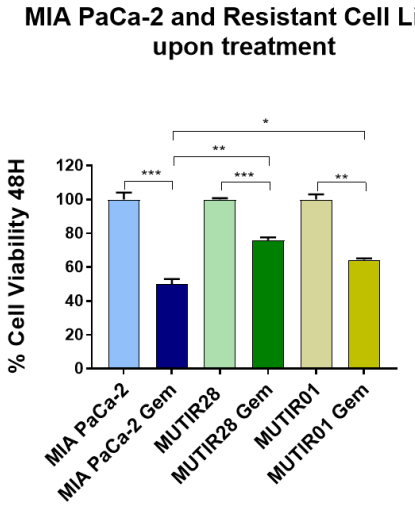
MIA PaCa-2 and Resistant Cell Lines upon treatment
% Cell Viability 48H
*
**
***
***
**
120
100
80
60
40
20
0
MIA PaCa-2
MIA PaCa-2 Gem
MUTIR28
MUTIR28 Gem
MUTIR01
MUTIR01 Gem

D

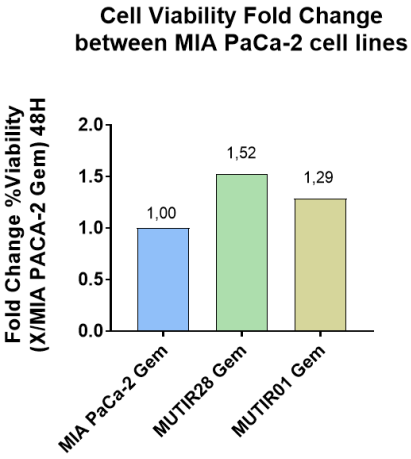
Cell Viability Fold Change between MIA PaCa-2 cell lines
Fold Change %Viability (X/MIA PACA-2 Gem) 48H
2.0
1.5
1.0
0.5
0.0
1,00
1,52
1,29
MIA PaCa-2 Gem
MUTIR28 Gem
MUTIR01 Gem

E

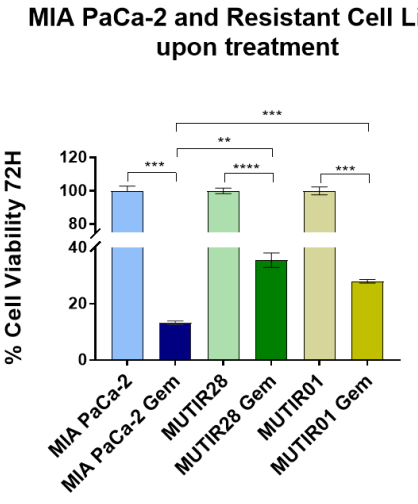
MIA PaCa-2 and Resistant Cell Lines upon treatment
% Cell Viability 72H
***
**
***
****
***
120
100
80
40
20
0
MIA PaCa-2
MIA PaCa-2 Gem
MUTIR28
MUTIR28 Gem
MUTIR01
MUTIR01 Gem

F

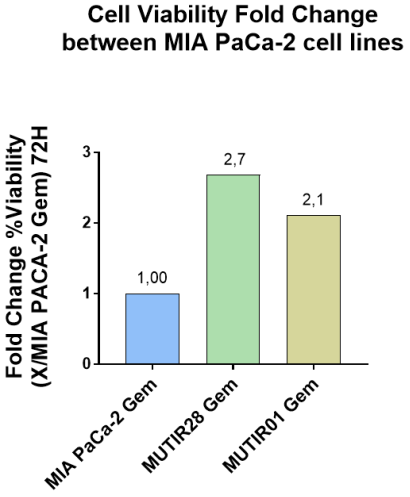
Cell Viability Fold Change between MIA PaCa-2 cell lines
Fold Change %Viability (X/MIA PACA-2 Gem) 72H
3
2
1
0
1,00
2,7
2,1
MIA PaCa-2 Gem
MUTIR28 Gem
MUTIR01 Gem

Figure III.9. MIA PaCa-2 and its derived resistant cell lines under high dose of Gemcitabine treatment at T5. To evaluate the treatment protocol success, we exposed MIA PaCa-2, MUTIR28 and MUTIR01 to 300nM of Gemcitabine, for 24 **(A)**,48 **(C)** and 72 hours **(E)**. We performed MTT assays to calculate cell viability and compare it to the DMSO-treated control (100% of cell viability). Statistical significance was determined by unpaired t test with Welch's correction, (ns) p>0,05, * p<0,05, ** p<0,005, *** p<0,001, **** p<0,0001. IC50 fold change of the % of cell viability is represented for the 24 **(B)**, 48 **(D)** and 72 hours **(F)** timepoints. We calculated the fold change of cell viability considering the viability for MIA PaCa-2 cell line the baseline for Gemcitabine sensitivity.

3.3.2 Characterization of MUTIR28, MUTIR01 and PUTIR23 cell lines after treatment with the Gemcitabine IC50 concentration for the parental cell lines at T9

3.3.2.1 Determination of cell viability by MTT assay

To determine the cell viability of parental and resistant cell lines after we treated them with the IC50 concentration of Gemcitabine previously determined for the parental cell line, we used the MTT assay as described in section 2.3.

We used MUTIR28, MUTIR01, PUTIR23 cell lines generated at time point T9 and the corresponding parental matches (MIA PaCa-2 and PANC-1) and analyzed cell viability using Gemcitabine IC50 concentrations determined in section 3.1. For MIA PaCa-2 and the derived resistant cell lines (MUTIR28 and MUTIR01) we used 22nM of Gemcitabine and for PANC-1 and the derived resistant cell lines and PUTIR23 we used 26nM of Gemcitabine. We treated the cells for 48 and 72 hours and determined the percentage of cell viability at each timepoint.

At 48 hours of treatment with 22nM of Gemcitabine, the MIA PaCa-2 and derived cell lines showed high levels of cell viability, close to the 100% value. Only MUTIR28 cell line showed around 138% of cell viability, however without statistical significance by the Welch's t-test analysis (Figure III.10A and B). We did not observe differences when comparing the parental cell line with the resistant cells or the cells treated with DMSO, and the cells treated with Gemcitabine. We verified similar results for PANC-1 and

PUTIR23, without differences between DMSO treatment or the Gemcitabine treatment (Figure III.10C and D).

However, after 72 hours of drug exposure, MIA PaCa-2 treatment with 22nM of Gemcitabine reduced the percentage of viable cells in about 31%. Only 69,0 ± 5,0 % of the cells were viable (Figure III.11A). For MUTIR28 and MUTIR01, we saw a decrease in cell viability upon Gemcitabine treatment. The cell viability decreased to 88,7 ± 4,6% and 64,1 ± 6,6 % in MUTIR28 and MUTIR01, respectively (Figure III.11A). This represents a fold change of 0,69 ± 0,05 for MIA PaCa-2, 0,88 ± 0,054 for MUTIR28 and 0,64 ± 0,07 for MUTIR01 cell lines, when comparing with the DMSO-treated controls (Figure III.11B). According to Welch's t-test analysis, the Gemcitabine treatment decreased the percentage of cell viability with statistical significance of $p<0,05$, only in MIA PaCa-2 and MUTIR01 cell lines. According to the same test, differences between the cell lines when treated with Gemcitabine did not demonstrate statistical significance. These data showed that 22nM of Gemcitabine produced significant decreasing effects in MIA PaCa-2 and MUTIR01 cell's viability but not in the MUTIR28 cell line, indicating the last one as less sensitive to Gemcitabine.

PANC-1 and PUTIR23 cell lines were treated with 26nM of Gemcitabine. As our data suggested, both cell line's viability decreased upon Gemcitabine treatment, however, without statistical significance. About 77,5 ± 2,1 % of PANC-1 cells and 74,7 ± 10,8 % of PUTIR23 cells were viable after 72 hours of treatment (Figure III.11C). This represents a fold change of 0,78 ± 0,02 for PANC-1 and 0,75 ± 0,1 for PUTIR23 cell lines, when compared with the correspondent DMSO-treated cells (Figure III.11D). Our results suggested that both cell lines responded similarly to the treatment with 26nM of Gemcitabine.

In conclusion, we did not observe significant changes in the cell viability of the cell lines after 48 hours of Gemcitabine exposure with 22nM (MIA PaCa-2 and derived cell lines) or 26nM (PANC-1 and derived cell lines). However, when the cells were exposed to Gemcitabine for 72 hours, we saw a decrease effect in all the cell lines viability when comparing with the DMSO-treated cells. From all the cell lines, the resistant MUTIR28 cell line showed higher levels of cell viability, when comparing with MIA PaCa-2 and MUTIR01. PANC-1 and PUTIR23 showed similar levels of the cell viability.

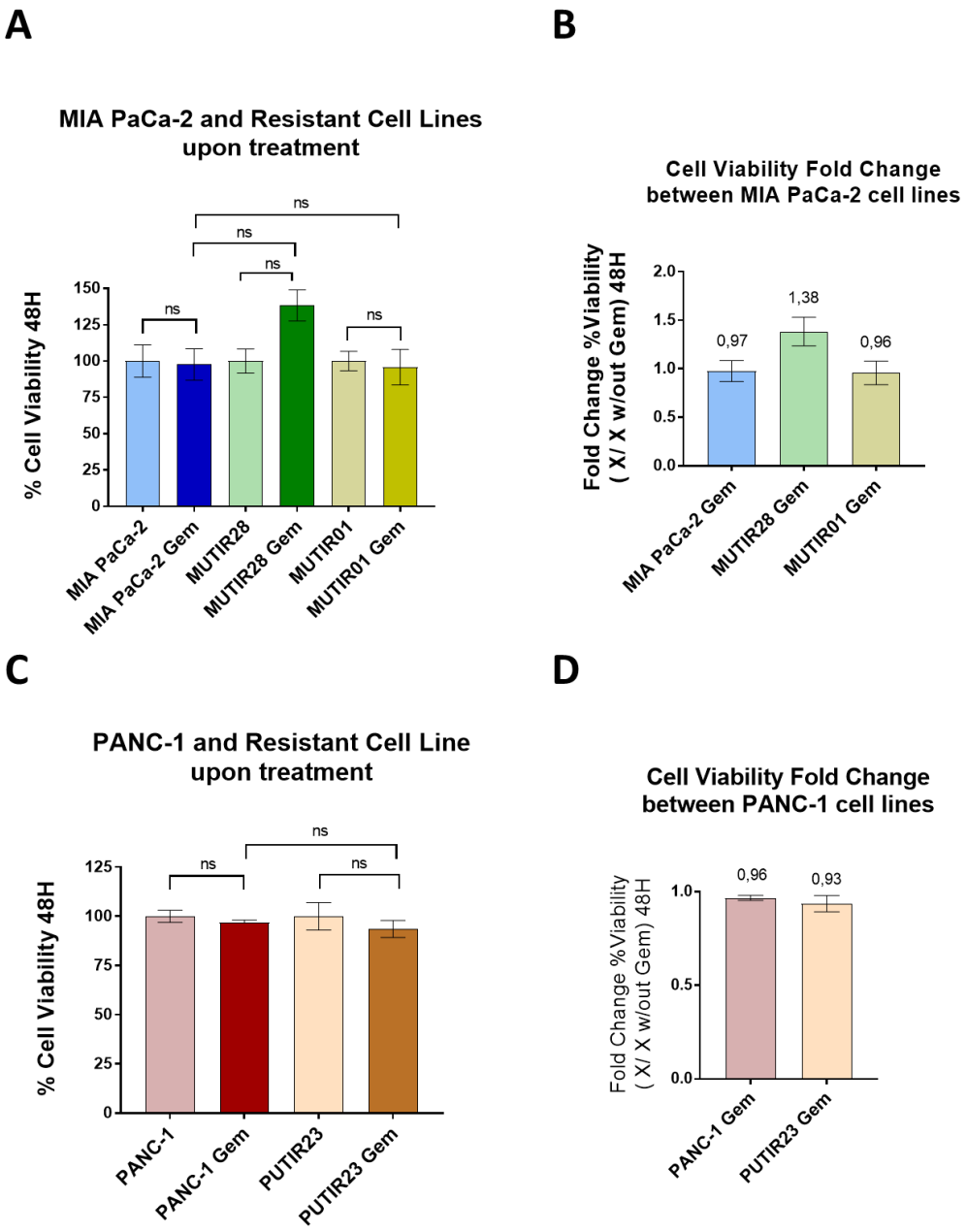

Figure III.10. Evaluation of the cell viability levels for the Parental versus Resistant cell lines when exposed to low levels of Gemcitabine for 48 hours. We used MTT assays to evaluate the percentage of cell viability after Gemcitabine administration (Gem) and for the controls (DMSO treated cells). For MIA PaCa-2, MUTIR28 and MUTIR01 cell lines we used 22nM of Gemcitabine and for PANC-1 and PUTIR23 we used 26nM of Gemcitabine. We evaluated the percentage of cell viability at 48 hours of drug exposure for MIA PaCa-2 and its derived cell lines **(A)**, and for PANC-1 and PUTIR23 cell line **(C)**. The experiments were performed in triplicate. The statistical significance was determined by unpaired t test with Welch's correction (ns) p>0,05. We calculated the cell viability fold change for each cell line comparing the values obtained under Gemcitabine treatment (Gem) with the DMSO-treated controls (100% of cell viability), for MIA PaCa-2 and its derived cell lines **(B)** and PANC-1 and its correspondent resistant cell line **(D)**.

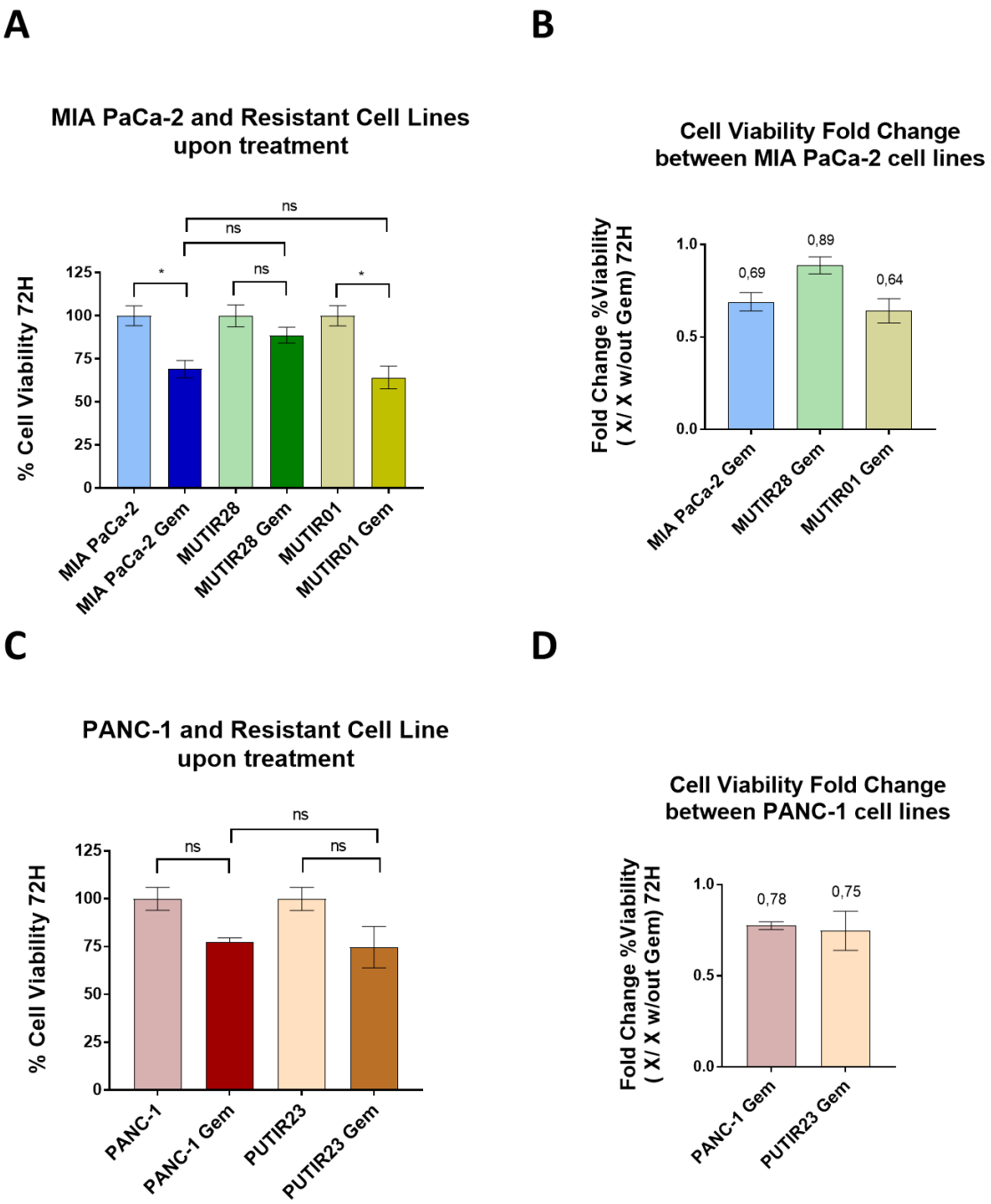

Figure III.11. Evaluation of the cell viability levels for the Parental versus Resistant cell lines when exposed to low levels of Gemcitabine for 72 hours. We exposed MIA PaCa-2, MUTIR28 and MUTIR01 to 22nM of Gemcitabine and PANC-1 and PUTIR23 to 26nM of Gemcitabine. We evaluated the percentage of cell viability at 72 hours of drug exposure for MIA PaCa-2 and its derived cell lines **(A)**, and for PANC-1 and PUTIR23 cell line **(C)**, using the MTT assay. The experiments were performed in triplicate. Statistical significance was determined by unpaired t test with Welch's correction, (ns) $p>0,05$, * $p<0,05$. Fold change of cell viability was determined comparing the values after Gemcitabine treatment (Gem) with the results obtained for the DMSO-treated controls, for both MIA PaCa-2 and its resistant cell lines **(B)** and PANC-1 and its resistant cell line **(D)**.

3.3.2.2 Determination of cell death by Trypan Blue exclusion assay

The cell viability experiments were performed by using the MTT assay. However, MTT assay does not allows to distinguish between cell cycle arrest and cell death. To differentiate between the Gemcitabine induced cell cycle arrest and cell death levels in the parental and the resistant cell lines, we performed the Trypan Blue Exclusion assay. After 48 and 72 hours of treatment, we evaluated the percentage of Gemcitabine-induced cell death. This assay allows us to verify if the decrease in the cell viability corresponded to an increase of cell death of the treated cell lines (Table III.1).

Table III.1. Calculation of the percentage of viable and non-viable cells upon Gemcitabine treatment for 48 and 72 hours. We used the Trypan Blue Exclusion Assay to evaluate the number of viable and non-viable cell after Gemcitabine exposure. We used 22nM of Gemcitabine for MIA PaCa-2, MUTIR28 and MUTIR01 and 26nM of Gemcitabine to PANC-1 and PUTIR23. The percentage of cells was calculated as represented in Equation II.1.

	%Cells (DMSO treatment)		%Cells (Gemcitabine treatment)	
48H	Viable	Unviable	Viable	Unviable
MIA-PACA-2	90	10	88	13
MUTIR28	79	21	82	18
MUTIR01	91	9	88	12
PANC-1	92	8	85	15
PUTIR23	92	8	90	10
72H	Viable	Unviable	Viable	Unviable
MIA-PACA-2	91	9	80	20
MUTIR28	90	10	88	12
MUTIR01	93	7	91	9
PANC-1	95	5	73	27
PUTIR23	95	5	77	23

Our results showed that at 48 hours of treatment, Gemcitabine induced higher cell death levels in MIA PaCa-2 (1,30-fold increase) and MUTIR01 (1,39-fold increase) compared with the cells treated with 0,1% of DMSO (Figure III.12A). We did not verify the same effect on MUTIR28 cell line, where cell death percentage did not seem to increase in the presence of Gemcitabine (fold change of 0,85), compared with the 0,1% of DMSO treatment (Figure III.12A). However, after 72 hours of Gemcitabine exposure, MIA PaCa-2, MUTIR28, and MUTIR01 cell lines showed an increase in the cell death percentage. The parental cell line showed the highest cell death percentage with a fold increase of 2,19, whereas MUTIR28 and MUTIR01 showed values of 1,25 and 1,17 (Figure III.12C). These data suggested that Gemcitabine induced more cellular death in the parental cell line than in the resistant cells and that after 48 hours, it did not seem to increase MUTIR28 cell death percentage.

For PANC-1 and PUTIR23 cell lines, our results showed that Gemcitabine induced cell death at higher levels in the PANC-1 cell line at both 48 and 72-hour time points. At 48-hour timepoint, we verified a cell death fold increase of 1,94 for PANC-1 and 1,24 for PUTIR23 cell line (Figure III.12B). At the 72-hour timepoint, both cell death percentages increased, representing a fold change of 5,48 for PANC-1 and 4,94 for the PUTIR23 cell line (Figure III.12D).

In conclusion, we observed that MIA PaCa-2 showed higher cell death levels when treated with Gemcitabine when compared with MUTIR28 and MUTIR01. According to our previous results, the cells presenting less cell viability levels when treated with this drug also showed higher cell death levels. For PANC-1 and PUTIR23 we did not observe differences in their cell death percentage upon treatment, concordant with the similar values of cell viability calculated for both these cell lines. However, we only performed this experiment once, and we need to repeat it for concise conclusions.

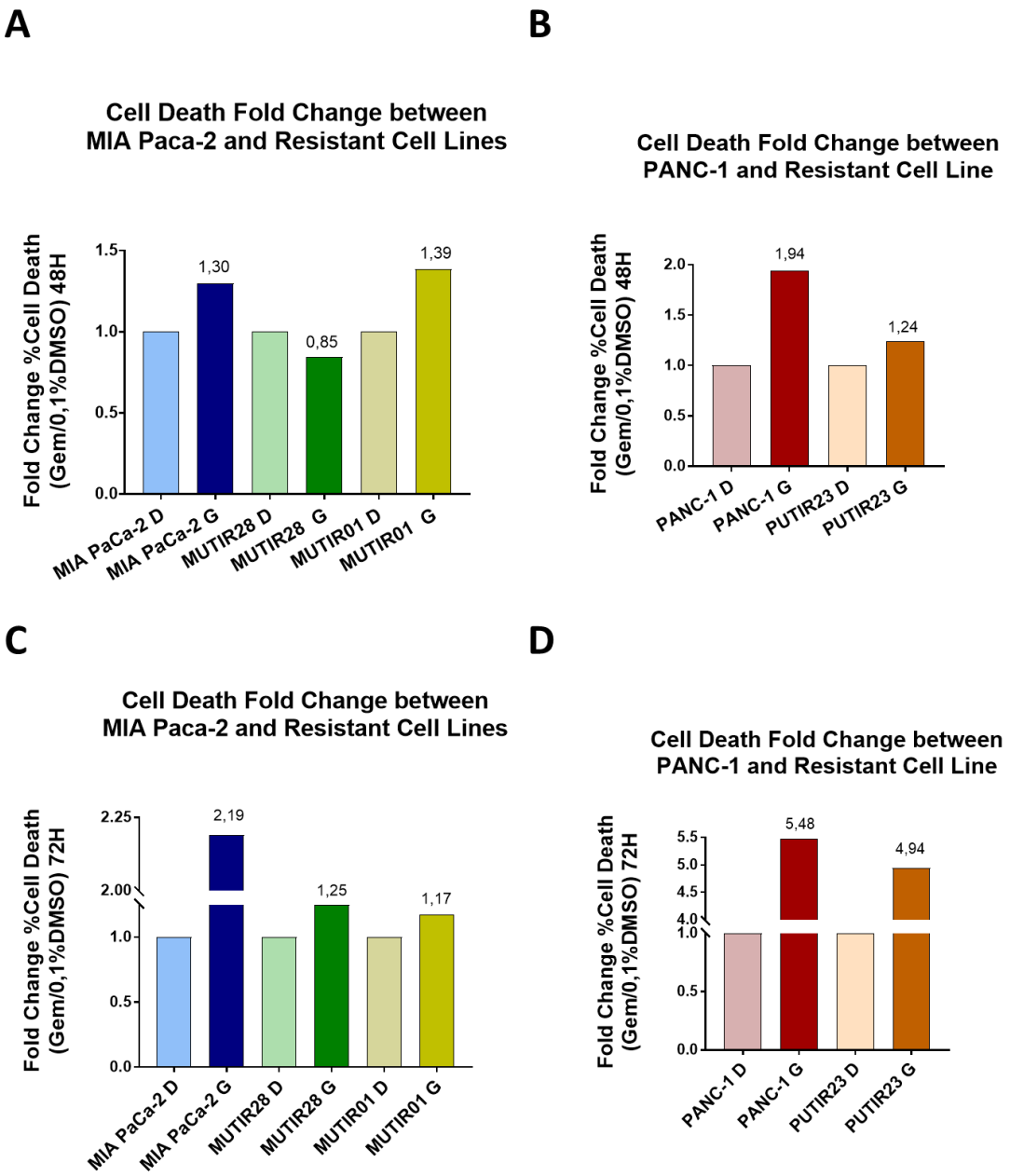

Figure III.12. Evaluation of the parental versus resistant cell lines cell death after Gemcitabine treatment. After the evaluation of cell viability of the newly generated cell lines, we performed a cell death experiment. We used the Trypan Blue Exclusion assay to calculate the percentage of cell death. In this experiment we compared the cells treated with DMSO (D) with the cells treated with Gemcitabine (G). For Gemcitabine treatments, we used 22nM for MIA PaCa-2, MUTIR28 and MUTIR01 and 26nM for PANC-1 and PUTIR23 cell lines and performed treatments of 48 and 72 hours. To calculate the number of viable or non-viable cells we diluted the cell suspension (1:2) in Trypan Blue and count the cells in a Neubauer chamber. The percentage of cell death values were calculated considering the following equation: (number of dead cells/numbers of total cells (viable + dead cells)) x 100.The represented IC50 values were calculated comparing the % of cell death under Gemcitabine treatment with the correspondent DMSO-treated controls. This experiment was only performed once.

3.4 Resistant versus Parental cell lines motility capacity

Cell migration is an important event in cancer invasion and metastasis and represent features of an aggressive tumor. To evaluate if the Gemcitabine resistant cell lines presented higher migration ability than the parental cell lines, possibly associated with an aggressive phenotype, we performed a 15-hour wound-healing assay. All migration experiments were performed under starvation conditions. This impairs cell proliferation and guarantees that the wound closure is due to migration capability.

3.4.1 Optimization of the starvation protocol

To evaluate the most suitable conditions of starvation during the wound-healing assay, we performed a pilot experiment. We used MIA PaCa-2, MUTIR28 and MUTIR01 cell lines and exposed them to DMEM supplemented with 0,5% or 2% FBS. The wound size was measured in pixels (PX) and the values at each time point are represented in Table III.2.

Table III.2. Wound size measurements for optimization of the starvation conditions. For starvation optimization we maintained the cells in culture with DMEM complemented with 0,5% or 2% FBS. We measured the wound size at every 3 hours. We used the *VisiCam® 5 Plus (VWR, USA)* microscopic camera to take the pictures and the *Wave Image software* to perform the measurements. These values are represented in pixels (PX) and in FC. The fold change was calculated considering the values at T=0.

IN PX	FBS	0H	3H	6H	9H	12H	15H
MIA-PACA-2	0,5%	459,0	318,0	380,0	376,0	290,0	196,0
	2%	606,0	579,0	529,0	476,0	466,8	377,1
MUTIR28	0,5%	664,0	643,0	620,1	589,9	570,0	566,6
	2%	474,0	440,0	432,1	422,1	390,0	378,9
MUTIR01	0,5%	729,6	680,0	667,0	620,0	614,0	607,0
	2%	663,9	658,0	601,0	596,2	549,0	469,8
IN FC	**FBS**	**0H**	**3H**	**6H**	**9H**	**12H**	**15H**
MIA-PACA-2	0,5%	1	0,693	0,828	0,819	0,632	0,427
	2%	1	0,956	0,873	0,786	0,770	0,622
MUTIR28	0,5%	1	0,968	0,934	0,888	0,858	0,853
	2%	1	0,928	0,912	0,891	0,823	0,799
MUTIR01	0,5%	1	0,932	0,914	0,850	0,841	0,832
	2%	1	0,991	0,905	0,898	0,827	0,708

As represented in Figures III.13 and III.14, both conditions appeared to result in similar wound closure and cell migration. At the 15-hour timepoint in the MIA PaCa-2 experiment, the results indicated a wound closure of 57% for 0,5% FBS and 48% for 2% FBS, indicating a higher motility capacity for cells under 0,5% FBS. However, for MUTIR28 and MUTIR01, 2% FBS was associated with higher motility ability (20% and 29% wound closure), comparing to the results obtained from the 0,5% FBS treatment (15% and 17% wound closure) (Table III.2).

Both FBS conditions allowed cells to migrate and did not interfere in the cell's adhesion to the culture plate along the experimental time course. Since we performed a long-term experiment in starvation conditions, we choose DMEM supplemented with 2% of FBS for future assays.

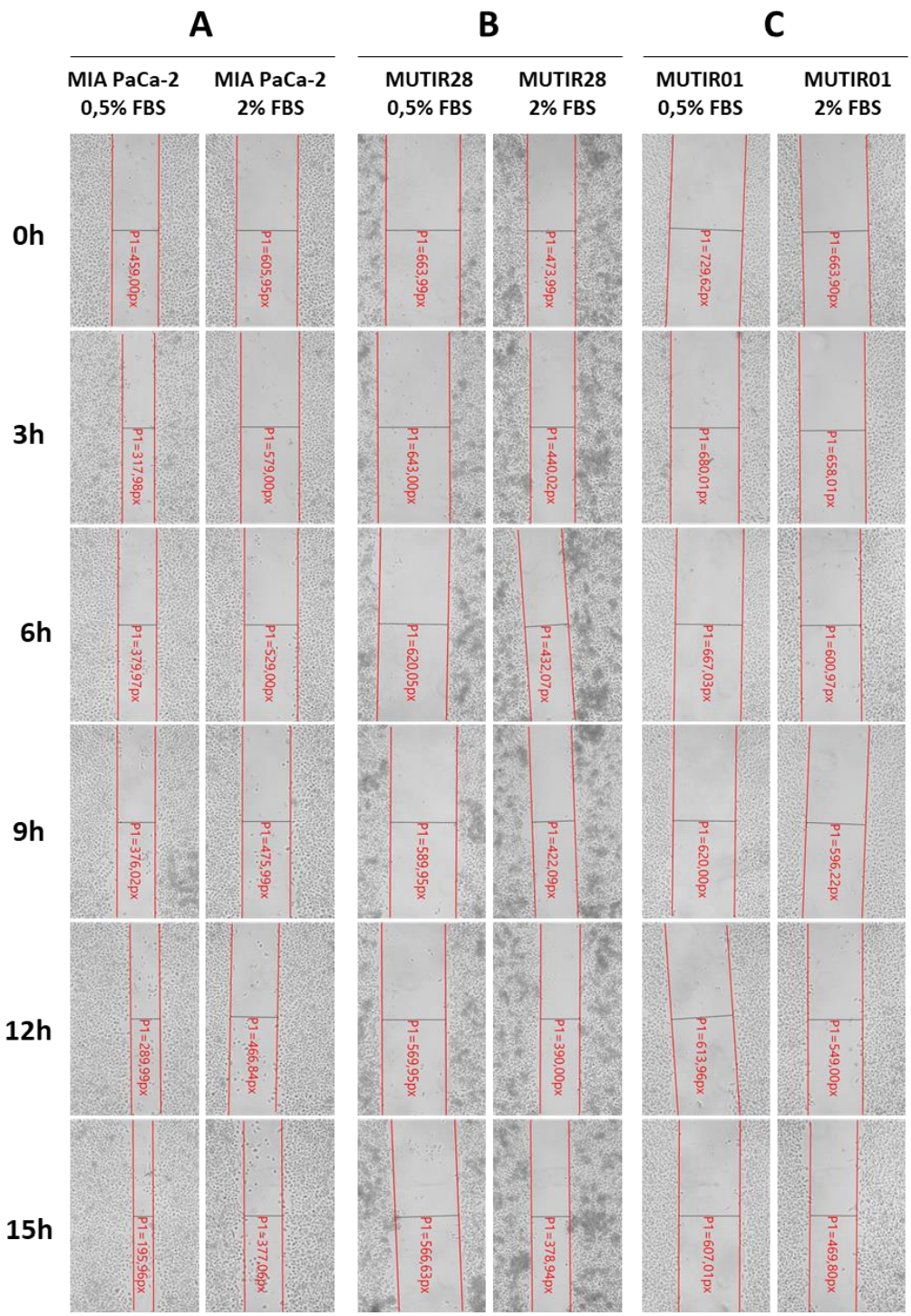

Figure III.13. Wound healing assay performed for 15 hours to evaluate starvation conditions. To evaluate the best starvation conditions to perform the wound healing assay, we tested two different FBS concentrations, 0,5% and 2%. For this experiment we used MIA PaCa-2 **(A)**, MUTIR28 **(B)** and MUTIR01 **(C)** cell lines. The wound size was measured at every 3 hours for each condition in a 15-hour time course. We used the *VisiCam® 5 Plus (VWR, USA)* microscopic camera and the *Wave Image software,* coupled to a microscope to register the wound size at each timepoint. Red lines indicate the wound margins, and the values represents the distance between the margins in pixels (PX).

A

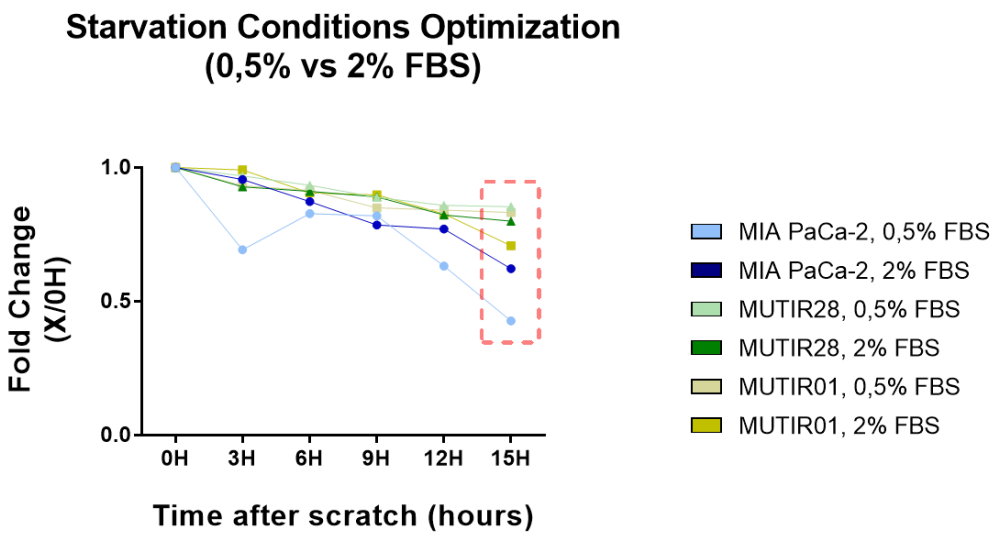

B

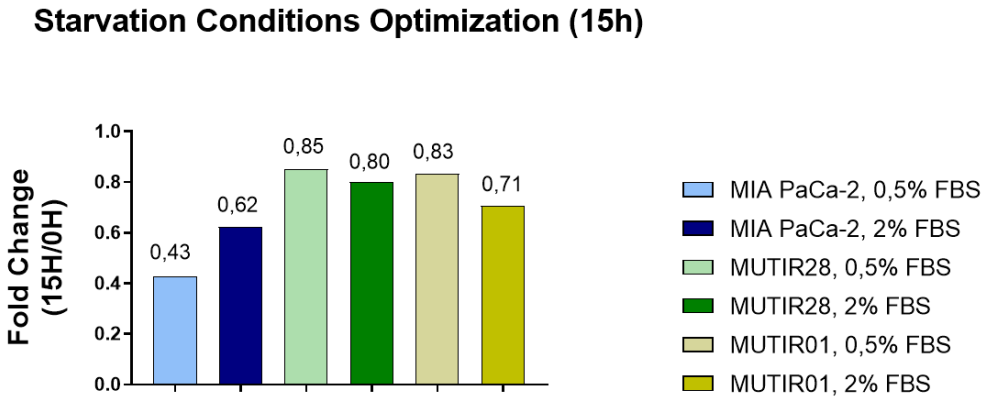

Figure III.14. Optimization of starvation conditions for the wound healing migration assay. We performed a wound healing migration assay to evaluate the best FBS conditions for the cell lines in the study. **A)** In this experiment, we used 0,5% and 2%of FBS for MIA PaCa-2, MUTIR28 and MUTIR01 cell lines. We evaluated the wound size every 3 hours for both conditions in a 15-hour duration assay. To register the wound size, we used the *VisiCam® 5 Plus (VWR, USA)* microscopic camera coupled to a microscope and the *Wave Image software.* The results were represented in fold change regarding the wound size at the T=0 timepoint. **B)** Representation of the fold change in a bar graph. The fold change was calculated comparing the wound closure size at each timepoint with the initial size at T=0.

3.4.1 Wound healing of MIA Paca-2 and PANC-1 and the derived resistant cell lines

After defining the optimal starvation conditions, we tested the motility of the parental cell lines, MIA PaCa-2 and PANC-1, and compared it with the resistant cell lines, MUTIR28, MUTIR01 and PUTIR23. The size of the wound was evaluated at each time and the corresponding values are represented Table III.3.

Table III.3. Wound size measurements in the 15 hours Migration Assay. During the 15 hours experiments, we measured the wound size at every 3 hours. We used the *VisiCam® 5 Plus (VWR, USA)* microscopic camera to take the pictures and the *Wave Image software* to perform the measurements. These values are represented in pixels (PX) and in FC. The fold change was calculated considering the values at T=0.

	N=1						N=2					
IN PX	0H	3H	6H	9H	12H	15H	0H	3H	6H	9H	12H	15H
MIA-PACA-2	356,0	315,6	270,0	199,7	153,7	118,0	206,1	194,0	138,0	100,0	93,0	78,0
MUTIR28	288,0	276,0	228,9	223,0	211,0	198,0	295,0	292,0	232,9	215,0	203,0	200,0
MUTIR01	572,9	519,9	517,0	426,9	474,9	464,0	900,0	892,0	881,0	789,9	751,9	723,8
PANC-1	496,9	462,8	428,9	413,3	382,5	307,0	536,1	474,0	410,9	382,1	372,0	343,0
PUTIR23	463,9	444,0	353,9	276,9	271,0	248,0	343,1	313,0	232,9	200,0	189,0	160,2
IN FC	0H	3H	6H	9H	12H	15H	0H	3H	6H	9H	12H	15H
MIA-PACA-2	1	0,887	0,758	0,561	0,432	0,331	1	0,941	0,670	0,485	0,451	0,378
MUTIR28	1	0,958	0,795	0,774	0,733	0,688	1	0,990	0,790	0,729	0,688	0,678
MUTIR01	1	0,907	0,902	0,745	0,829	0,810	1	0,991	0,979	0,878	0,835	0,804
PANC-1	1	0,931	0,863	0,832	0,770	0,618	1	0,884	0,767	0,713	0,694	0,640
PUTIR23	1	0,957	0,763	0,597	0,584	0,535	1	0,912	0,679	0,583	0,551	0,467

Our results demonstrated that all cell lines, the parental and the resistant cells, showed migration ability and wound closure capacity along the experimental time course, however, at different levels (Table III.3). MIA PaCa-2 showed a higher capacity to close the wound at every time-point than the resistant cell lines, as represent in Figure III.15. At 15-hour after scratch, the MIA PaCa-2 cell line showed a 64,6 ± 3,3% wound closure, while MUTIR28 and MUTIR01 presented about 31,8 ± 0,6% and 19,3 ± 0,4%, respectively (Figure III.15 and III.17). These results indicated that MIA PaCa-2 had a higher ability to migrate than the correspondent resistant cell lines, with a statistical significance of $p<0,05$ according to the Welch's t-test.

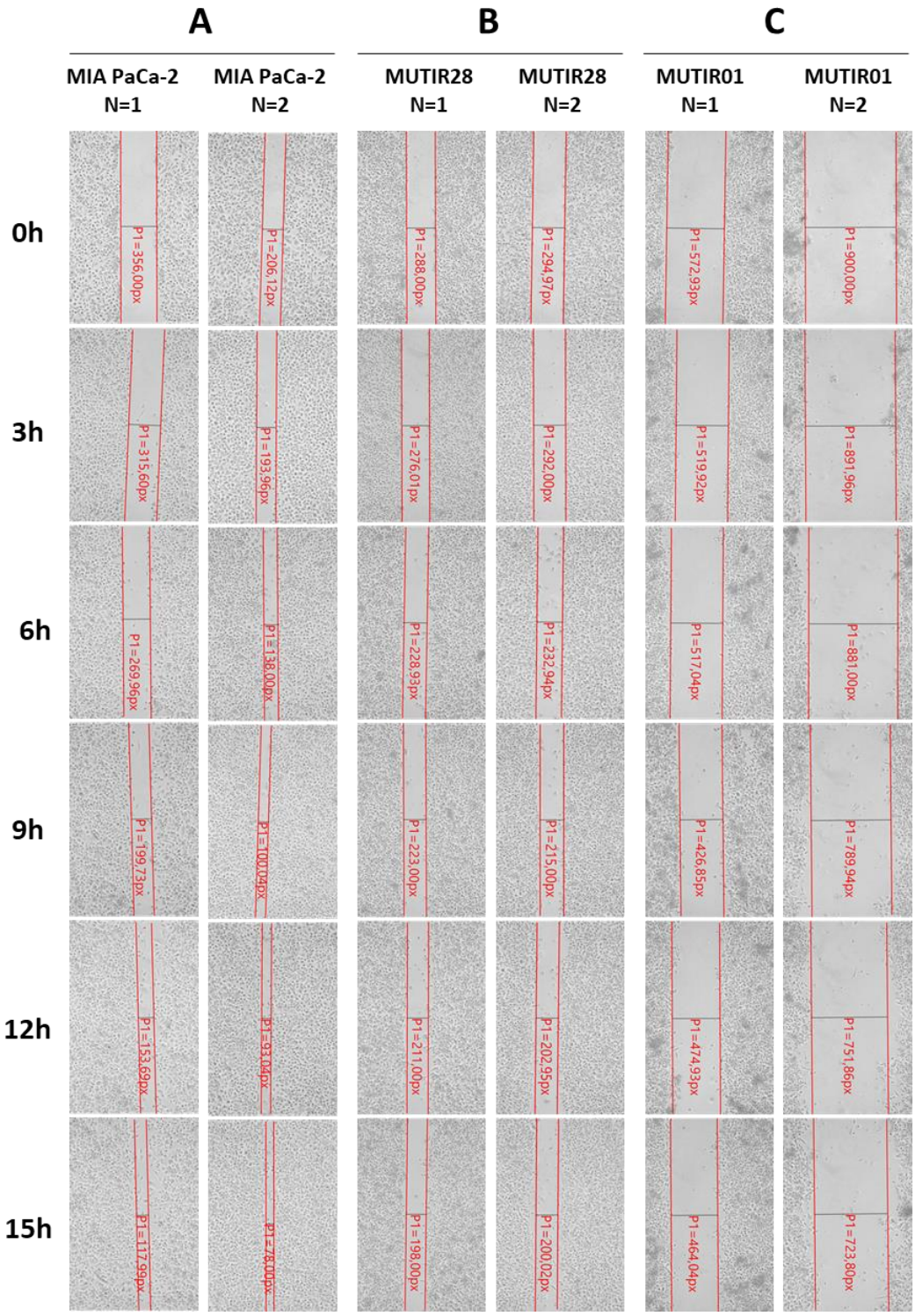

Figure III.15. Wound healing assay to analyze the migration ability of MIA PaCa-2 and the derived cell lines. We performed a wound healing assay to evaluate the migration ability of the sensitive MIA PaCa-2 cell line **(A)**, and the resistant cell lines MUTIR28 **(B)** and MUTIR01 **(C).** We evaluated the wound closure of each cell line at every 3 hours in a 15-hour duration experiment and microscopy photographs were taken with the used the *VisiCam® 5 Plus (VWR, USA)* microscopic camera and the *Wave Image software*, coupled to a microscope. The cells were cultured in DMEM with 2% FBS. This experiment was performed twice, and the results are represented for the n=1 and the n=2, for each cell line. Red lines indicate the wound margins, and the values

For PANC-1 and its derived cell line, we observed the most prominent effect at the 9-hour time-point. The PANC-1 cell line showed a wound closure of 22,8 ± 8,4%, while PUTIR23, contrary to the other resistant cell lines, showed an increased wound healing capacity of 41,1 ± 0,9% (Figures III.16 and III.18). However, PANC-1 and PUTIR23 differences were not statistically significant, according to the Welch's t-test analysis. In conclusion, we observed that both of the MIA PaCa-2 derived cell lines showed lower wound closure ability, and consequently, lower ability to migrate. Whereas PUTIR23, the PANC-1 derived cell line seemed to present higher migration ability than de parental cell line, however without statistical significance.

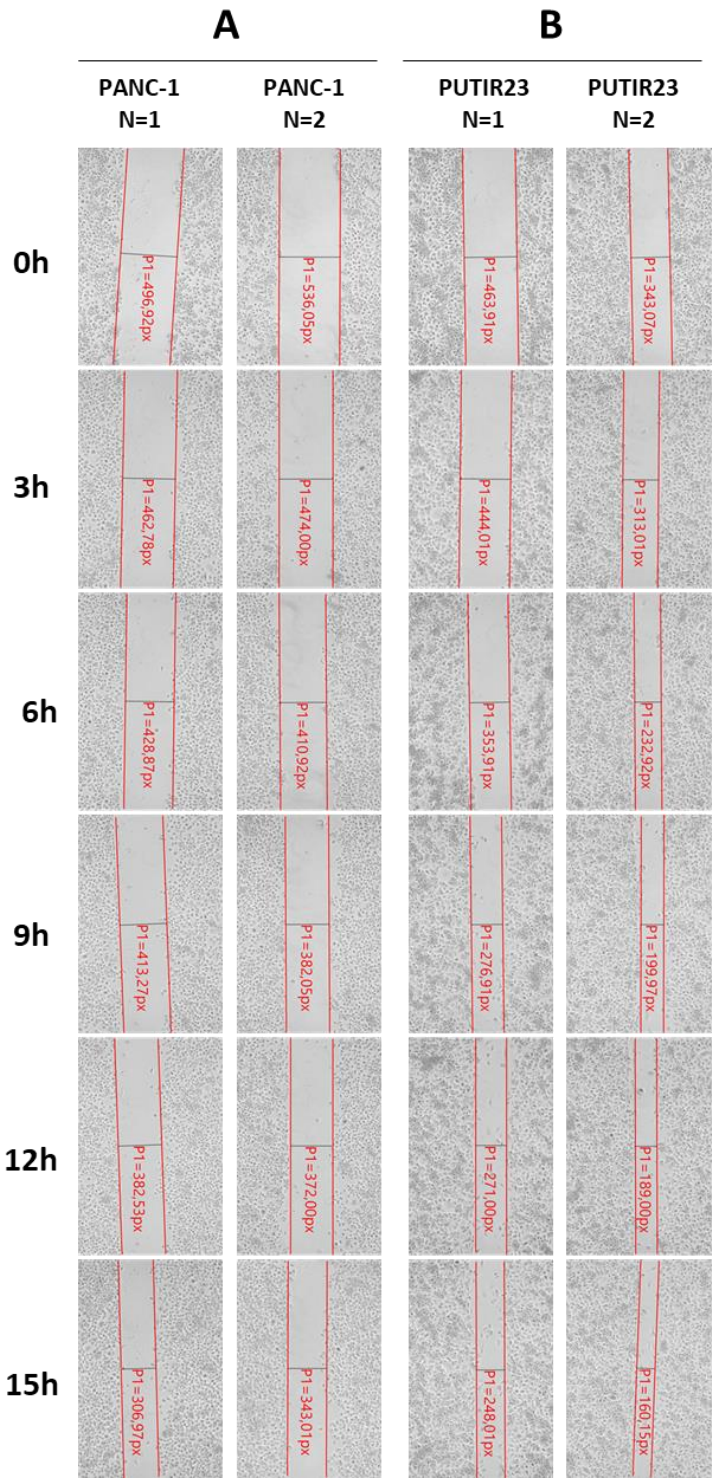

Figure III.16. Wound healing assay to analyze the migration ability of PANC-1 and derived cell line. We analyzed the wound closure ability of the sensitive cell line, PANC-1 and the resistant cell line, PUTIR23. Both of the cells were cultured in DMEM with 2% of FBS. We took microscopic photographs at every 3 hours after scratch, in a 15-hour duration assay, using the used the *VisiCam® 5 Plus (VWR, USA)* microscopic camera and the *Wave Image software*, coupled to a microscope. We performed this experiment twice. The results are represented for both the experiments, n=1 and n=2. Red lines indicate the wound margins, and the values represents the distance between the margins in pixels (PX).

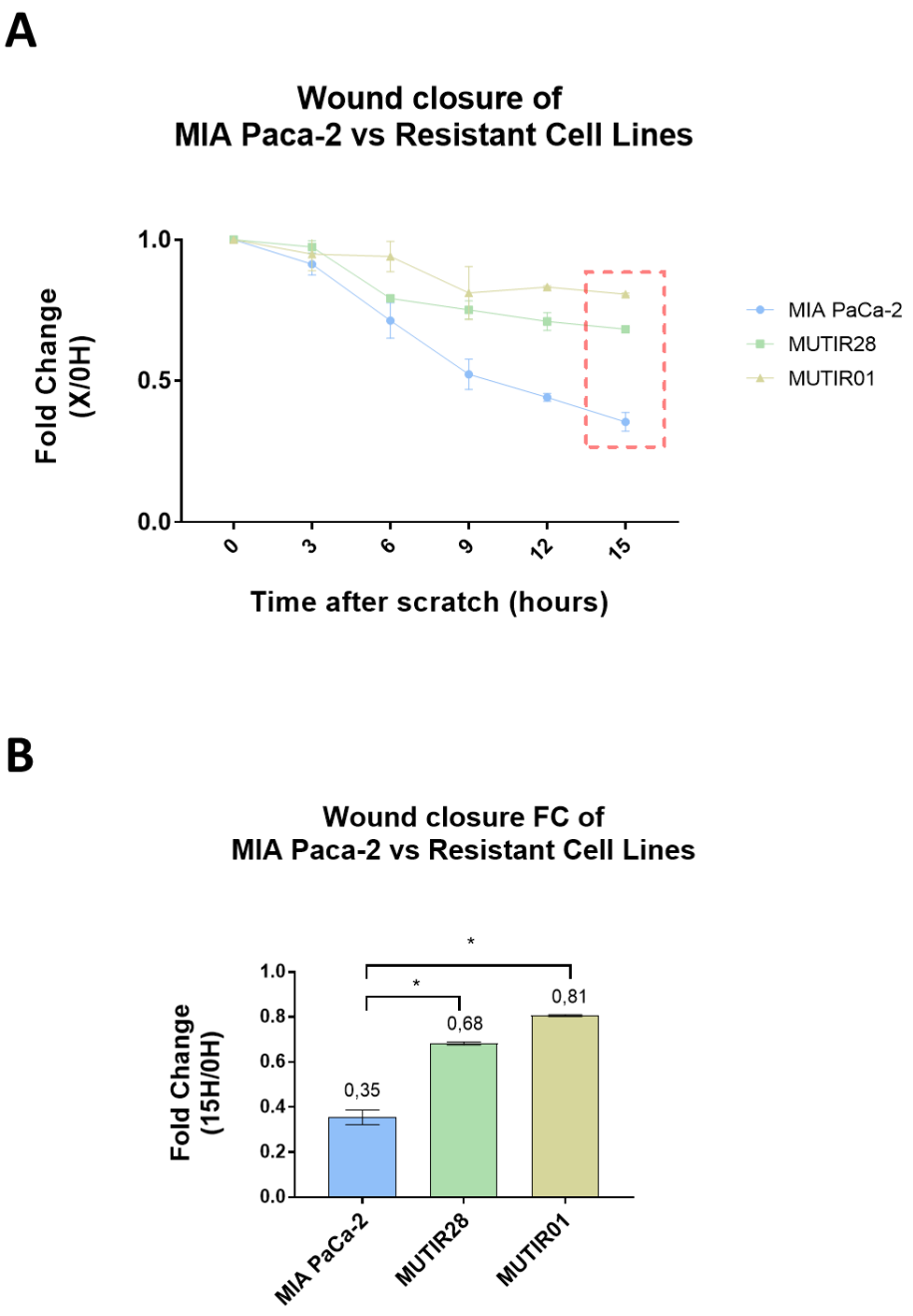

Figure III.17. MIA PaCa-2 and derived cell lines present different levels of wound closure ability. To analyze cell line's ability to migrate, we performed a wound-healing assay during a 15-hour time course. **A)** After the scratch, we evaluated the wound size in every 3 hours, in starvation conditions, with cells maintained in DMEM complemented with only 2% FBS. The dotted red square indicates the 15-hour timepoint, where the wound closure differences were more evident between the studied cell lines. The results were represented in fold change of the wound size at each timepoint, comparing with the initial size at T=0 (FC=1). Experiments were performed in duplicate, and the represented data is the mean ± SEM, with n=2. **B)** Bar graphic representing the results at the 15-hours timepoint. We compared each cell line migration ability to the ability of the sensitive cell line, MIA PaCa-2. Statistical significance was determined by unpaired t test with Welch's correction: * $p<0,05$.

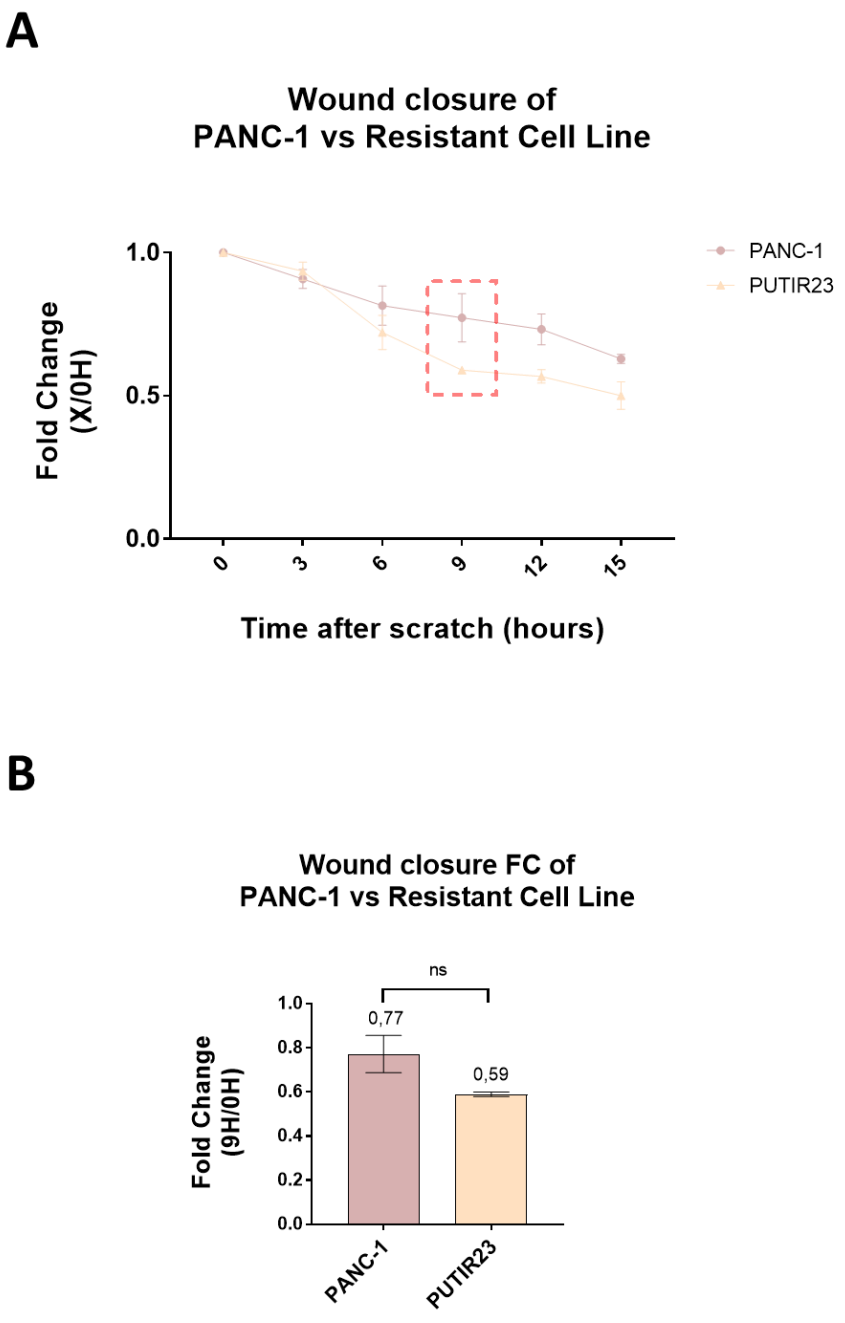

Figure III.18. PANC-1 and PUTIR23 cell lines wound closure ability. To evaluate the migration ability of the parental versus the resistant cell line, we performed a wound-healing assay with a 15-hour time course. **A)** We analyzed the wound closure at every 3 hours, in starvation conditions (DMEM with 2% of FBS). Both PANC-1 and PUTIR23 seemed to be able to close the wound during this assay. We observed the most evident differences between cell lines at the 9-hour timepoint (dotted red square). The results were represented in fold change of the wound closure comparing with the wound size at T=0. Experiments were performed in duplicate, and the represented data is the mean ± SEM, with n=2. **B)** Bar graph representation of the results at the 9-hour timepoint. Statistical significance was determined by unpaired t test with Welch's correction: ns p>0,05.

3.5 TRIBBLES expression in the generated cell lines

Since TRIBBLES, specially TRIB2 and TRIB3, were previously associated with resistant phenotypes in other cancer types, we decided to evaluate their expression in the parental cells and newly generated resistant cell lines. This allowed us to evaluate if TRIBBLES proteins represent potential therapeutic targets in the context of PC and contribute to the mechanism underlying acquired resistance.

3.5.1 TRIB1, TRIB2 and TRIB3 mRNA levels

3.5.1.1 Characterization of MIA PaCa-2 and PANC-1 cell lines

To evaluate the endogenous expression of TRIB1, TRIB2 and TRIB3 in the parental cell lines MIA PaCa-2 and PANC-1 at the mRNA level we performed an RT-qPCR.

As our results demonstrate, both MIA PaCa-2 and PANC-1 cell lines seemed to express TRIBBLES at the transcriptional level. However, PANC-1 cell line showed higher TRIB1, TRIB2 and TRIB3 mRNA levels, when compared with MIA PaCa-2 cell line. We demonstrated a fold increase of 20,5 ± 3,0 for TRIB1 mRNA levels, a fold increase of 4,99 ± 1,25 for TRIB2 mRNA levels, and a fold increase of 2,23 ±0,34 for TRIB3 mRNA levels (Figure III.19). Overall, PANC-1 cell line presented higher TRIBBLES gene expression.

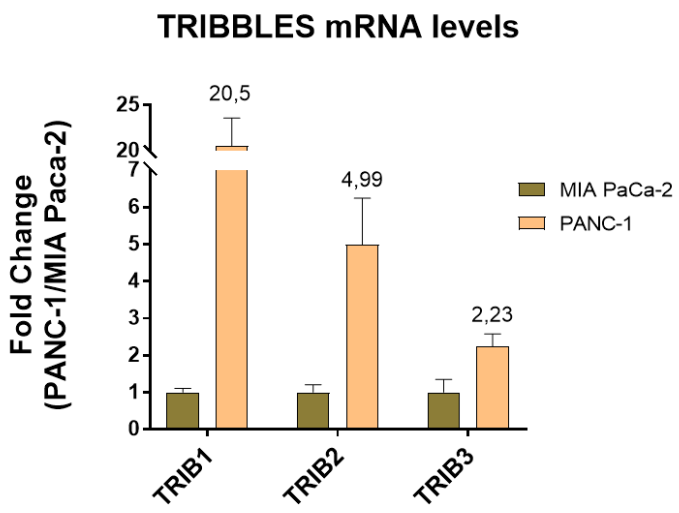

Figure III.19. Characterization of MIA PaCa-2 and PANC-1 cell lines regarding TRIBBLES mRNA levels. We evaluated TRIBBLES mRNA expression in the parental sensitive cell lines, MIA PaCa-2 and PANC-1, by RT-qPCR analyses. We evaluated TRIB1, TRIB2 and TRIB3 gene expression and is represented as fold change relative to the MIA PaCa-2 cell line. We used *the CFX384 Touch Real-Time PCR Detection System* to perform the experiment and analyzed the results with the *CFX Maestro Software.*

3.5.1.2 TRIBBLES expression in Parental versus Resistant cell lines

After characterization of the parental cell lines, we assessed TRIBBLES expression in the Gemcitabine-resistant cell lines. However, during these cells' generation, we observed different emerging phenotypes of the MIA PaCa-2 cell line, which we named DR (with drug), ROU (rounder) and FUS (fusiform), as represented in Figure III.4. For PANC-1 cell line, we did not verify these events. In line with this, we also included samples from the emerging phenotypes in our analysis and evaluated TRIBBLES expression among them.

As we can observe in Figure III.20, when the resistant cell lines, MUTIR28 and MUTIR01, were rounder (ROU), after Gemcitabine treatment, we observed higher TRIB1 and TRIB2 mRNA levels, when compared with MIA PaCa-2 cell line. These results represented a fold increase of 1,6 for MUTIR28 and 1,21 for MUTIR01 in the TRIB1 mRNA levels (Figure III.20A). However, in basal conditions, MUTIR28 and MUTIR01 seemed to present lower TRIB1 expression when compared with these cells under phenotypic changes and when compared with MIA PaCa-2 cell line (0,55- and 0,41- fold decrease, respectively) (Figure III.20A). Regarding TRIB2 expression, we saw a considerable increment in its mRNA levels when cells undergo the phenotypic changes. Our data showed a fold increase of 31,4 for MUTIR28 and a fold increase of 51,0 for MUTIR01 in TRIB2 mRNA levels when compared with MIA PaCa-2 cell line (Figure III.20C). Furthermore, when MUTIR28 and MUTIR01 present a fusiform appearance (FUS) and in basal conditions, we saw a decrease in TRIB2 mRNA levels. However, in contrary to the observed in TRIB1 analyzes, the resistant cell lines MUTIR28 and MUTIR01 in normal conditions showed higher TRIB2 levels when compared with the parental cell line, MIA PaCa-2 (12,9- and 5,9- fold increase, respectively) (Figure III.20C). Respecting TRIB3 expression, we observed a decreased its mRNA levels in the majority of the emerging phenotypes (Figure III.20E).

In PANC-1 cell line we did not observe a phenotypic switch when the cells undergo Gemcitabine treatments. For that reason, in this experiment we only compared the parental cell line (PANC-1) and the resistant cell line (PUTIR23), in basal conditions. As our results showed, PANC-1 cell line present higher levels of TRIB1, TRIB2 and TRIB3, when compared with MIA PaCa-2 cell line. For PUTIR23, we verified increased levels of TRIB1 (3,53-fold increase) (Figure III.20B), but lower levels of TRIB2 (0,14-fold increase) (Figure III.20D) and TRIB3 (0,81-fold increase) (Figure III.20F), when compared with MIA PaCa-2 cell line. Overall, when comparing PANC-1 with the

corresponded derived resistant cell line, we demonstrated that PUTIR23 presented lower TRIBBLES mRNA levels.

Taken together, these data indicate that TRIB1 and, particularly, TRIB2 levels are increased in the new emerging phenotypes of the MIA PaCa-2 cell line. In fact, the TRIB2 expression profile seemed to follow the phenotypic switch that we observed, with higher mRNA levels when the cells presented a rounder and in suspension phenotype. Conversely, we saw an overall decrease or no changes in the TRIB3 mRNA levels, along the new phenotypes. For PUTIR23, we observed a decrease in all of the three TRIBBLES expression.

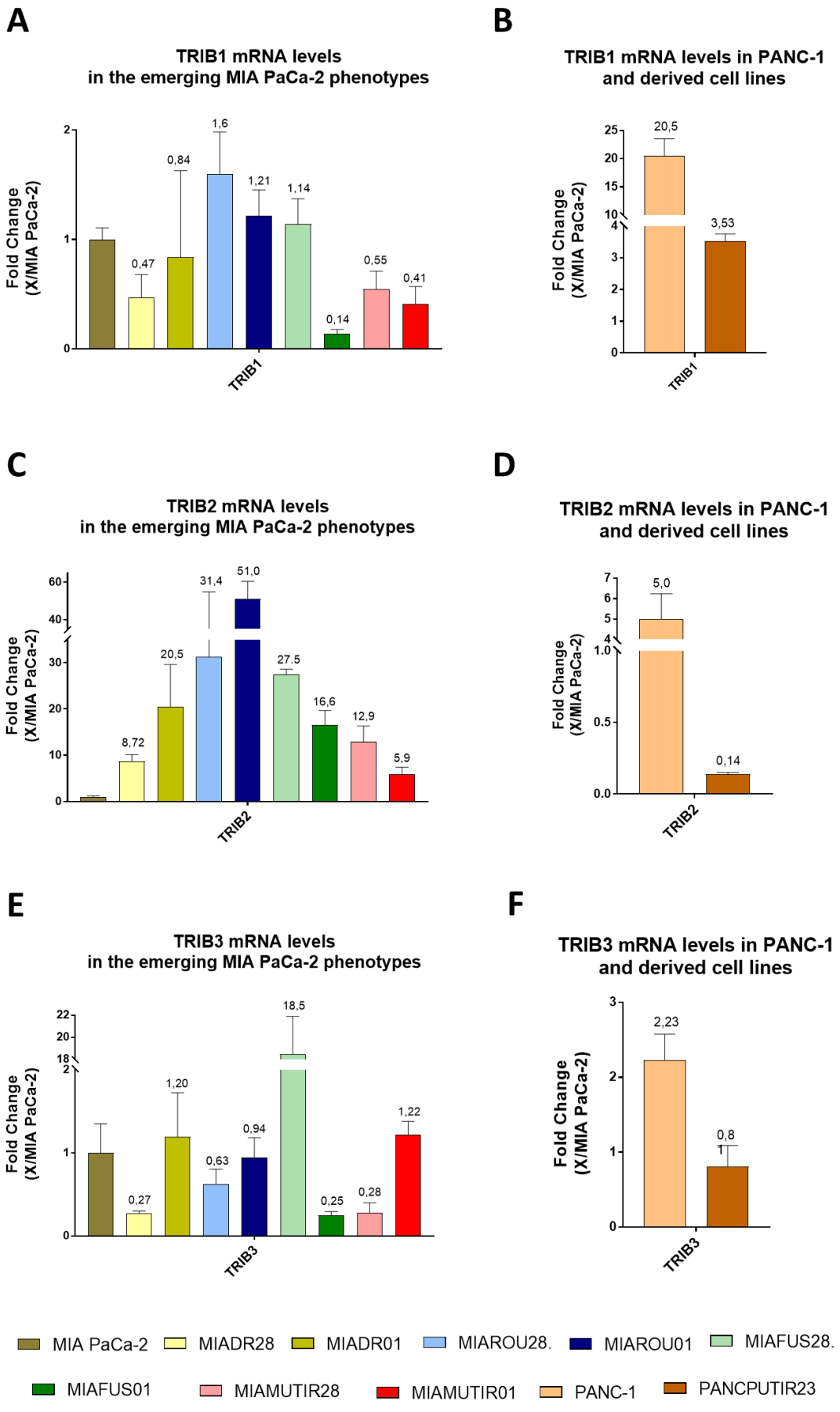
A
TRIB1 mRNA levels
in the emerging MIA PaCa-2 phenotypes
Fold Change
(X/MIA PaCa-2)
0,47
0,84
1,6
1,21
1,14
0,14
0,55
0,41
TRIB1
B
TRIB1 mRNA levels in PANC-1
and derived cell lines
Fold Change
(X/MIA PaCa-2)
20,5
3,53
TRIB1
C
TRIB2 mRNA levels
in the emerging MIA PaCa-2 phenotypes
Fold Change
(X/MIA PaCa-2)
8,72
20,5
31,4
51,0
27.5
16,6
12,9
5,9
TRIB2
D
TRIB2 mRNA levels in PANC-1
and derived cell lines
Fold Change
(X/MIA PaCa-2)
5,0
0,14
TRIB2
E
TRIB3 mRNA levels
in the emerging MIA PaCa-2 phenotypes
Fold Change
(X/MIA PaCa-2)
0,27
1,20
0,63
0,94
18,5
0,25
0,28
1,22
TRIB3
F
TRIB3 mRNA levels in PANC-1
and derived cell lines
Fold Change
(X/MIA PaCa-2)
2,23
0,8
TRIB3
MIA PaCa-2
MIADR28
MIADR01
MIAROU28.
MIAROU01
MIAFUS28.
MIAFUS01
MIAMUTIR28
MIAMUTIR01
PANC-1
PANCPUTIR23

Figure III.20. TRIBBLES mRNA levels in the newly generated Gemcitabine-resistant cell lines. To evaluate TRIBBLES contribution in the emerging resistant phenotypes, we performed an RT-qPCR analysis. We analyzed TRIB1 **(A,B)**, TRIB2 **(C,D)** and TRIB3 **(E,F)** expression patterns in all the resistant phenotypes (DR, ROU and FUS) and in the resistant cell lines in normal conditions (MUTIR28, MUTIR01 and PUTIR23). TRIBBLES gene expression is represented in fold change relative to MIA PaCa-2 cell line. We used *the CFX384 Touch Real-Time PCR Detection System* to perform the experiment and analyzed the results with the *CFX Maestro Software.*

3.5.2 TRIB2 and TRIB3 protein levels

3.5.2.1 Characterization of MIA PaCa-2 and PANC-1 cell lines

To evaluate TRIB2 and TRIB3 protein expression, we initially characterized the parental cell lines by performing a Western Blot. We used the established melanoma cell line UACC-62 as our control for endogenous expression of both TRIB2 and TRIB3 proteins. Our results demonstrated that both pancreatic cancer cell lines, MIA PaCa-2 and PANC-1, expressed less TRIB2 protein than our control cell line, UACC-62 (Figure III.21). We could not detect differences between MIA PaCa-2 and PANC-1 cell lines regarding TRIB2 protein expression. Furthermore, PANC-1 cell line showed higher levels of TRIB3 protein expression when compared with the MIA PaCa-2 cell line (Figure III.21).

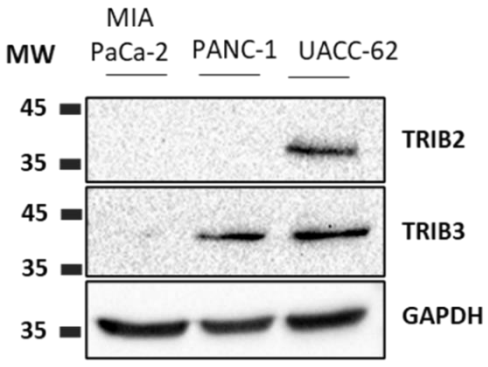

Figure III.21. Levels of TRIB2 and TRIB3 proteins in MIA PaCa-2, PANC-1, and UACC-62. We performed Western Blot analysis to determine TRIBBLES protein levels, using specific antibodies for TRIB2 and TRIB3 detection. GAPDH was used as housekeeping gene for loading control and UACC-62 cell line as a control for endogenous expression. We loaded 20 µL (3 µg/µL) of each protein sample and 3 µL of the NZY Blue Protein Marker per well in each gel. MW indicates the molecular weight of the proteins in kilodaltons (kDa), that are in the range between 35 and 45 kDa. We used 10% running gels. We detected the signal using the ChemiDoc XRS+ System (BioRad, USA) and the ImageLab software.

3.5.2.2 TRIBBLES expression in Parental vs Resistant cell lines

After generation of the Gemcitabine-resistant cell lines, we decided to evaluate TRIB2 and TRIB3 expression in these cells and in both the parental MIA PaCa-2 and PANC-1 cell lines. In our analysis we also included samples from the emerging phenotypes and evaluated TRIB2 and TRIB3 proteins expression among them.

According to our results, TRIB2 and TRIB3 expression seemed to be different in both the resistant MUTIR28 and MUTIR01 cells lines when compared to the parental cell line and to be phenotype dependent. TRIB2 protein expression was induced when cells presented a rounder phenotype (ROU) and when they attached to the plate with a fusiform shape (FUS), after a cycle of Gemcitabine treatment (Figure III.22A). Conversely, TRIB3 expression appeared to be attenuated in the drug-resistant cell lines, when compared with the parental MIA PaCa-2 cell line (Figure III.22B). However, among the emerging phenotypes, we verified the lowest expression of TRIB3 when the cells were in the ROU phenotype (Figure III.22B). These results were consistent among the two MIA PaCa-2-derived cell lines, MUTIR28 and MUTIR01.

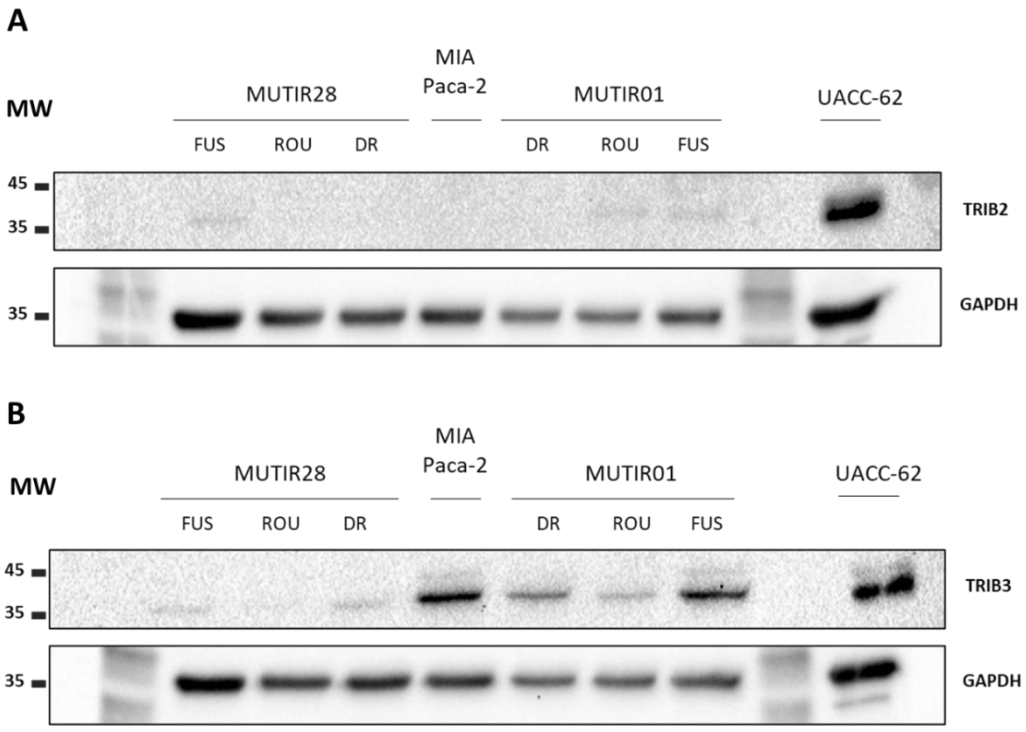

Figure III.22. TRIB2 and TRIB3 proteins expression levels in the emerging MIA PaCa-2 resistant phenotypes. MUTIR28 and MUTIR01 were submitted to Gemcitabine during treatment protocol. The emerging phenotypes of both cell lines, DR, FUS and ROU were analyzed regarding TRIB2 **(A)** and TRIB3 **(B)** protein levels. We used GAPDH as the housekeeping gene for loading control for the Western Blot analysis and UACC-62 as the control for endogenous expression of TRIBBLES. We loaded 20 µL (3 µg/µL) of each protein sample and 3 µL of the NZY Blue Protein Marker per well in each gel. MW indicates the molecular weight of the proteins in kilodaltons (kDa), that are in the range between 35 and 45 kDa. We used 10% running gels. We detected the signal using the ChemiDoc XRS+ System (BioRad, USA) and the ImageLab software.

In PANC-1 and PUTIR23 cell lines, TRIB2 protein expression remained undetectable, indicating that both of these cell lines present lower TRIB2 expression than the UACC-62 cell line (Figure III.23A). Moreover, we also observed less TRIB3 expression in PANC-1 and PUTIR23 when compared with our control. We could not detect differences in TRIB2 and TRIB3 expression between the parental and the resistant cell lines (Figure III.23B).

Overall, our results corroborate our previous RT-qPCR data. We observed higher TRIB2 protein levels in the new phenotypes for the resistant cell lines when compared with the levels for MIA PaCa-2 cell line. In fact, we could not detect TRIB2 protein expression in the parental cell line, MIA PaCa-2. Moreover, the levels of TRIB2 and TRIB3 seemed to be phenotype dependent.

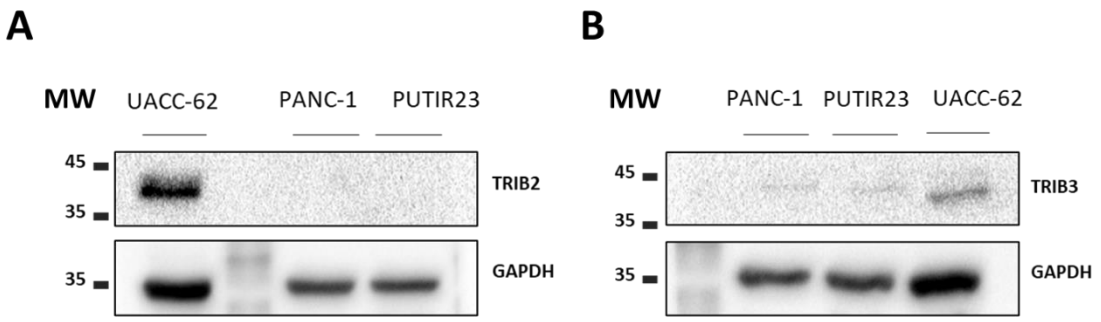

Figure III.23. TRIB2 and TRIB3 proteins expression levels in PANC-1 and PUTIR23 cell lines. To verify if TRIB2 and TRIB3 expression profiles differ between the sensitive and the resistant phenotype in PANC-1 cell line, we analyzed TRIB2 and TRIB3 expression in both of the cell lines. GAPDH was used as housekeeping gene as a control for protein loading. UACC-62 was used as control cell line for TRIB2 and TRIB3 expression. We loaded 20 µL (3 µg/µL) of each protein sample and 3 µL of the NZY Blue Protein Marker per well in each gel. MW indicates the molecular weight of the proteins in kilodaltons (kDa), that are in the range between 35 and 45 kDa. We used 10% running gels. We detected the signal using the ChemiDoc XRS+ System (BioRad, USA) and the ImageLab software.

3.5.2.3 TRIBBLES expression under Gemcitabine treatment

After the initial characterization, we compared all the cell lines in basal normal conditions and under Gemcitabine treatment. For this experiment we used the parental MIA PaCa-2 and PANC-1 cell lines and compare them with the correspondent resistant cells, MUTIR28 and MUTIR01, and PUTIR23, respectively. All these cell lines were submitted Gemcitabine treatment. Cells treated with 0,1% of DMSO were used as experimental controls.

In both situations, we could not detect TRIB2 expression in MIA PaCa-2 cell line, indicating that the Gemcitabine treatment did not induce TRIB2 protein expression by itself. However, we could detect TRIB2 in the MIA PaCa-2-derived resistant cell lines, MUTIR28 and MUTIR01, with no differences when comparing the DMSO-treated cells with the cells treated with Gemcitabine (Figure III.24A). About TRIB3 protein, it appeared to be expressed regardless to the condition (Figure III.24B).

In PANC-1 and PUTIR23 cell lines, we could not detect TRIB2 expression, and we did not see any differences in TRIB3 protein expression, when comparing the cells treated with Gemcitabine with the DMSO-treated controls (Figure III.25).

Overall, we did not observed differences in the TRIBBLES protein expression when comparing the cells treated with DMSO or the cells treated with Gemcitabine. This indicates that Gemcitabine administration did not induce TRIB2 expression. However, we could detect TRIB2 expression in both MUTIR28 and MUTIR01 resistant cell lines, regardless the experimental condition.

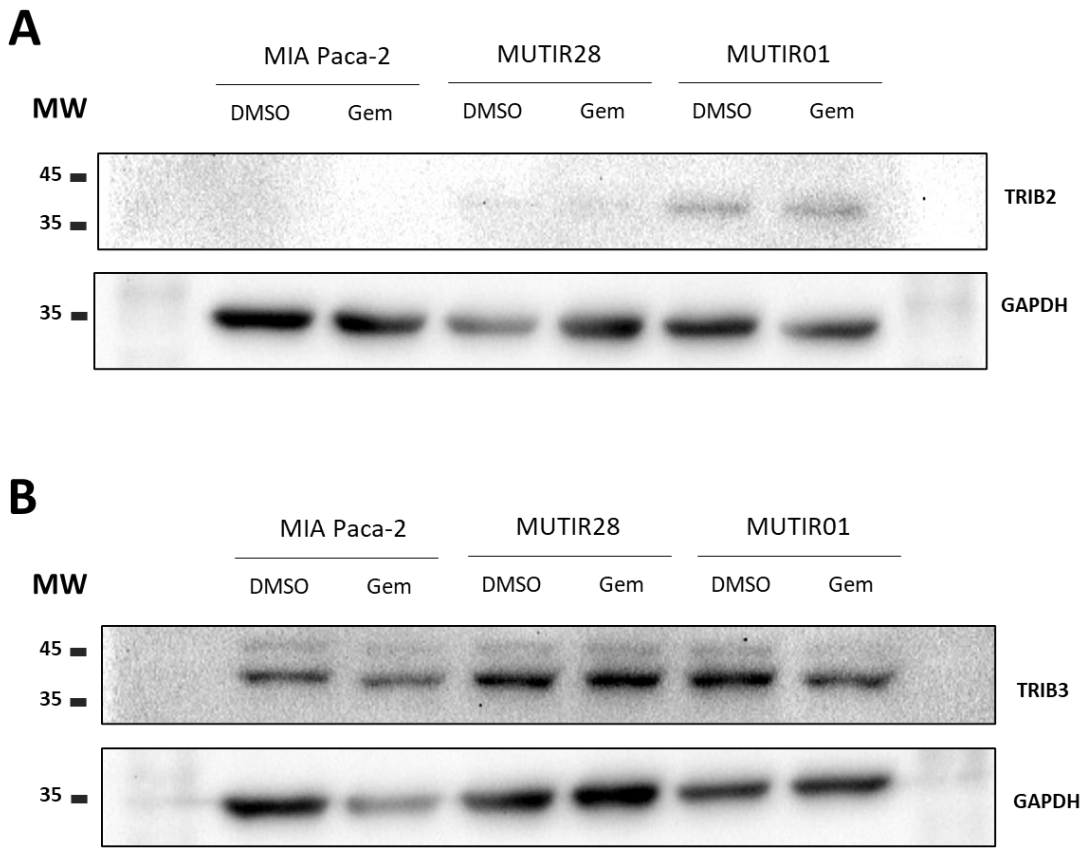

Figure III.24. TRIB2 and TRIB3 levels in MIA PaCa-2, MUTIR28 and MUTIR01 cell lines under Gemcitabine treatment. MIA PaCa-2, MUTIR28 and MUTIR01 were treated with 22nM of Gemcitabine (IC50 value for the parental cell line) and with 0,1% of DMSO. The expression of TRIB2 **(A)** and TRIB3 **(B)** proteins was evaluated for both of the conditions. The GAPDH housekeeping gene was used as loading control. We loaded 20 µL (3 µg/µL) of each protein sample and 3 µL of the NZY Blue Protein Marker per well in each gel. MW indicates the molecular weight of the proteins in kilodaltons (kDa), that are in the range between 35 and 45 kDa. We used 10% running gels. We detected the signal using the ChemiDoc XRS+ System (BioRad, USA) and the ImageLab software.

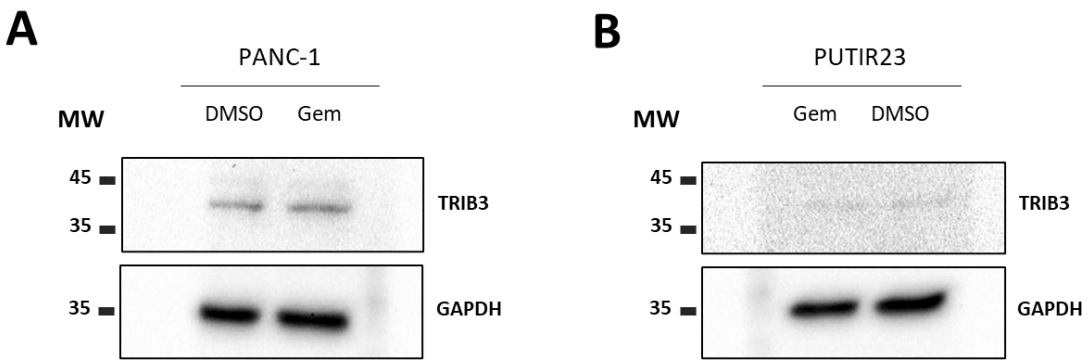

Figure III.25. TRIB2 and TRIB3 levels in PANC-1 and PUTIR23 cell lines under Gemcitabine treatment. PANC-1 and PUTIR23 were treated with 26nM of Gemcitabine and with 0,1% of DMSO. GAPDH was used as a reference gene for loading control We loaded 20 µL (3 µg/µL) of each protein sample and 3 µL of the NZY Blue Protein Marker per well in each gel. MW indicates the molecular weight of the proteins in kilodaltons (kDa), that are in the range between 35 and 45 kDa. We used 10% running gels. We detected the signal using the ChemiDoc XRS+ System (BioRad, USA) and the ImageLab software.

3.6 Epithelial to mesenchymal transition markers evaluation

As previously mentioned, we were confronted with phenotypic changes of the resistant cell lines during the Gemcitabine treatment protocol. The epithelial to mesenchymal transition (EMT) is a process that occurs when epithelial cells undergo biological changes and adopt a mesenchymal like phenotype. EMT has been characterized as an important step in cellular resistance to some drugs. To test the hypothesis that the observed reversible phenotypic switch is associated with the activation of the EMT process, we decided to evaluate some of the EMT markers expression in the cell lines.

3.6.1 EMT mRNA levels

To analyze if the cells with fibroblastic-like features undergo activation of the EMT process, we decided to evaluate EMT markers mRNA levels in all the phenotypes of MUTIR28 and MUTIR01 and in PUTIR23 cell line. For this experiment we chose *β-Catenin* as an epithelial marker and *Slug*, *Snail*, *Vimentin* and *Zeb-1* as mesenchymal markers. We also included *E-CADHERIN* and *N-CADHERIN* to our analysis, however MIA PaCa-2 and PANC-1 cell lines showed low or no expression of their respective mRNA levels.

As our results show, MUTIR28 and MUTIR01 slightly increased *β-Catenin* mRNA levels upon a cycle of Gemcitabine treatment, when comparing with the parental cell line (MIA PaCa-2 cell line). Moreover, *β-Catenin* levels of both of the resistant cell lines in basal conditions seemed to be higher than the sensitive cell line MIA PaCa-2 (Figure III.26A). When analyzing PANC-1 and its derived cell line, PUTIR23, we observed an increase in *β-Catenin* levels in the resistant cell line (Figure III.26A).

Concerning the expression of mesenchymal markers, all of the resistant cell lines, regardless of their phenotypes, showed low expression or did not express *Slug,* indicating a decrease in its mRNA levels when compared with MIA PaCa-2 cell line (Figure III.26B). We verified the same for both PANC-1 and PUTIR23 cell lines, with PUTIR23 showing higher *Slug* levels than the correspondent sensitive cell line (Figure III.26B). *Snail* and *Zeb-1* mRNA levels seemed to follow a similar expression pattern among the resistant phenotypes, with MUTIR28 and MUTIR01 showing increased levels of these genes when in the DR and ROU appearance (Figures III.26C and E). We verified a following decrease in these genes mRNA levels when the cells attached to the plate (FUS) and in their basal conditions. Regarding *Vimentin* expression, we did not observe major differences in its expression, regardless the phenotype of the resistant cell lines (Figure III.26D). However, MUTIR28 and MUTIR01 in normal conditions seemed to present higher *Vimentin* levels when compare with the sensitive MIA PaCa-2 cell line. For PUTIR23, we verified higher mRNA levels of most of the mesenchymal markers (*Snail*, *Vimentin*, *Zeb-1*) when compared with the sensitive cell line, PANC-1.

In summary, we verified that all of the resistant cell lines showed slightly higher levels of the epithelial marker, *β-Catenin*, when compared with the parental cells. Moreover, the resistant cell lines MUTIR28 and MUTIR01 showed increased mRNA levels of *Snail*, *Vimentin* and *Zeb-1* when they undergo the phenotypic changes. In basal conditions they also seemed to present higher mesenchymal marker expression than

MIA PaCa-2 cell line. Regarding PUTIR23 we observed an overall decrease in all the mesenchymal markers expression.

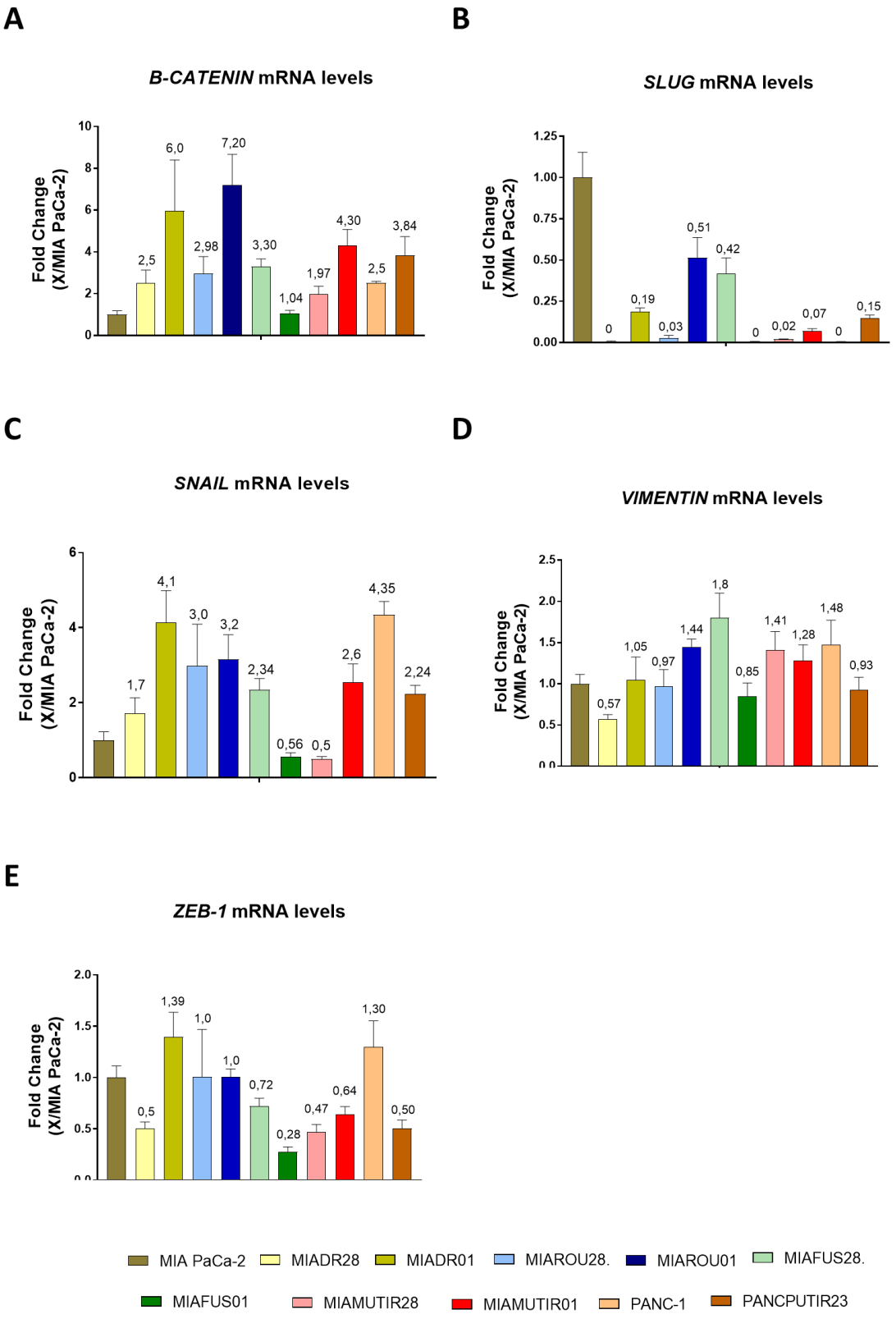

Figure III.26. Epithelial to mesenchymal markers mRNA expression levels in the Parental versus Resistant cell lines and in the emerging MIA PaCa-2 phenotypes and in PANC-1 derived resistant cell line. To analyze if the phenotypic switch could be associated with the epithelial to mesenchymal process activation, we analyzed EMT markers expression in the resistant cell lines. We evaluated B-CATENIN **(A)** as an epithelial marker and SLUG **(B)**, SNAIL **(C)**, VIMENTIN **(D)** and ZEB-1 **(E)** as mesenchymal markers. To determine gene expression, we performed an RT-qPCR analysis. Gene expression is represented in fold change relative to the expression levels detected in MIA PaCa-2 cell line. We used *the CFX384 Touch Real-Time PCR Detection System* to perform the experiment and analyzed the results with the *CFX Maestro Software.*

CHAPTER IV

DISCUSSION

4 Discussion

Despite the progress in cancer research and the development of new therapeutic approaches, there is an urgent need for new effective therapeutics to improve the clinical outcome of patients with PC. The acquired therapy resistance, developed during drug exposure, limits the success of the current oncologic treatment protocols [213] and targeting the underlying mechanisms has become a major focus of research. Understanding the mechanisms of acquired therapy resistance will contribute to the improvement of treatment protocols and ultimately to improve patient's prognosis.

In the present study, we focused on generating cell lines resistant to the current first line chemotherapeutic drug for the majority of PC patients, Gemcitabine, and the subsequent characterization of the obtained cell lines. According with previous studies on drug resistance generation [133,154,189–191,214,215], we hypothesized that chronic exposure to Gemcitabine would induce drug-resistance, characterized by phenotypic and molecular changes in the cells.

To establish the Gemcitabine-resistant cell lines we exposed the cells to consecutive cycles of increasing Gemcitabine concentrations, interspaced by recovery moments [189–191]. Our objective was to generate clinically relevant resistant models, replicating the chemotherapeutic cycles applied to cancer patients. As described by *McDermott et al. 2014*, clinical samples show low levels of resistance and, for that reason, our goal was to accomplish a 2 to 5-fold resistance level. To generate the resistant cells, we opted for two different pancreatic cancer cell lines, MIA PaCa-2 and PANC-1, described as sensitive to Gemcitabine at the nanomolar range [217–219].

Our evaluation of the IC50 values on MIA PaCa-2 and PANC-1 cells upon Gemcitabine treatment, showed that they are concordant with the literature, with IC50 values of 22nM for the MIA PaCa-2 cell line and 26nM for the PANC-1 cell line, for 72 hours of drug exposure. According to these values, we decided to start the treatment protocol with 40nM of Gemcitabine. The generation of resistant cells is a stepwise process, and for that reason we divided our work into two different temporal moments, T5 and T9 (which corresponds to 5 and 9 months after the first Gemcitabine administration).

To analyze the success of the treatment regimen, we evaluated MUTIR28 and MUTIR01 sensitivity to Gemcitabine at T5, by calculating their IC50 values. According with our results, MUTIR28 and MUTIR01 showed higher IC50 values for MUTIR28 and

MUTIR01 when compared with the parental MIA PaCa-2 cell line. These values represented a 3 and 2-fold increase for MUTIR28 and MUTIR01, respectively, when compared with the parental cell line, indicating that Gemcitabine treatment promoted changes in these cells and seemed to turn them resistant.

Moreover, in T5, we aimed to understand how the newly generated cell lines would react in terms of cell viability to high Gemcitabine doses comparing with MIA PaCa-2 cell line. To evaluate this, we exposed MIA PaCa-2, MUTIR28 and MUTIR01 to 300nM of Gemcitabine (the maximum Gemcitabine concentration at the moment) and calculated the percentage of cell viability under these conditions. Our results showed a fold change of 2,7 and 2,1 of the levels of cell viability for MUTIR28 and MUTIR01, respectively, when comparing with MIA PaCa-2 cell line. This indicates that the resistant cells tolerate higher levels of drug induced stress, and that the resistance levels maintains under these conditions. Overall, the results obtained at T5 were concordant with the development of a resistant phenotype by MUTIR28 and MUTIR01 cell lines. MUTIR28 showed the highest IC50 value between both of the resistant cells and seemed to be less affected when treated with higher Gemcitabine concentrations. MUTIR28 was the first cell line to be generated, thus this cell line underwent the greatest number of treatment cycles up to this moment (T5). This could justify the differences between MUTIR28 and MUTIR01cell lines resistance levels.

The Gemcitabine protocol used to generate resistant cell lines was finalized after 9 months of the first Gemcitabine treatment. The final cell lines IC50 values calculated for MUTIR28 and MUTIR01, represented a fold increase of 2,7 ± 1,2 and 1,4 ± 0,2, respectively, when compared with MIA PaCa-2 cell line. These values were similar to the ones calculated at T5. According with these values, MUTIR28 continued showing the highest resistance level when comparing with the sensitive cell line and with MUTIR01, with no changes verified in the resistance levels when comparing with the values calculated at T5.

Since we increased the number of treatments and their correspondent concentrations between T5 and T9, we were expecting to observe higher levels of resistance at T9. However, during the generation of resistant cells, we needed to freeze the cells and restart the treatment two and a half months later, due to the pandemic and the lockdown. As described in *McDermott et al.* 2014, freezing the cells could influence their resistance after thawing if the resistance level is not yet stable. For that reason, further experiments are crucial to evaluate the stability of the phenotype and to evaluate the effect of the freezing in the maintenance of the resistant cell lines.

Concerning PUTIR23 cell line, we saw an increase in the IC50 value of around 7 ± 1,5 times when compared to the parental PANC-1, considering three different experiments. However, PUTIR23 showed a different response profile to Gemcitabine when compared with the MIA PaCa-2 resistant cells. Despite its increased resistance, PUTIR23 seemed to behave differently in the presence of higher Gemcitabine concentrations, showing less viable cells when compared to the parental cell line. We could only observe this phenomenon in the PANC-1 derived cell line, and we are interested in studying it in the future, because it is not a feature associated with the phenotype of the resistant cells.

Chemotherapeutic drugs induce both cytostatic and cytotoxic effects in the cells. However, previous works demonstrated that the level of stress necessary for each of these events is different. The cytostatic effect, characterized by proliferation arrest, can be achieved by exposure to low concentrations of a specific drug. On the contrary, higher levels of stress and higher drug doses are necessary to induce apoptosis. Furthermore, other studies have demonstrated the important role of drug induced senescence in the chemotherapy outcome and its cytostatic effect [220]. Taken together, these findings suggest that the levels of drug induced stress are crucial to either activate senescence or the apoptosis of the cells. In addition, Gemcitabine acts in the DNA synthesis, causing DNA damage in the cells, a mechanism that is known to drive drug induced senescence [221,222].

Considering that we treated our cells with Gemcitabine and according to the role of drug induced senescence in the chemotherapy outcome, we can suggest that chronic exposure of PUTIR23 cells to this drug is increasing their basal stress levels. These could be causing lower levels of cell viability when the cells are exposed to high doses of Gemcitabine, as we verified in our results on the PUTIR23 cell line viability assays. Moreover, lower doses of Gemcitabine in cells presenting low levels of drug stress could induce a senescent phenotype and proliferation arrest, with low levels of apoptosis, which is concordant with our results in the cell viability analysis of the PANC-1 cell line These observations are very intriguing and could justify the differences that we observed for both PANC-1 and PUTIR23 cell lines response to Gemcitabine.

Moreover, the PUTIR23 cell line took longer to recover from each cycle of Gemcitabine, when compared with MUTIR28 and MUTIR01 and seemed to maintain a different appearance during the recovery process. PUTIR23 cell line showed a bigger and disperse cytoplasm with cytoplasmic extensions after two treatments with Gemcitabine. Senescent cells also undergo morphologic changes, such as increased

size and a flat appearance, with vacuoles, possible multiple nuclei, and cytoplasmic bridges formation, similar to what we observed in our cells [221,223]. According with the morphologic features of the senescent cells, our observations on the PUTIR23 cells morphology and the information mentioned on the previous paragraph, we suggest that Gemcitabine treatments could be activating the senescence of these cells. For those reasons, we suggest evaluating the senescence activation in the PUTIR23 cell line, especially when treated with Gemcitabine. To accomplish that, we could analyze the activity of β-galactosidase, the p21 and p16 proteins expression and the accumulation of high-mobility group HMGA proteins on the chromatin, which are biomarkers of cellular senescence [223–226].

However, this hypothesis does not explain the increased resistance in the PUTIR23 cell line. In fact, the ability of a cancer cell to evade drug induced senescence is associated with drug resistance and tumor progression [227]. Smaller changes in response to critical and intermediate concentrations of Gemcitabine justifies differences in the IC50 values calculated for these cells. A shift to the right in the slope of the nonlinear regression used to calculate the IC50 value, caused by the different responses at higher Gemcitabine doses, could be associated with the greater IC50 value for PUTIR23.

The IC50 value is extrapolated from a non-linear regression, which is applied to a dose response analysis plot. To understand how the resistant cells varied from the original cell line in response to a specific Gemcitabine concentration, we performed an MTT assay comparing the cell viability of the resistant versus the parental cell line viability under a specific drug concentration. Our results showed that MIA PaCa-2 and MUTIR01 cell lines showed significant decreases in their viability in response to Gemcitabine (0,69 ± 0,05 and 0,64 ± 0,07-fold changes, respectively, when compared with the DMSO-treated control). On the contrary, MUTIR28 cell line was less responsive to treatment, showing a 0,88-fold increase of the cell viability levels when compared with the DMSO-treated control. These observations were concordant with our previous results, indicating that MUTIR28 is the cell line displaying the highest level of resistance, even under low Gemcitabine concentrations.

PUTIR23 cell line did not show any differences when compared with PANC-1 cell line when treated with 26nM of Gemcitabine, indicating that both of the cell lines respond similarly to low Gemcitabine concentrations. According to our previous results, the PUTIR23 IC50 value could not reflect its response in terms of cell viability to low levels of Gemcitabine. Drug resistance is usually evaluated by cell viability assays, which allow

us to determine the sensibility/resistance of a determined cell line, when exposed to a specific compound. The most commonly cell-based assay to evaluate cell viability is the MTT assay. According to this assay principle, only living and metabolically active cells are able to reduce MTT [192,193,199,228,229]. However, the cell viability measurements with MTT assay does not allows to distinguish between cell cycle arrest and cell death.

Considering the principle of MTT assay and that we used this technique for the above experiments, we decided to complement the characterization of the resistant cell lines with a cell death experiment. The direct Gemcitabine mechanism of action is characterized by the incorporation of this compound into the DNA chain, affecting chain elongation, and inducing cell death [105,109,114]. Considering that Gemcitabine possesses a cytotoxic effect, we analyzed the Gemcitabine-induced cell death of the sensitive and resistant cells. To accomplish that, we used Trypan Blue Exclusion assay, that is based on the incorporation of Trypan Blue dye into non-viable cells [203,230,231]. According to this assay principle, viable cells would appear with a clear cytoplasm whereas non-viable/dead cells would appear with a blue stained cytoplasm [201].

As we observed, Gemcitabine administration induced higher cell death levels in MIA PaCa-2 cell line when comparing with the resistant cells. These results were calculated considering residual levels of cell death that normally occurs, treating the cells with our solvent control, DMSO. We observed lower levels of cell death for MUTIR28 when comparing with MIA PaCa-2 and MUTIR01 cell lines, at 48 hours of treatment. However, at the 72 hours treatments we did not observe differences between both the resistant cell lines. This could be associated with a lack of space for the cells to continue proliferating after 72 hours, especially the resistant ones, reaching the limit of confluence in culture, which masks the real percentage of cell death. Moreover, our results showed that Gemcitabine administration also induced higher levels of cell death in PANC-1 cell line, compared with PUTIR23 cell line at both 48- and 72-hours treatments.

Overall, exposing cells to repetitive cycles of Gemcitabine with the objective of generating resistant cells seems to induce alterations in the levels of cell death upon treatment. The cell lines presenting higher IC50 values and, for that reason, classified as resistant (MUTIR28, MUTIR01 and PUTIR23) presented lower percentage of cell death upon Gemcitabine treatment, when compared with the sensitive cells.

Taken together, the results obtained for cell viability with the MTT assay and for cell death with the Trypan Blue Exclusion assay for the same conditions (low Gemcitabine concentrations) are concordant, especially for the 72 hours timepoint. In fact, we observed better results for all the MTT assays when the cells were exposed for

72 hours instead of 48 hours. This could be associated with the cells doubling time and consequent incorporation rate of Gemcitabine.

Comparing both the experiments, we observed cell viability decreases of 31%, 11%, 36%, 22% and 26% and cell death levels of 20%, 12%, 9%, 27% and 23% for MIA PaCa-2, MUTIR28, MUTIR01, PANC-1 and PUTIR23, respectively. These values indicated that 11% of the decrease in the cell viability for MIA PaCa-2 might be due to cell cycle arrest, as well as around 27% of the decrease in the cell viability levels of MUTIR01. To the remaining MUTIR28, PANC-1 and PUTIR23 cell lines, the cell viability and cell death values are similar, suggesting that the total decrease in the levels of cell viability might be due to cell death. However, more cell death experiments need to be performed in all of the cell lines to take further conclusions.

During the treatments of the cell lines, we observed phenotypic changes on cells exposed to consecutive cycles of Gemcitabine. As we observed, after a cycle of Gemcitabine exposure, the resistant cells switch their appearance. After drug removal, the cells presented a rounder phenotype and were in suspension. Conversely to what happens normally with these cell lines, that attach to the plate in around 12 hours, they remained around 5 days in suspension, before attach to the culture surface with a fibroblastic and spindle like morphology.

A similar phenomenon was previously observed in other studies [152–154,232]. They also detected morphological changes in the Gemcitabine resistant cell lines, with cells showing elongated and fibroblastic like features. However, less is known about the rounder morphology that we observed. In fact, in the studies where the authors report morphologic changes on the resistant cells [152–154,232,233], they did not included recovery periods between the cycles of Gemcitabine exposure. In line with this, our study contributed to complement what is already known about the phenotypic switch process in the pancreatic resistant cell lines.

As described by *Z. Wang et al. 2009,* the cell ability to attach and detach to different places is a hallmark of the migration capacity of these cells. Considering the morphological changes that we observed and the ability of our cells to maintain longer periods in suspension, we analyzed their migration ability by performing Wound-Healing Migration assays. Previous studies showed that Gemcitabine resistant cell lines are frequently associated with higher migration ability [152,153,232].

According to our results, the MIA PaCa-2 derived resistant cell lines, MUTIR28 and MUTIR01, showed a surprisingly decreased migration ability when compared with the parental cell line. As mentioned above, we were expecting to observe higher levels

of migration on the resistant cells [152,153,232]. On the contrary, we verified an increase in the wound closure rate in PUTIR23 cell line. Differences in the resistance levels of MUTIR28, MUTIR01 and PUTIR23 could be contributing to these discrepancies. Lower resistance levels could be correlated with lower levels of aggressiveness and impaired migration ability, while higher resistance levels are associated with increased invasion and migration capacity. Our results showed PUTIR23 with the greatest resistance levels (IC50 value of 141nM), when comparing with the MIA PaCa-2 derived cell lines. Additional experiments comparing non-treated resistant cells and Gemcitabine treated cells would help us to understand if an increase in migration could be induced by external stress.

Actually, the fibroblastic and mesenchymal phenotype observed has been associated with Gemcitabine resistance and the activation of the EMT process in different cancer types [147,151,154,232–236].

In order to understand if these phenotypic changes were correlated with the activation of the EMT process in our cells, we evaluated the mRNA expression of epithelial and mesenchymal markers. For both MIA PaCa-2 and PANC-1 derived cell lines we observed a small increase in the *β-Catenin* mRNA levels. Previous studies demonstrated that *β-Catenin* activation by nuclear translocation is associated with EMT induction in resistant cells, with no significant differences observed in its total levels. *β-Catenin* can also function as a transcription factor when in the nucleus, activating the transcription of genes associated with migration and invasion [152,153]. For the above reasons, we aim to analyze *β-Catenin* cellular localization and phosphorylation status at the protein level.

Regarding the expression of the mesenchymal markers, we expected to observe higher levels of *Slug*, *Snail*, *Zeb-1* and *Vimentin*, since these transcription factors are associated with the transcription of genes related with the mesenchymal phenotype [147,153,154,232,234]. As our results show, we observed a general decrease in *Slug* expression for the MIA PaCa-2 cell lines and no significant differences for the PANC-1 derived cell line. Conversely, we observed an increase in both *Snail* and *Zeb-1* mRNA levels, correlated with the administration of a treatment cycle and the phenotypic switch in the MIA PaCa-2 derived cell lines. In the PUTIR23 cell line we saw a decrease expression of *Snail* and *Zeb-1*. Regarding *Vimentin* expression, we did not see significant changes in its transcriptional levels.

In conclusion, the increased levels of *Snail* and *Zeb-1* observed in the cells that undergo the phenotypic switch are associated with higher migration and invasion ability

of the MIA PaCa-2 derived cell lines and the activation of EMT process. These results are concordant with the new morphologies that we observed for these cells, but not with our results on the Migration Assay since we did not see higher migration ability of these cells. To complement our study, we aim to analyze these markers expression at the protein level for further conclusions in the EMT activation.

According to our results for PUTIR23 cell line, the decrease in the mRNA levels of mesenchymal markers could be associated with the fact that this cell line did not undergo the morphologic changes that we observed for the remaining resistant cells and that corresponds with the moment where we observed the increased mesenchymal markers. Moreover, we need to evaluate if changes in the expression of these markers are induced upon Gemcitabine treatment of these cells

Previous works from our lab and others have demonstrated an association between high *Tribbles pseudokinase homologue 2* and decreased *Tribbles pseudokinase homologue* 3 expression with cancer progression and resistant phenotypes in other cancers. The overexpression of TRIB2 contributes to the malignance and progression of a diversity of cancer types, such as melanoma, glioblastoma and colorectal cancer [168–170,175,225,237–239]. Moreover, overexpression of TRIB2 has been identified as important driver of drug resistance, being associated with the activation of the PI3K/AKT signaling pathway [176,179,238,240–242]. On the other hand, the *Tribbles pseudokinase homologue 3* (TRIB3) has been associated with apoptotic signaling and the inhibition of survival pathways. Higher expression of TRIB3 is associated with lower tumorigenesis ability, by inhibition of AKT activation [181–184].

Since both of this pseudokinases have important roles in resistance and apoptosis, we decided to evaluate TRIBBLES expression in the sensitive and Gemcitabine resistant cell lines. According to our results, the mRNA levels of TRIB2 are highly increased in the MIA PaCa-2 resistant cell lines, especially when these cells undergo the phenotypic switch and where in the DR and ROU phenotypes. For TRIB3 we observed an overall decreased expression, when comparing the resistant cells with MIA PaCa-2 cell line. The PANC-1 derived cell line, PUTIR23, showed a decrease in the three TRIBBLES mRNA expression.

We also evaluated TRIB2 and TRIB3 proteins expression. This allowed us to evaluate if the changes observed at the mRNA level are also present at the protein level, the effector molecule of these protein kinases. Our experiments for protein levels detection revealed similar results when compared with the RT-qPCR data. We observed higher TRIB2 expression, and lower TRIB3 protein levels associated with the resistant

phenotypes. Both TRIB2 and TRIB3 protein seemed to be dependent on the phenotype of the resistant.

Taken together, these results are concordant with the role of TRIB2 in AKT signaling activation, tumorigenesis and with its contribution on driving drug resistance. Moreover, the TRIB3 decreased expression in the resistant cells could be related with enhanced signaling by survival pathways, no longer inhibited by TRIB3 phosphorylation, such as the AKT signaling. Furthermore, we also conclude that Gemcitabine administration is not causing the changes of TRIB2 and TRIB3 protein levels by itself. Overall, our findings indicate that chronic exposure to Gemcitabine generated a drug resistant phenotype, which is associated with higher levels of TRIB2 and an impaired TRIB3 expression. The chronic exposure to Gemcitabine induced changes in mRNA and protein levels of TRIBBLES, that might be causing or be a cause of the resistant phenotype.

Importantly, the only publication describing the role of TRIB2 in PC, associates higher levels of TRIB2 with cancer progression, poor prognosis and migration and invasion ability [172]. All these features are associated with our results on the resistance phenotype and the phenotypic switch that we observed in the generated resistant cell lines. Furthermore, TRIB2 overexpression has been associated with the somatic cells reprogramming and self-renewal ability of stem cells [169]. Additionally, the Gemcitabine induced stemness of PC cells was already described and the authors suggested that it is possibly associated with drug resistance [243,244]. In fact, previous works demonstrated that Gemcitabine resistant PC cells express stemness and EMT markers [245]. According with this literature, Gemcitabine is also able to induce the appearance of Cancer Stem Cells (CSC) in PC, with the cells presenting different morphology, with increased ability to form spheres [150,243,245].

Our results are in line with this literature in several aspects. First, we observed morphologic changes that are concordant with the changes related on the EMT process, and the appearance of a new rounder phenotype, similar to the one described for CSCs. Second, we detected higher *Snail* and *Zeb-1 mRNA* levels in the resistant cells that underwent the morphologic changes, which is associated with the EMT activation.

Considering our results and the literature, we can suggest that our resistant cells undergo a reprogramming process when stimulated by Gemcitabine, driving by TRIB2 signaling. Further evaluation of stemness markers in our cells could contribute to unveil the mechanism by which TRIB2 could be contributing to the resistant phenotype. To accomplish that we could perform experiments to determine the expression of tumor

stem markers in the resistant cells, when exposed to Gemcitabine. Previous studies demonstrated an important role of CD24, CD44, CD133 as stemness markers, and the role of Bmi1, Nanog, and SOX2 has stemness associated genes in PC [243,245].

As previously mentioned, both TRIB2 and TRIB3 seem to interfere with the AKT signaling [176,179,182,183]. Moreover, the PI3K/AKT signaling pathway, one of the most mutated pathways in cancer, is related with metabolic changes, survival, and cell proliferation [246]. The PI3K/AKT signaling pathway induces the EMT process, a relevant phenomenon in our study and drug resistance. This can happen by direct activation of the integrin-linked kinase (ILK) which downregulates E-cadherin or cooperation with other signaling pathways, such as TGF-β, e NF-κβ and Wnt/β-catenin pathways [247].

The PI3K/AKT pathway is also frequently associated with the inactivation of FOXO proteins [178,248,249]. The phosphorylation of FOXO transcription factors by AKT, results in their sequestration in the cells cytoplasm, inhibiting their target genes expression. FOXOs play an important role in apoptosis, drug-induced cell death and drug response, being considered tumor suppressors in different cancer types [249–251]. Interestingly, both TRIB2 and TRIB3 proteins have been associated with FOXOs modulation [168,175,180,184].

In fact, the AKT regulation of MYC induces the expression of important factors for purine and pyrimidine synthesis [252]. As previously mentioned, Gemcitabine is a pyrimidine analogue and compete with nucleotides in the DNA synthesis [105]. Previous studies in other cancer types have demonstrated c-MYC as an important driver of drug resistance ad apoptosis inhibition [253–255]. With these observations, it would be very interesting to analyze MYC expression in our resistant models. This would allow us to evaluate if the network TRIB2-AKT-MYC could be increasing the nucleotides pool in the cells, that competes with Gemcitabine in the DNA incorporation, acting like a resistance mechanism.

In conclusion, understand the stability of the resistant phenotype and the role of TRIB2 and TRIB3 in our resistant model is crucial to understand the resistance mechanisms. We aim to analyze if the inversion of the TRIB2 and TRIB3 protein levels restores the sensitivity of the pancreatic cancer cells to Gemcitabine and by which mechanisms are they contributing to this resistance. As previously mentioned in the previous paragraphs, we suggest that PI3K/AKT signaling pathway is possibly contributing (via TRIB2 activation) in the activation of several pathways, associated with survival, proliferation, aggressiveness, EMT activation and drug resistance.

CHAPTER V

CONCLUSION

5 Conclusion

The chronic exposure of pancreatic cancer sensitive cell lines, MIA PaCa-2 and PANC-1 to Gemcitabine, a chemotherapeutic drug used in PC treatment, induced the development of drug resistance in these cells. Similar to what happens in the clinic, our results showed that the administration of consecutive cycles of Gemcitabine for 9 months, interspaced by recovery periods, decreased the sensitivity of the exposed cell lines to the drug.

The MIA PaCa-2 derived cell lines, MUTIR28 and MUTIR01, showed a 2,7 ± 1,2 and 1,4 ± 0,2-fold increase in their IC50 values, respectively. For PANC-1 derived cell line, PUTIR23, we observed a 7 ± 1,5-fold increase in its IC50. These data shows that we successfully achieved our initial goal, with the generation of clinically relevant resistant cell lines, that will contribute to study the resistance mechanisms.

According to the characterization of the resistant cell lines, we observed an increase in the cell viability of MUTIR28 and MUTIR01 compared to the parental cell line MIA PaCa-2 cells, upon exposure to Gemcitabine. Moreover, the resistant cells showed a decrease in the Gemcitabine-induced cell death levels. These results are concordant with the development of a resistant phenotype. In the case of the PANC-1 and PUTIR23 cell lines, despites the differences in their IC50 values, they showed no significant changes in the levels of cell viability and cell death when exposed to lower doses of Gemcitabine.

Our results on the drug-response evaluation of PANC-1 and PUTIR23 cell lines also showed lower cell viability levels on the resistant cell line, when compared with the parental cell line, when exposed to high doses of Gemcitabine. These findings indicate that PUTIR23 cell line is less tolerant to high doses of Gemcitabine than PANC-1 cell line. According with our findings and with previous works, we suggest that this could be an effect of the chronic exposure to Gemcitabine [220–222]. We exposed PUTIR23 to consecutive cycles of treatment that possibly increased the levels of cell stress, influencing the therapeutic outcome. Conversely, PANC-1 cell line was not subjected to the Gemcitabine cycles, being only exposed momentarily to the drug. According to the literature, low levels of drug exposure are able to induce senescence in the cells, while high doses of the drug are required to induce apoptosis, which is concordant with our results for both of these cell lines. Moreover, we also observed a different morphology of

the PUTIR23 cell line after Gemcitabine exposure, with enlarge cytoplasm and extensions, which could also be associated with a senescence activation [220–222].

We need to test this new hypothesis by analyzing the levels of stress in these cell lines in two different conditions, normal conditions and with Gemcitabine administration. Moreover, we need to evaluate if Gemcitabine induces the senescence of PANC-1 cells and if it contributes to the results that we described above.

During the treatment protocol, we observed different phenotypes and morphologies in MUTIR28 and MUTIR01 cell lines. Similar observations were made in previous studies and the authors correlated these findings with the activation of the EMT process and development of drug resistance [147,151,154,232–236]. Besides the changes from an epithelial to a fusiform morphology, we observed an intermediary step, with the cells presenting a rounder and in suspension phenotype, while viable. Our work contributed with this finding to complement what was already known about the phenotypic switch in the resistant cells.

As mentioned above, the EMT process was previously indicated as a cause for the phenotypic switch. For that reason, we evaluated if its activation is inducing the morphologic changes in the resistant cells and if it is associated with the resistant phenotype. The EMT process involves the activation of a set of genes at the mRNA and protein level. Our RT-qPCR results on the mRNA levels expression of EMT related genes revealed an interesting pattern in *Slug* and *Zeb*-1 expression when the resistant cells undergo the phenotypic switch. Both *Slug* and *Zeb*-1 showed an increase expression when the cells undergo a cycle of Gemcitabine and go through the phenotypic switch, with their levels decreasing again when the cells attach to the plate and showed a fusiform morphology. Our data from the analysis of *β-Catenin*, *Snail* and *Vimentin* were not conclusive and showed no significant differences. We were able to conclude that *Slug* and *Zeb*-1 seem to be associated with the phenotypic switch, however we need to further analyze the EMT activation process, especially at the protein level.

Regarding the migration ability of the resistant cell lines, we observed a significant decrease in MUTIR28 and MUTIR01 cell lines. According to the literature, we were expecting to observe an increased migration capacity in the resistant cells, which we did not verified. Surprisingly, for PUTIR23 we observed higher capacity for wound closure. Nonetheless, these differences in the resistant cells should be evaluated under Gemcitabine treatment, to analyze if the drug induced stress could contribute to activate this process, associated with tumor progression and metastasis.

Because TRIB2 is part of a wider family of proteins that comprehends TRIB3 and TRIB1, we analyzed the levels of TRIB3 protein by western blot. Our treatment regimen increased TRIB2 and decreased TRIB3 protein levels in the MIA PaCa-2 derived cell lines. We were able to associate an increased TRIB2 expression with the resistant phenotype and not with the parental cell line, suggesting that Gemcitabine chronic exposure of these cells increased their TRIB2 levels. However, Gemcitabine administration by itself did not induce these changes, suggesting that increased expression of TRIB2 in the resistant cells is related to the resistance mechanism itself.

In conclusion, we were able to confirm our initial hypothesis that Gemcitabine chronic exposure develops drug resistance and that TRIB2 is associated with the resistant phenotype. We were able to generate clinically relevant resistance models through chronic exposure to Gemcitabine and verified important phenotypic and mechanistic changes associated with this resistance. Importantly, we were able to generate crucial tools for drug resistance research on pancreatic cancer.

Overall, our study provided novel information that could contribute to understand the mechanisms behind pancreatic cancer resistance to Gemcitabine, complementing previous studies. We demonstrated the importance of the treatment protocol chosen and the relevance of the morphologic switch in the resistant cells. Finally, we emphasize the role of TRIBBLES proteins in drug resistance and demonstrated that the increased TRIB2 expression in the resistant cells could contribute to Gemcitabine resistance in our model.

CHAPTER VI

FUTURE PERSPECTIVES

6 Future Perspectives

We generated resistant cell lines and suggested some mechanisms for the resistance in pancreatic cancer. However, some questions remain to be answer. Firstly, we would like to evaluate the resistance levels of our cells overtime. Our study was too short to understand the long-term durability of this phenotype, and if it is dependent of constant Gemcitabine administration.

Beyond that, we aim to unveil the role of TRIB2 and TRIB3 in the resistance phenotype and in its maintenance. Are TRIB2 overexpression and/or TRIB3 downregulation a cause or a consequence of the resistant phenotype? According to the literature we have evidence that these changes could be provoked by chronic exposure to Gemcitabine, contributing to the resistance phenotype. Experiments reverting these proteins expression, such as abrogation of TRIB2 levels and overexpression of TRIB3 should be performed to evaluate if they reverse the resistance in these cells and restores Gemcitabine sensitivity.

Furthermore, it is possible that there are multiple factors contributing to the resistant phenotype. For example, we clearly see different phenotypes depending on the original cell line from which the resistant cells were derived. According to the literature, it is possible that the activation of EMT could be contributing to the resistant phenotype in these cells. However, we need to evaluate the expression of the EMT markers at the protein level to further conclusions in its contribution.

To complement and test the relevance of our findings, it would be very interesting to use an *in vivo* model to extend our study, evaluating the tumorigenic potential of these cells and investigate if they can develop Gemcitabine resistant tumors. An orthotopic tumor model could allow to determine the contribution of tumor heterogeneity and the tumor microenvironment to therapy resistance.

Finally, we aim to understand the impact and clinical relevance of TRIB2 and TRIB3 expression in pancreatic cancer patients. We suggest an analysis of TRIBBLES expression by comparing tumor *versus* normal tissues of PC patients using the data available in different public databases. This evaluation and its association with the clinical records of PC patients, such as their treatment protocols, could contribute to improve the treatments regimens of these patients in the future and improve their prognosis.

CHAPTER VII

BIBLIOGRAPHY

7 Bibliography

1. Sung, H. *et al.* Global Cancer Statistics 2020: GLOBOCAN Estimates of Incidence and Mortality Worldwide for 36 Cancers in 185 Countries. *CA. Cancer J. Clin.* **71**, 209–249 (2021).
2. Hanahan, D. & Weinberg, R. A. Hallmarks of cancer: The next generation. *Cell* vol. 144 646–674 (2011).
3. You, J. S. & Jones, P. A. Cancer Genetics and Epigenetics: Two Sides of the Same Coin? *Cancer Cell* vol. 22 9–20 (2012).
4. Curtius, K., Wright, N. A. & Graham, T. A. Evolution of premalignant disease. *Cold Spring Harb. Perspect. Med.* **7**, 19 (2017).
5. Weinberg, R. A. *The Biology of Cancer: Second Edition*. (Garland Science, 2013).
6. Vogelstein, B. *et al.* Cancer genome landscapes. *Science* vol. 340 1546–1558 (2013).
7. Alexandrov, L. B. *et al.* Signatures of mutational processes in human cancer. *Nature* **500**, 415–421 (2013).
8. Peters, J. M. & Gonzalez, F. J. The Evolution of Carcinogenesis. *Toxicol. Sci.* **165**, 272–276 (2018).
9. Michor, F., Iwasa, Y. & Nowak, M. A. Dynamics of cancer progression. *Nature Reviews Cancer* vol. 4 197–205 (2004).
10. Stratton, M. R., Campbell, P. J. & Futreal, P. A. The cancer genome. *Nature* vol. 458 719–724 (2009).
11. Deans, C. & Maggert, K. A. What do you mean, “Epigenetic”? *Genetics* **199**, 887–896 (2015).
12. Holliday, R. Epigenetics: An overview. *Developmental Genetics* vol. 15 453–457 (1994).
13. Wu, C. T. & Morris, J. R. Genes, genetics, and epigenetics: A correspondence. *Science* vol. 293 1103–1105 (2001).
14. Feinberg, A. P., Koldobskiy, M. A. & Göndör, A. Epigenetic modulators, modifiers

and mediators in cancer aetiology and progression. *Nature Reviews Genetics* vol. 17 284–299 (2016).

15. Feinberg, A. P., Ohlsson, R. & Henikoff, S. The epigenetic progenitor origin of human cancer. *Nature Reviews Genetics* vol. 7 21–33 (2006).

16. Rawla, P., Sunkara, T. & Gaduputi, V. Epidemiology of Pancreatic Cancer: Global Trends, Etiology and Risk Factors. *World J. Oncol.* **10**, 10–27 (2019).

17. Ferlay, J., Partensky, C. & Bray, F. More deaths from pancreatic cancer than breast cancer in the EU by 2017. *Acta Oncol. (Madr).* **55**, 1158–1160 (2016).

18. Siegel, R. L., Miller, K. D. & Jemal, A. Cancer statistics, 2020. *CA. Cancer J. Clin.* **70**, 7–30 (2020).

19. Cancer Facts & Figures 2020 | American Cancer Society. https://www.cancer.org/research/cancer-facts-statistics/all-cancer-facts-figures/cancer-facts-figures-2020.html.

20. ESMO. What is Pancreatic Cancer ? Let us answer some of your questions. *Eur. Soc. Med. Oncol.* 1–55 (2018).

21. Ilic, M. & Ilic, I. Epidemiology of pancreatic cancer. *World Journal of Gastroenterology* vol. 22 9694–9705 (2016).

22. Bray, F. *et al.* Global cancer statistics 2018: GLOBOCAN estimates of incidence and mortality worldwide for 36 cancers in 185 countries. *CA. Cancer J. Clin.* **68**, 394–424 (2018).

23. Fearon, E. R. & Vogelstein, B. A genetic model for colorectal tumorigenesis. *Cell* vol. 61 759–767 (1990).

24. Hruban, R. H., Goggins, M., Parsons, J. & Kern, S. E. Progression model for pancreatic cancer. *Clinical Cancer Research* vol. 6 2969–2972 (2000).

25. Cubilla, A. L. & Fitzgerald, P. J. Morphological Lesions Associated with Human Primary Invasive Nonendocrine Pancreas Cancer. *Cancer Res.* **36**, 2690–2698 (1976).

26. Koorstra, J. B. M., Hustinx, S. R., Offerhaus, G. J. A. & Maitra, A. Pancreatic carcinogenesis. *Pancreatology* **8**, 110–125 (2008).

27. Grant, T. J., Hua, K. & Singh, A. Molecular Pathogenesis of Pancreatic Cancer. in *Progress in Molecular Biology and Translational Science* vol. 144 241–275

(Elsevier B.V., 2016).

28. Hruban, R. H. *et al.* K-ras oncogene activation in adenocarcinoma of the human pancreas: A study of 82 carcinomas using a combination of mutant-enriched polymerase chain reaction analysis and allele-specific oligonucleotide hybridization. *Am. J. Pathol.* **143**, 545–554 (1993).

29. Almoguera, C. *et al.* Most human carcinomas of the exocrine pancreas contain mutant c-K-ras genes. *Cell* **53**, 549–554 (1988).

30. Wei, S. *et al.* Patterns of K-ras codon 12 and 13 mutations found in pancreatic adenocarcinoma of 30 Chinese patients by microdissection, PCR and direct sequencing. *J. Gastroenterol. Hepatol.* **20**, 67–72 (2005).

31. Collins, M. A. *et al.* Oncogenic Kras is required for both the initiation and maintenance of pancreatic cancer in mice. *J. Clin. Invest.* **122**, 639–653 (2012).

32. Vatansever, S., Erman, B. & Gümüş, Z. H. Oncogenic G12D mutation alters local conformations and dynamics of K-Ras. *Sci. Rep.* **9**, 1–13 (2019).

33. Jiang, W. *et al.* Precise and efficient silencing of mutant krasG12D by CRISPR-CasRx controls pancreatic cancer progression. *Theranostics* **10**, 11507–11519 (2020).

34. Calhoun, E. S. *et al.* BRAF and FBXW7 (CDC4, FBW7, AGO, SEL10) mutations in distinct subsets of pancreatic cancer: Potential therapeutic targets. *Am. J. Pathol.* **163**, 1255–1260 (2003).

35. Witkiewicz, A. K. *et al.* Whole-exome sequencing of pancreatic cancer defines genetic diversity and therapeutic targets. *Nat. Commun.* **6**, 1–11 (2015).

36. Mann, K. M., Ying, H., Juan, J., Jenkins, N. A. & Copeland, N. G. KRAS-related proteins in pancreatic cancer. *Pharmacology and Therapeutics* vol. 168 29–42 (2016).

37. Davies, H. *et al.* Mutations of the BRAF gene in human cancer. *Nature* **417**, 949–954 (2002).

38. Day, J. D. *et al.* Immunohistochemical evaluation of HER-2/neu expression in pancreatic adenocarcinoma and pancreatic intraepithelial neoplasms. *Hum. Pathol.* **27**, 119–124 (1996).

39. Satoh, K. *et al.* An immunohistochemical study of the c-erbB-2 oncogene product in intraductal mucin-hypersecreting neoplasms and in ductal cell carcinomas of

the pancreas. *Cancer* **72**, 51–56 (1993).

40. Yamao, K. *et al.* A mucous histochemical and immunohistochemical study of precancerous and neoplastic lesions in the human pancreas. *Int. J. Pancreatol.* **14**, 37–44 (1993).

41. Akiyama, T., Sudo, C., Ogawara, H., Toyoshima, K. & Yamamoto, T. The product of the human c-erbB-2 gene: A 185-kilodalton glycoprotein with tyrosine kinase activity. *Science (80-.).* **232**, 1644–1646 (1986).

42. Slamon, D. J. *et al.* Human breast cancer: Correlation of relapse and survival with amplification of the HER-2/neu oncogene. *Science (80-.).* **235**, 182–191 (1987).

43. Yonemura, Y. *et al.* Evaluation of Immunoreactivity for erbB-2 Protein as a Marker of Poor Short Term Prognosis in Gastric Cancer. *Cancer Res.* **51**, 1034–1038 (1991).

44. Yamano, M. *et al.* Genetic progression and divergence in pancreatic carcinoma. *Am. J. Pathol.* **156**, 2123–2133 (2000).

45. Wilentz, R. E. *et al.* Inactivation of the p16 (INK4A) tumor-suppressor gene in pancreatic duct lesions: Loss of intranuclear expression. *Cancer Res.* **58**, 4740–4744 (1998).

46. Zhao, R., Choi, B. Y., Lee, M. H., Bode, A. M. & Dong, Z. Implications of Genetic and Epigenetic Alterations of CDKN2A (p16INK4a) in Cancer. *EBioMedicine* vol. 8 30–39 (2016).

47. Moskaluk, C. A., Hruban, R. H. & Kern, S. E. p16 and K-ras gene mutations in the intraductal precursors of human pancreatic adenocarcinoma. *Cancer Res.* **57**, 2140–2143 (1997).

48. Sigal, A. & Rotter, V. Oncogenic mutations of the p53 tumor suppressor: The demons of the guardian of the genome. *Cancer Research* vol. 60 6788–6793 (2000).

49. Levine, A. J. p53, the cellular gatekeeper for growth and division. *Cell* vol. 88 323–331 (1997).

50. Zhao, M., Mishra, L. & Deng, C. X. The role of TGF-β/SMAD4 signaling in cancer. *Int. J. Biol. Sci.* **14**, 111–123 (2018).

51. Liu, F. SMAD4/DPC4 and pancreatic cancer survival. Commentary re: M. Tascilar et al., The SMAD4 protein and prognosis of pancreatic ductal adenocarcinoma.

Clin. Cancer Res., 7: 4115-4121, 2001. *Clinical Cancer Research* vol. 7 3853–3856 (2001).

52. Yoshida, K. & Miki, Y. Role of BRCA1 and BRCA2 as regulators of DNA repair, transcription, and cell cycle in response to DNA damage. *Cancer Science* vol. 95 866–871 (2004).

53. Wilentz, R. E. *et al.* Loss of expression of Dpc4 in pancreatic intraepithelial neoplasia: Evidence that DPC4 inactivation occurs late in neoplastic progression. *Cancer Res.* **60**, 2002–2006 (2000).

54. Goggins, M., Hruban, R. H. & Kern, S. E. BRCA2 is inactivated late in the development of pancreatic intraepithelial neoplasia: Evidence and implications. *Am. J. Pathol.* **156**, 1767–1771 (2000).

55. Makohon-Moore, A. & Iacobuzio-Donahue, C. A. Pancreatic cancer biology and genetics from an evolutionary perspective. *Nature Reviews Cancer* vol. 16 553–565 (2016).

56. Haeberle, L. & Esposito, I. Pathology of pancreatic cancer. *Translational Gastroenterology and Hepatology* vol. 4 (2019).

57. Reichert, M., Saur, D., Hamacher, R., Schmid, R. M. & Schneider, G. Phosphoinositide-3-kinase signaling controls S-phase kinase-associated protein 2 transcription via E2F1 in pancreatic ductal adenocarcinoma cells. *Cancer Res.* **67**, 4149–4156 (2007).

58. Schönleben, F. *et al.* PIK3CA mutations in intraductal papillary mucinous neoplasm/carcinoma of the pancreas. *Clin. Cancer Res.* **12**, 3851–3855 (2006).

59. Asano, T. *et al.* The PI 3-kinase/Akt signaling pathway is activated due to aberrant Pten expression and targets transcription factors NF-κB and c-Myc in pancreatic cancer cells. *Oncogene* **23**, 8571–8580 (2004).

60. Di Magliano, M. P. *et al.* Hedgehog/Ras interactions regulate early stages of pancreatic cancer. *Genes Dev.* **20**, 3161–3173 (2006).

61. Taipale, J. & Beachy, P. A. The Hedgehog and Wnt signalling pathways in cancer. *Nature* vol. 411 349–354 (2001).

62. Feldmann, G. *et al.* Blockade of hedgehog signaling inhibits pancreatic cancer invasion and metastases: A new paradigm for combination therapy in solid cancers. *Cancer Res.* **67**, 2187–2196 (2007).

63. Ji, Z., Mei, F. C., Xie, J. & Cheng, X. Oncogenic KRAS activates hedgehog signaling pathway in pancreatic cancer cells. *J. Biol. Chem.* **282**, 14048–14055 (2007).

64. Torres, C. & Grippo, P. J. Pancreatic cancer subtypes: a roadmap for precision medicine. *Annals of Medicine* vol. 50 277–287 (2018).

65. Luo, G. *et al.* Characteristics and Outcomes of Pancreatic Cancer by Histological Subtypes. *Pancreas* **48**, 817–822 (2019).

66. Mostafa, M. E., Erbarut-Seven, I., Pehlivanoglu, B. & Adsay, V. Pathologic classification of 'pancreatic cancers': Current concepts and challenges. *Chinese Clinical Oncology* vol. 6 (2017).

67. Becker, A. E., Hernandez, Y. G., Frucht, H. & Lucas, A. L. Pancreatic ductal adenocarcinoma: Risk factors, screening, and early detection. *World Journal of Gastroenterology* vol. 20 11182–11198 (2014).

68. Collisson, E. A., Bailey, P., Chang, D. K. & Biankin, A. V. Molecular subtypes of pancreatic cancer. *Nature Reviews Gastroenterology and Hepatology* vol. 16 207–220 (2019).

69. Regel, I., Mayerle, J. & Mukund Mahajan, U. Current strategies and future perspectives for precision medicine in pancreatic cancer. *Cancers* vol. 12 1024 (2020).

70. Bailey, P. *et al.* Genomic analyses identify molecular subtypes of pancreatic cancer. *Nature* **531**, 47–52 (2016).

71. The Lancet Oncology. Undruggable KRAS—time to rebrand? *The Lancet Oncology* vol. 22 289 (2021).

72. Waddell, N. *et al.* Whole genomes redefine the mutational landscape of pancreatic cancer. *Nature* **518**, 495–501 (2015).

73. Collisson, E. A. *et al.* Subtypes of pancreatic ductal adenocarcinoma and their differing responses to therapy. *Nat. Med.* **17**, 500–503 (2011).

74. Moffitt, R. A. *et al.* Virtual microdissection identifies distinct tumor- and stroma-specific subtypes of pancreatic ductal adenocarcinoma. *Nat. Genet.* **47**, 1168–1178 (2015).

75. Daemen, A. *et al.* Metabolite profiling stratifies pancreatic ductal adenocarcinomas into subtypes with distinct sensitivities to metabolic inhibitors.

Proc. Natl. Acad. Sci. U. S. A. **112**, E4410–E4417 (2015).

76. Lomberk, G. *et al.* Distinct epigenetic landscapes underlie the pathobiology of pancreatic cancer subtypes. *Nat. Commun.* **9**, 1–10 (2018).

77. Kanji, Z. S. & Gallinger, S. Diagnosis and management of pancreatic cancer. *CMAJ* vol. 185 1219–1226 (2013).

78. McGuigan, A. *et al.* Pancreatic cancer: A review of clinical diagnosis, epidemiology, treatment and outcomes. *World Journal of Gastroenterology* vol. 24 4846–4861 (2018).

79. Canto, M. I. *et al.* International cancer of the pancreas screening (CAPS) consortium summit on the management of patients with increased risk for familial pancreatic cancer. *Gut* **62**, 339–347 (2013).

80. Ducreux, M. *et al.* Cancer of the pancreas: ESMO Clinical Practice Guidelines for diagnosis, treatment and follow-up. *Ann. Oncol.* **26**, v56–v68 (2015).

81. Goral, V. Pancreatic cancer: Pathogenesis and diagnosis. *Asian Pacific Journal of Cancer Prevention* vol. 16 5619–5624 (2015).

82. Meng, Q. *et al.* Diagnostic and prognostic value of carcinoembryonic antigen in pancreatic cancer: A systematic review and meta-analysis. *OncoTargets and Therapy* vol. 10 4591–4598 (2017).

83. Vincent, A., Herman, J., Schulick, R., Hruban, R. H. & Goggins, M. Pancreatic cancer. in *The Lancet* vol. 378 607–620 (Lancet, 2011).

84. Varadhachary, G. R. *et al.* Borderline resectable pancreatic cancer: Definitions, management, and role of preoperative therapy. *Annals of Surgical Oncology* vol. 13 1035–1046 (2006).

85. National Cancer Institute. Cancer Staging - National Cancer Institute. *NCI Cancer Staging* https://www.cancer.gov/about-cancer/diagnosis-staging/staging (2015).

86. Zhu, H., Li, T., Du, Y. & Li, M. Pancreatic cancer: Challenges and opportunities. *BMC Medicine* vol. 16 (2018).

87. Hartwig, W., Werner, J., Jäger, D., Debus, J. & Büchler, M. W. Improvement of surgical results for pancreatic cancer. *The Lancet Oncology* vol. 14 (2013).

88. Neoptolemos, J. P. *et al.* Therapeutic developments in pancreatic cancer: Current and future perspectives. *Nature Reviews Gastroenterology and Hepatology* vol.

15 333–348 (2018).

89. Hermanek, P. & Wittekind, C. Residual tumor (R) classification and prognosis. *Semin. Surg. Oncol.* **10**, 12–20 (1994).

90. Neoptolemos, J. P. *et al.* Adjuvant chemoradiotherapy and chemotherapy in resectable pancreatic cancer: A randomised controlled trial. *Lancet* **358**, 1576–1585 (2001).

91. Oettle, H. *et al.* Adjuvant chemotherapy with gemcitabine and long-term outcomes among patients with resected pancreatic cancer: The CONKO-001 randomized trial. *JAMA - J. Am. Med. Assoc.* **310**, 1473–1481 (2013).

92. Neoptolemos, J. P. *et al.* Comparison of adjuvant gemcitabine and capecitabine with gemcitabine monotherapy in patients with resected pancreatic cancer (ESPAC-4): a multicentre, open-label, randomised, phase 3 trial. *Lancet* **389**, 1011–1024 (2017).

93. Corporation, C. Nab-paclitaxel and Gemcitabine vs Gemcitabine Alone as Adjuvant Therapy for Patients With Resected Pancreatic Cancer (the 'Apact' Study) - NCT01964430. 2–5 (2015).

94. Trial Comparing Adjuvant Chemotherapy With Gemcitabine Versus mFolfirinox to Treat Resected Pancreatic Adenocarcinoma - Full Text View - ClinicalTrials.gov. https://clinicaltrials.gov/ct2/show/NCT01526135.

95. Zhan, H. X. *et al.* Neoadjuvant therapy in pancreatic cancer: a systematic review and meta-analysis of prospective studies. *Cancer Med.* **6**, 1201–1219 (2017).

96. Goess, R. & Friess, H. A look at the progress of treating pancreatic cancer over the past 20 years. *Expert Review of Anticancer Therapy* vol. 18 295–304 (2018).

97. Fathi, A. *et al.* Neoadjuvant therapy for localized pancreatic cancer: Guiding principles. *Journal of Gastrointestinal Oncology* vol. 6 418–429 (2015).

98. Ghaneh, P. *et al.* ESPAC-5F: Four-arm, prospective, multicenter, international randomized phase II trial of immediate surgery compared with neoadjuvant gemcitabine plus capecitabine (GEMCAP) or FOLFIRINOX or chemoradiotherapy (CRT) in patients with borderline resectable pan. *J. Clin. Oncol.* **38**, 4505–4505 (2020).

99. Trial to Investigate Intensified Neoadjuvant Chemotherapy in Locally Advanced Pancreatic Cancer - Full Text View - ClinicalTrials.gov.

https://clinicaltrials.gov/ct2/show/NCT02125136.

100. Definition of palliative therapy - NCI Dictionary of Cancer Terms - National Cancer Institute. https://www.cancer.gov/publications/dictionaries/cancer-terms/def/palliative-therapy.

101. Pancreatic Cancer: Statistics | Cancer.Net. *American Society of Clinical Oncology* https://www.cancer.net/cancer-types/pancreatic-cancer/statistics (2019).

102. Burris, H. A. *et al.* Improvements in survival and clinical benefit with gemcitabine as first- line therapy for patients with advanced pancreas cancer: A randomized trial. *J. Clin. Oncol.* **15**, 2403–2413 (1997).

103. Conroy, T. *et al.* FOLFIRINOX versus Gemcitabine for Metastatic Pancreatic Cancer. *N. Engl. J. Med.* **364**, 1817–1825 (2011).

104. Goldstein, D. *et al.* Nab-paclitaxel plus gemcitabine for metastatic pancreatic cancer: Long-term survival from a phase III trial. *J. Natl. Cancer Inst.* **107**, (2015).

105. De Sousa Cavalcante, L. & Monteiro, G. Gemcitabine: Metabolism and molecular mechanisms of action, sensitivity and chemoresistance in pancreatic cancer. *European Journal of Pharmacology* vol. 741 8–16 (2014).

106. Mackey, J. R. *et al.* Functional nucleoside transporters are required for gemcitabine influx and manifestation of toxicity in cancer cell lines. *Cancer Res.* **58**, 4349–4357 (1998).

107. Mini, E., Nobili, S., Caciagli, B., Landini, I. & Mazzei, T. Cellular pharmacology of gemcitabine. *Ann. Oncol.* **17**, (2006).

108. Hu, R., Lam, W., Hsu, C. H. & Cheng, Y. C. Ump/cmpk is not the critical enzyme in the metabolism of pyrimidine ribonucleotide and activation of deoxycytidine analogs in human rko cells. *PLoS One* **6**, e19490 (2011).

109. Plunkett, W., Grindey, G. B. & Plunkett, W. Action of 2',2'-Difluorodeoxycytidine on DNA Synthesis. *Cancer Res.* **51**, 6110–6117 (1991).

110. Heinemann, V. *et al.* Cellular Elimination of 2′,2′-Difluorodeoxycytidine 5′-Triphosphate: A Mechanism of Self-Potentiation. *Cancer Res.* **52**, 533–539 (1992).

111. Xu, H., Faber, C., Uchiki, T., Racca, J. & Dealwis, C. Structures of eukaryotic ribonucleotide reductase I define gemcitabine diphosphate binding and subunit assembly. *Proc. Natl. Acad. Sci. U. S. A.* **103**, 4028–4033 (2006).

112. Amrutkar, M. & Gladhaug, I. P. Pancreatic cancer chemoresistance to gemcitabine. *Cancers* vol. 9 (2017).

113. Habiro, A. *et al.* Involvement of p38 mitogen-activated protein kinase in gemcitabine-induced apoptosis in human pancreatic cancer cells. *Biochem. Biophys. Res. Commun.* **316**, 71–77 (2004).

114. Zhu, J. *et al.* Gemcitabine induces apoptosis and autophagy via the AMPK/mTOR signaling pathway in pancreatic cancer cells. *Biotechnol. Appl. Biochem.* **65**, 665–671 (2018).

115. Holohan, C., Van Schaeybroeck, S., Longley, D. B. & Johnston, P. G. Cancer drug resistance: An evolving paradigm. *Nat. Rev. Cancer* **13**, 714–726 (2013).

116. Panda, M. & Biswal, B. K. Cell signaling and cancer: a mechanistic insight into drug resistance. *Molecular Biology Reports* vol. 46 5645–5659 (2019).

117. U.S Department of Health and Human Services. Definition of progression-free survival - NCI Dictionary of Cancer Terms - National Cancer Institute. *National Cancer Institute* https://www.cancer.gov/publications/dictionaries/cancer-terms/def/progression-free-survival (2018).

118. Binenbaum, Y., Na'Ara, S. & Gil, Z. Gemcitabine resistance in pancreatic ductal adenocarcinoma. *Drug Resist. Updat.* **23**, 55–68 (2015).

119. Sarvepalli, D. *et al.* Gemcitabine: A review of chemoresistance in pancreatic cancer. *Crit. Rev. Oncog.* **24**, 199–212 (2019).

120. Quiñonero, F. *et al.* The challenge of drug resistance in pancreatic ductal adenocarcinoma: a current overview. *Cancer Biol. Med.* **16**, 688–699 (2019).

121. Du, J., Gu, J. & Li, J. Mechanisms of drug resistance of pancreatic ductal adenocarcinoma at different levels. *Bioscience Reports* vol. 40 (2020).

122. Spratlin, J. *et al.* The absence of human equilibrative nucleoside transporter 1 is associated with reduced survival in patients with gemcitabine-treated pancreas adenocarcinoma. *Clin. Cancer Res.* **10**, 6956–6961 (2004).

123. Bhutia, Y. D., Hung, S. W., Patel, B., Lovin, D. & Govindarajan, R. CNT1 expression influences proliferation and chemosensitivity in drug-resistant pancreatic cancer cells. *Cancer Res.* **71**, 1825–1835 (2011).

124. Maréchal, R. *et al.* Human equilibrative nucleoside transporter 1 and human concentrative nucleoside transporter 3 predict survival after adjuvant gemcitabine

therapyin resected pancreatic adenocarcinoma. *Clin. Cancer Res.* **15**, 2913–2919 (2009).

125. Giovannetti, E. *et al.* Transcription analysis of human equilibrative nucleoside transporter-1 predicts survival in pancreas cancer patients treated with gemcitabine. *Cancer Res.* **66**, 3928–3935 (2006).

126. Farrell, J. J. *et al.* Human Equilibrative Nucleoside Transporter 1 Levels Predict Response to Gemcitabine in Patients With Pancreatic Cancer. *Gastroenterology* **136**, 187–195 (2009).

127. Nakano, Y. *et al.* Gemcitabine chemoresistance and molecular markers associated with gemcitabine transport and metabolism in human pancreatic cancer cells. *Br. J. Cancer* **96**, 457–463 (2007).

128. Saiki, Y. *et al.* DCK is frequently inactivated in acquired gemcitabine-resistant human cancer cells. *Biochem. Biophys. Res. Commun.* **421**, 98–104 (2012).

129. Kroep, J. R. *et al.* Pretreatment deoxycytidine kinase levels predict in vivo gemcitabine sensitivity. *Mol. Cancer Ther.* **1**, 371–376 (2002).

130. Funamizu. Is the resistance of gemcitabine for pancreatic cancer settled only by overexpression of deoxycytidine kinase? *Oncol. Rep.* **23**, (2009).

131. Nakano, T. *et al.* Acquisition of chemoresistance to gemcitabine is induced by a loss-of-function missense mutation of DCK. *Biochem. Biophys. Res. Commun.* **464**, 1084–1089 (2015).

132. Weizman, N. *et al.* Macrophages mediate gemcitabine resistance of pancreatic adenocarcinoma by upregulating cytidine deaminase. *Oncogene* **33**, 3812–3819 (2014).

133. Wang, C. *et al.* Establishment of human pancreatic cancer gemcitabine-resistant cell line with ribonucleotide reductase overexpression. *Oncol. Rep.* **33**, 383–390 (2015).

134. Nielsen, M. F. B., Mortensen, M. B. & Detlefsen, S. Key players in pancreatic cancer-stroma interaction: Cancer-associated fibroblasts, endothelial and inflammatory cells. *World Journal of Gastroenterology* vol. 22 2678–2700 (2016).

135. Feig, C. *et al.* The pancreas cancer microenvironment. *Clinical Cancer Research* vol. 18 4266–4276 (2012).

136. Neesse, A. *et al.* Stromal biology and therapy in pancreatic cancer. *Gut* vol. 60

861–868 (2011).

137. Olive, K. P. *et al.* Inhibition of Hedgehog signaling enhances delivery of chemotherapy in a mouse model of pancreatic cancer. *Science (80-.).* **324**, 1457–1461 (2009).

138. Fletcher, J. I., Williams, R. T., Henderson, M. J., Norris, M. D. & Haber, M. ABC transporters as mediators of drug resistance and contributors to cancer cell biology. *Drug Resist. Updat.* **26**, 1–9 (2016).

139. Domenichini, A., Adamska, A. & Falasca, M. ABC transporters as cancer drivers: Potential functions in cancer development. *Biochimica et Biophysica Acta - General Subjects* vol. 1863 52–60 (2019).

140. Mohelnikova-Duchonova, B. *et al.* Differences in transcript levels of ABC transporters between pancreatic adenocarcinoma and nonneoplastic tissues. *Pancreas* vol. 42 707–716 (2013).

141. Adamska, A. *et al.* Molecular and cellular mechanisms of chemoresistance in pancreatic cancer. *Advances in Biological Regulation* vol. 68 77–87 (2018).

142. Santos Ramos, F., Wons, L., João Cavalli, I. & M.S.F. Ribeiro, E. Epithelial-mesenchymal transition in cancer: An overview. *Integr. Cancer Sci. Ther.* **4**, (2017).

143. Tian, X. *et al.* E-Cadherin/β-catenin complex and the epithelial barrier. *Journal of Biomedicine and Biotechnology* vol. 2011 (2011).

144. Dongre, A. & Weinberg, R. A. New insights into the mechanisms of epithelial–mesenchymal transition and implications for cancer. *Nature Reviews Molecular Cell Biology* vol. 20 69–84 (2019).

145. Huber, M. A., Kraut, N. & Beug, H. Molecular requirements for epithelial-mesenchymal transition during tumor progression. *Current Opinion in Cell Biology* vol. 17 548–558 (2005).

146. Arumugam, T. *et al.* Epithelial to mesenchymal transition contributes to drug resistance in pancreatic cancer. *Cancer Res.* **69**, 5820–5828 (2009).

147. Smigiel, J. M., Parameswaran, N. & Jackson, M. W. Potent EMT and CSC phenotypes are induced by oncostatin-M in pancreatic cancer. *Mol. Cancer Res.* **15**, 478–488 (2017).

148. Wang, W., Dong, L., Zhao, B., Lu, J. & Zhao, Y. E-cadherin is downregulated by

microenvironmental changes in pancreatic cancer and induces EMT. *Oncol. Rep.* **40**, 1641–1649 (2018).

149. Yang, Y., Bai, Y. S. & Wang, Q. CDGSH iron sulfur domain 2 activates proliferation and EMT of pancreatic cancer cells via Wnt/ß-catenin pathway and has prognostic value in human pancreatic cancer. *Oncol. Res.* **25**, 605–615 (2017).

150. Zhou, P. *et al.* The epithelial to mesenchymal transition (EMT) and cancer stem cells: Implication for treatment resistance in pancreatic cancer. *Molecular Cancer* vol. 16 (2017).

151. Wang, R. *et al.* Gemcitabine Resistance is Associated with Epithelial-Mesenchymal Transition and Induction of HIF-1a; in Pancreatic Cancer Cells. *Curr. Cancer Drug Targets* **14**, 407–417 (2014).

152. Shah, A. N. *et al.* Development and characterization of gemcitabine-resistant pancreatic tumor cells. *Ann. Surg. Oncol.* **14**, 3629–3637 (2007).

153. Wang, Z. *et al.* Acquisition of epithelial-mesenchymal transition phenotype of gemcitabine-resistant pancreatic cancer cells is linked with activation of the notch signaling pathway. *Cancer Res.* **69**, 2400–2407 (2009).

154. El Amrani, M. *et al.* Gemcitabine-induced epithelial-mesenchymal transition-like changes sustain chemoresistance of pancreatic cancer cells of mesenchymal-like phenotype. *Mol. Carcinog.* **58**, 1985–1997 (2019).

155. Ma, J. *et al.* Down-regulation of miR-223 reverses epithelial-mesenchymal transition in gemcitabine-resistant pancreatic cancer cells. *Oncotarget* **6**, 1740–1749 (2015).

156. Li, J. *et al.* Knockdown of FOXO3a induces epithelial-mesenchymal transition and promotes metastasis of pancreatic ductal adenocarcinoma by activation of the β-catenin/TCF4 pathway through SPRY2. *J. Exp. Clin. Cancer Res.* **38**, 38 (2019).

157. Wang, X. *et al.* AMPK-related kinase 5 (ARK5) enhances gemcitabine resistance in pancreatic carcinoma by inducing epithelial-mesenchymal transition. *Am. J. Transl. Res.* **10**, 4095–4106 (2018).

158. Ayob, A. Z. & Ramasamy, T. S. Cancer stem cells as key drivers of tumour progression. *Journal of Biomedical Science* vol. 25 1–18 (2018).

159. Walcher, L. *et al.* Cancer Stem Cells—Origins and Biomarkers: Perspectives for Targeted Personalized Therapies. *Frontiers in Immunology* vol. 11 1280 (2020).

160. Cho, Y. & Kim, Y. K. Cancer Stem Cells as a Potential Target to Overcome Multidrug Resistance. *Frontiers in Oncology* vol. 10 (2020).

161. Lee, C. J., Dosch, J. & Simeone, D. M. Pancreatic cancer stem cells. *Journal of Clinical Oncology* vol. 26 2806–2812 (2008).

162. Hermann, P. C. *et al.* Distinct Populations of Cancer Stem Cells Determine Tumor Growth and Metastatic Activity in Human Pancreatic Cancer. *Cell Stem Cell* **1**, 313–323 (2007).

163. Li, C. *et al.* Identification of pancreatic cancer stem cells. *Cancer Res.* **67**, 1030–1037 (2007).

164. Yao, J. *et al.* Cyclopamine reverts acquired chemoresistance and down-regulates cancer stem cell markers in pancreatic cancer cell lines. *Swiss Med. Wkly.* **141**, (2011).

165. Eyers, P. A., Keeshan, K. & Kannan, N. Tribbles in the 21st Century: The Evolving Roles of Tribbles Pseudokinases in Biology and Disease. *Trends in Cell Biology* vol. 27 284–298 (2017).

166. Hegedus, Z., Czibula, A. & Kiss-Toth, E. Tribbles: A family of kinase-like proteins with potent signalling regulatory function. *Cellular Signalling* vol. 19 238–250 (2007).

167. Yokoyama, T. & Nakamura, T. Tribbles in disease: Signaling pathways important for cellular function and neoplastic transformation. *Cancer Science* vol. 102 1115–1122 (2011).

168. Zanella, F. *et al.* Human TRIB2 is a repressor of FOXO that contributes to the malignant phenotype of melanoma cells. *Oncogene* **29**, 2973–2982 (2010).

169. Fang, Y. *et al.* Tribbles homolog 2 (Trib2), a pseudo serine/threonine kinase in tumorigenesis and stem cell fate decisions. *Cell Communication and Signaling* vol. 19 (2021).

170. Link, W. Tribbles breaking bad: TRIB2 suppresses FOXO and acts as an oncogenic protein in melanoma. *Biochem. Soc. Trans.* **43**, 1085–1088 (2015).

171. Hannon, M. M. *et al.* Elevated TRIB2 with NOTCH1 activation in paediatric/adult T-ALL. *Br. J. Haematol.* **158**, 626–634 (2012).

172. Wei, G., Lu, T., Shen, J. & Wang, J. LncRNA ZEB1-AS1 promotes pancreatic cancer progression by regulating miR-505-3p/TRIB2 axis. *Biochem. Biophys.*

Res. Commun. **528**, 644–649 (2020).

173. Wang, J. *et al.* Impaired phosphorylation and ubiquitination by p70 S6 kinase (p70S6K) and smad ubiquitination regulatory factor 1 (Smurf1) promote tribbles homolog 2 (TRIB2) stability and carcinogenic property in liver cancer. *J. Biol. Chem.* **288**, 33667–33681 (2013).

174. Foulkes, D. M., Byrne, D. P., Bailey, F. P. & Eyers, P. A. Tribbles pseudokinases: Novel targets for chemical biology and drug discovery? *Biochem. Soc. Trans.* **43**, 1095–1103 (2015).

175. Mayoral-Varo, V., Jiménez, L. & Link, W. The critical role of trib2 in cancer and therapy resistance. *Cancers* vol. 13 (2021).

176. Hill, R. *et al.* TRIB2 confers resistance to anti-cancer therapy by activating the serine/threonine protein kinase AKT. *Nat. Commun.* **8**, 14687 (2017).

177. Revathidevi, S. & Munirajan, A. K. Akt in cancer: Mediator and more. *Seminars in Cancer Biology* (2019) doi:10.1016/j.semcancer.2019.06.002.

178. Hill, R. *et al.* A novel phosphatidylinositol 3-kinase (PI3K) inhibitor directs a potent FOXO-dependent, p53-independent cell cycle arrest phenotype characterized by the differential induction of a subset of FOXO-regulated genes. *Breast Cancer Res.* **16**, (2014).

179. Machado, S. *et al.* Harmine and piperlongumine revert TRIB2-mediated drug resistance. *Cancers (Basel).* **12**, 1–20 (2020).

180. Salazar, M. *et al.* TRIB3 suppresses tumorigenesis by controlling mTORC2/AKT/FOXO signaling. *Mol. Cell. Oncol.* **2**, (2015).

181. Su, J. *et al.* Emodin induces apoptosis of lung cancer cells through ER stress and the TRIB3/NF-κB pathway. *Oncol. Rep.* **37**, 1565–1572 (2017).

182. Qu, J. *et al.* TRIB3 suppresses proliferation and invasion and promotes apoptosis of endometrial cancer cells by regulating the AKT signaling pathway. *Onco. Targets. Ther.* **12**, 2235–2245 (2019).

183. Erazo, T. *et al.* The New Antitumor Drug ABTL0812 Inhibits the Akt/mTORC1 Axis by Upregulating Tribbles-3 Pseudokinase. *Clin. Cancer Res.* **22**, 2508–2519 (2016).

184. Salazar, M. *et al.* Loss of Tribbles pseudokinase-3 promotes Akt-driven tumorigenesis via FOXO inactivation. *Cell Death Differ.* **22**, 131–144 (2015).

185. Wu, I. J., Lin, R. J., Wang, H. C., Yuan, T. M. & Chuang, S. M. TRIB3 downregulation enhances doxorubicin-induced cytotoxicity in gastric cancer cells. *Arch. Biochem. Biophys.* **622**, 26–35 (2017).

186. Dong, S. *et al.* Overexpression of TRIB3 promotes angiogenesis in human gastric cancer. *Oncol. Rep.* **36**, 2339–2348 (2016).

187. Wennemers, M. *et al.* Tribbles homolog 3 denotes a poor prognosis in breast cancer and is involved in hypoxia response. *Breast Cancer Res.* **13**, (2011).

188. Fang, N. *et al.* TRIB3 alters endoplasmic reticulum stress-induced β-cell apoptosis via the NF-κB pathway. *Metabolism.* **63**, 822–830 (2014).

189. Takahashi, K. *et al.* Establishment of a 5-fluorouracil-resistant triple-negative breast cancer cell line. *Int. J. Oncol.* **43**, 1985–1991 (2013).

190. Zhang, X. *et al.* Establishment and characterization of multidrug-resistant gastric cancer cell lines. *Anticancer Res.* **30**, 915–922 (2010).

191. Zhou, J. *et al.* Identification of chemoresistance-related mRNAs based on gemcitabine-resistant pancreatic cancer cell lines. *Cancer Med.* **9**, 1115–1130 (2020).

192. Mosmann, T. Rapid colorimetric assay for cellular growth and survival: Application to proliferation and cytotoxicity assays. *J. Immunol. Methods* **65**, 55–63 (1983).

193. Liu, Y., Peterson, D. A., Kimura, H. & Schubert, D. Mechanism of Cellular 3-(4,5-Dimethylthiazol-2-yl)-2,5-Diphenyltetrazolium Bromide (MTT) Reduction. *J. Neurochem.* **69**, 581–593 (1997).

194. Lü, L., Zhang, L., Wai, M. S. M., Yew, D. T. W. & Xu, J. Exocytosis of MTT formazan could exacerbate cell injury. *Toxicol. Vitr.* **26**, 636–644 (2012).

195. van Tonder, A., Joubert, A. M. & Cromarty, A. Limitations of the 3-(4,5-dimethylthiazol-2-yl)-2,5-diphenyl-2H-tetrazolium bromide (MTT) assay when compared to three commonly used cell enumeration assays. *BMC Res. Notes* **8**, 47 (2015).

196. Plumb, J. A. Cell Sensitivity Assays: The MTT Assay. in *Methods in Molecular Medicine* vol. 88 165–170 (Humana Press, 2004).

197. American Type Culture Collection. MTT Cell Proliferation Assay Instruction Guide. vol. 6597 1–6 (2011).

198. Aldrich, S. Protocol Guide: MTT Assay for Cell Viability and Proliferation | Sigma-Aldrich. https://www.sigmaaldrich.com/technical-documents/protocols/biology/roche/cell-proliferation-kit-i-mtt.html.

199. Meerloo, J. van, Kaspers, G. J. L. & Cloos, J. Cell Sensitivity Assays: The MTT Assay. in *Cancer Cell Culture: Methods and Protocols* vol. 731 79–91 (2011).

200. GraphPad Prism 7 Curve Fitting Guide - Equation: log(inhibitor) vs. response -- Variable slope. https://www.graphpad.com/guides/prism/7/curve-fitting/REG_DR_inhibit_variable.htm.

201. Strober, W. Trypan blue exclusion test of cell viability. *Curr. Protoc. Immunol.* **Appendix 3**, 2–3 (2001).

202. Strober, W. Trypan Blue Exclusion Test of Cell Viability. *Curr. Protoc. Immunol.* **111**, A3.B.1-A3.B.3 (2015).

203. Crowley, L. C., Marfell, B. J., Christensen, M. E. & Waterhouse, N. J. Measuring cell death by trypan blue uptake and light microscopy. *Cold Spring Harb. Protoc.* **2016**, 643–646 (2016).

204. Trepat, X., Chen, Z. & Jacobson, K. Cell migration. *Comprehensive Physiology* vol. 2 2369–2392 (2012).

205. Christiansen, J. J. & Rajasekaran, A. K. Reassessing epithelial to mesenchymal transition as a prerequisite for carcinoma invasion and metastasis. *Cancer Research* vol. 66 8319–8326 (2006).

206. Friedl, P. & Wolf, K. Tumour-cell invasion and migration: Diversity and escape mechanisms. *Nature Reviews Cancer* vol. 3 362–374 (2003).

207. Liang, C. C., Park, A. Y. & Guan, J. L. In vitro scratch assay: A convenient and inexpensive method for analysis of cell migration in vitro. *Nat. Protoc.* **2**, 329–333 (2007).

208. Justus, C. R., Leffler, N., Ruiz-Echevarria, M. & Yang, L. V. In vitro cell migration and invasion assays. *J. Vis. Exp.* (2014) doi:10.3791/51046.

209. De Ieso, M. L. & Pei, J. V. An accurate and cost-effective alternative method for measuring cell migration with the circular wound closure assay. *Bioscience Reports* vol. 38 (2018).

210. Mahmood, T. & Yang, P.-C. Western blot: Technique, Theory, and Trouble Shooting. *N. Am. J. Med. Sci.* **4**, 429–434 (2012).

211. Hnasko, T. S. & Hnasko, R. M. The Western Blot. in *Methods in Molecular Biology* vol. 1318 87–96 (Humana Press Inc., 2015).

212. McDermott, M. *et al.* In vitro development of chemotherapy and targeted therapy drug-resistant cancer cell lines: A practical guide with case studies. *Front. Oncol.* **4 MAR**, (2014).

213. Holohan, C., Van Schaeybroeck, S., Longley, D. B. & Johnston, P. G. Cancer drug resistance: An evolving paradigm. *Nature Reviews Cancer* vol. 13 714–726 (2013).

214. Togawa, A. *et al.* Establishment of gemcitabine-resistant human pancreatic cancer cells and effect of brefeldin-A on the resistant cell line. *Pancreas* **27**, 220–224 (2003).

215. Xu, B. Q. *et al.* Gemcitabine enhances cell invasion via activating HAb18G/ CD147-EGFR-pSTAT3 signaling. *Oncotarget* **7**, 62177–62193 (2016).

216. McDermott, M. *et al.* In vitro development of chemotherapy and targeted therapy drug-resistant cancer cell lines: A practical guide with case studies. *Front. Oncol.* **4 MAR**, (2014).

217. Shi, X., Liu, S., Kleeff, J., Friess, H. & Büchler, M. W. Acquired resistance of pancreatic cancer cells towards 5-fluorouracil and gemcitabine is associated with altered expression of apoptosis-regulating genes. *Oncology* **62**, 354–362 (2002).

218. Hagmann, W., Jesnowski, R. & Löhr, J. M. Interdependence of gemcitabine treatment, transporter expression, and resistance in human pancreatic carcinoma cells. *Neoplasia* **12**, 740–747 (2010).

219. Samulitis, B. K. *et al.* Gemcitabine resistant pancreatic cancer cell lines acquire an invasive phenotype with collateral hypersensitivity to histone deacetylase inhibitors. *Cancer Biol. Ther.* **16**, 43–51 (2015).

220. Rebbaa, A. Targeting senescence pathways to reverse drug resistance in cancer. *Cancer Letters* vol. 219 1–13 (2005).

221. Calcinotto, A. *et al.* Cellular senescence: Aging, cancer, and injury. *Physiol. Rev.* **99**, 1047–1078 (2019).

222. Elmore, L. W., Di, X., Dumur, C., Holt, S. E. & Gewirtz, D. A. Evasion of a single-step, chemotherapy-induced senescence in breast cancer cells: Implications for treatment response. *Clin. Cancer Res.* **11**, 2637–2643 (2005).

223. Herranz, N. & Gil, J. Mechanisms and functions of cellular senescence. *Journal of Clinical Investigation* vol. 128 1238–1246 (2018).

224. Yuedi, D. *et al.* KLF2 induces the senescence of pancreatic cancer cells by cooperating with FOXO4 to upregulate p21. *Exp. Cell Res.* **388**, 111784 (2020).

225. Hou, Z. *et al.* TRIB2 functions as novel oncogene in colorectal cancer by blocking cellular senescence through AP4/p21 signaling 11 Medical and Health Sciences 1112 Oncology and Carcinogenesis 06 Biological Sciences 0601 Biochemistry and Cell Biology. *Mol. Cancer* **17**, (2018).

226. Itahana, K., Campisi, J. & Dimri, G. P. Methods to Detect Biomarkers of Cellular Senescence. in *Methods in molecular biology (Clifton, N.J.)* vol. 371 21–31 (Methods Mol Biol, 2007).

227. Yan, Q. & Wajapeyee, N. Exploiting cellular senescence to treat cancer and circumvent drug resistance. *Cancer Biology and Therapy* vol. 9 166–175 (2010).

228. Riss, T. L. *et al. Cell Viability Assays*. *Assay Guidance Manual* (Eli Lilly & Company and the National Center for Advancing Translational Sciences, 2004).

229. Kumar, P., Nagarajan, A. & Uchil, P. D. Analysis of Cell Viability by the MTT assay. *Cold Spring Harb. Protoc.* **2018**, 469–471 (2018).

230. Louis, K. S. & Siegel, A. C. Cell viability analysis using trypan blue: manual and automated methods. *Methods Mol. Biol.* **740**, 7–12 (2011).

231. Stoddart, M. J. Mammalian Cell Viability: Methods and Protocols - Cell Viability Assays. *Methods Mol. Biol.* **740**, 1–6 (2011).

232. Wu, Q. *et al.* Chemoresistance to gemcitabine in hepatoma cells induces epithelial-mesenchymal transition and involves activation of PDGF-D pathway. *Oncotarget* **4**, 1999–2009 (2013).

233. Samulitis, B. K. *et al.* Gemcitabine resistant pancreatic cancer cell lines acquire an invasive phenotype with collateral hypersensitivity to histone deacetylase inhibitors. *Cancer Biol. Ther.* **16**, 43–51 (2015).

234. Yan, T. *et al.* Astaxanthin inhibits gemcitabine-resistant human pancreatic cancer progression through EMT inhibition and gemcitabine resensitization. *Oncol. Lett.* **14**, 5400–5408 (2017).

235. Zheng, X. *et al.* Epithelial-to-mesenchymal transition is dispensable for metastasis but induces chemoresistance in pancreatic cancer. *Nature* **527**, 525–530 (2015).

236. Kalluri, R. & Weinberg, R. A. The basics of epithelial-mesenchymal transition. *Journal of Clinical Investigation* vol. 119 1420–1428 (2009).

237. Hill, R. *et al.* Trib2 as a biomarker for diagnosis and progression of melanoma. *Carcinogenesis* **36**, 469–477 (2014).

238. Wang, J. *et al.* Combined elevation of TRIB2 and MAP3K1 indicates poor prognosis and chemoresistance to temozolomide in glioblastoma. *CNS Neurosci. Ther.* **26**, 297–308 (2020).

239. Grandinetti, K. B. *et al.* Overexpression of TRIB2 in human lung cancers contributes to tumorigenesis through downregulation of C/EBPα. *Oncogene* **30**, 3328–3335 (2011).

240. Liang, Y., Yu, D., Perez-Soler, R., Klostergaard, J. & Zou, Y. TRIB2 contributes to cisplatin resistance in small cell lung cancer. *Oncotarget* **8**, 109596–109608 (2017).

241. O'Connor, C. *et al.* Trib2 expression in granulocyte-monocyte progenitors drives a highly drug resistant acute myeloid leukaemia linked to elevated Bcl2. *Oncotarget* **9**, 14977–14992 (2018).

242. Ma, X. *et al.* TRIB2 knockdown as a regulator of chemotherapy resistance and proliferation via the ERK/STAT3 signaling pathway in human chronic myelogenous leukemia K562/ADM cells. *Oncol. Rep.* **39**, 1910–1918 (2018).

243. Zhang, Z. *et al.* Gemcitabine treatment promotes pancreatic cancer stemness through the Nox/ROS/NF-κB/STAT3 signaling cascade. *Cancer Lett.* **382**, 53–63 (2016).

244. Kumazoe, M. *et al.* The FOXO3/PGC-1β signaling axis is essential for cancer stem cell properties of pancreatic ductal adenocarcinoma. *J. Biol. Chem.* **292**, 10813–10823 (2017).

245. Quint, K. *et al.* Pancreatic cancer cells surviving gemcitabine treatment express markers of stem cell differentiation and epithelial-mesenchymal transition. *Int. J. Oncol.* **41**, 2093–2102 (2012).

246. Hoxhaj, G. & Manning, B. D. The PI3K–AKT network at the interface of oncogenic signalling and cancer metabolism. *Nature Reviews Cancer* vol. 20 74–88 (2020).

247. Xu, W., Yang, Z. & Lu, N. A new role for the PI3K/Akt signaling pathway in the epithelial-mesenchymal transition. *Cell Adhes. Migr.* **9**, 317–324 (2015).

248. Tzivion, G. & Hay, N. PI3K-AKT-FoxO axis in cancer and aging. *Biochimica et Biophysica Acta - Molecular Cell Research* vol. 1813 1925 (2011).

249. Paik, J. H. *et al.* FoxOs Are Lineage-Restricted Redundant Tumor Suppressors and Regulate Endothelial Cell Homeostasis. *Cell* **128**, 309–323 (2007).

250. Zhang, X., Tang, N., Hadden, T. J. & Rishi, A. K. Akt, FoxO and regulation of apoptosis. *Biochim. Biophys. Acta - Mol. Cell Res.* **1813**, 1978–1986 (2011).

251. Beretta, G. L., Corno, C., Zaffaroni, N. & Perego, P. Role of FoxO proteins in cellular response to antitumor agents. *Cancers (Basel).* **11**, 1–16 (2019).

252. Liu, Y. C. *et al.* Global regulation of nucleotide biosynthetic genes by c-myc. *PLoS One* **3**, (2008).

253. Yang, X. *et al.* Inhibition of c-Myc by let-7b mimic reverses mutidrug resistance in gastric cancer cells. *Oncol. Rep.* **33**, 1723–1730 (2015).

254. Luanpitpong, S. *et al.* Hyper-O-GlcNAcylation induces cisplatin resistance via regulation of p53 and c-Myc in human lung carcinoma. *Sci. Rep.* **7**, (2017).

255. Krysan, K. *et al.* PGE2-driven expression of c-Myc and oncomiR-17-92 contributes to apoptosis resistance in NSCLC. *Mol. Cancer Res.* **12**, 765–774 (2014).